3-D P WAVE VELOCITY STRUCTURE OF MARMARA REGION
USING LOCAL EARTHQUAKE TOMOGRAPHY

by

Sezim Ezgi Işık

B.S. Geophysical Engineering, İstanbul University, 2008

3-D P WAVE VELOCITY STRUCTURE OF MARMARA REGION USING LOCAL EARTHQUAKE TOMOGRAPHY

APPROVED BY:

Prof. Dr. Cemil Gürbüz . . . .
(Thesis Supervisor)

Prof. Dr. Nurcan Meral Özel . . . .

Prof. Dr. Ali Pınar . . . .

DATE OF APPROVAL: ……. July 2013

ACKNOWLEDGEMENTS

ABSTRACT

The 3D P wave velocity model of upper and lower crust of the Marmara Region between 40.2^0 - 41.2^0 N and 26.5^0 - 30.5^0 E is obtained by tomographic inversion (Simulps) of 47034 P wave arrivals of local earthquakes recorded at 90 land stations, 30 OBO stations and 14162 shot arrivals recorded at 35 OBO stations (Seismarmara Survey, 2001) between October 2009 and December 2012. We first obtained a 1D minimum model with Velest code in order to use it as an initial model for 3D inversion with 648 well located earthquakes located within the study area.

We first developed a 1D model by VELEST code then used it as an initial model for 3D tomography. After trial 3D inversions we decided to create a more adequate initial model for 3D inversion. Choosing the initial model we estimated the 3D P wave velocity model representing the whole region both for land and sea. The results are tested by making Checkerboard Test, Restoring Resolution Test and Characteristic Test, and the reliable areas of the resulting model is defined in terms of RDE, DWS, SF and Hit count distributions.

By taking cross sections from the resulting model we observed the vertical velocity change along profiles crossing both land and sea. All the profiles crossing the basins showed that the high velocities of lower crust make extensions towards the basin area which looks like the force that gives a shape to the basins. Under the north of the Central Basin and Çınarcık Basin high velocity zones appeared which look like resisting walls holding the north of the basins between 5 km and 15 km. The same is also observed under the southern Tekirdağ Basin between 5 km and 15 km. These extensions of lower crust towards the basins appeared with an average velocity of 6.3 km/s. These extensions might be the result of the deformation due the shear in the region and it is also interpreted that the development of these high velocities coincides with the development of the basins. Thus, both the basins and the high velocity zones around them might be resulted from the entrance of the NAF into the Marmara Sea when also a shear regime is dominated due to the resistance of the northern Marmara Region (Yılmaz, 2010). The seismicity is observed between 5 km and 15 km after the 3D location of the earthquakes. The locations of the earthquakes improved and the seismogenic zone is determined well, between 5 km and 15 km. The depths of the pre-kinematic basement and crystalline basement showed great

differences under the sea. It is observed that the velocity under sea becomes compatible with land after 8 km.

ÖZET

Ekim, 2009 ve Aralık, 2012 tarihleri arasında 40.2-41.2 N ve 26.5-30.5 E koordinatları içerisinde kalan, 90 kara istasyonunda, 30 OBO istasyonunda kaydedilmiş 47034 bölgesel depremlerin P dalgası varış zamanları ve 35 OBO istasyonunda kaydedilmiş patlatma verisinin (Seismarmara Survey, France) ters çözümle değerlendirilmesi sonucu Marmara Bölgesi'nin 3 boyutlu P hızı değişimi modellenmiştir. Seçilen 648 iyi çözümlenmiş deprem ile 1 boyutlu hız modellemesi Velest kodu ile gerçekleştirilmiştir.

Öncelikle 3D tomografi için başlangıç modeli olarak kullanılmak üzere VELEST kodu ile 1D minimum model oluşturulmuştur. Farklı 3D ters çözümlerin ardından çalışma alnını daha iyi temsil edebilecek bir başlangıç modeli elde edilmesine karar verilmiştir. Başlangıç modeli seçilerek çalışma alanını hem karada hem de denizde temsil edecek 3D P dalgası hız modeli oluşturulmuştur. Oluşturulan modele Checkerboard Testi, Geri Dönüştürücü Test and Karakteristik Test yapılarak sonucun güvenilirliği RDE, DWS, SF and Hit count, değerleri ile belirlenmiştir.

Elde edilen modelden kesitler alınarak karayı ve denizi aynı anda kesen profiler boyunca hız değişimi gösterilmiştir. Basenleri kesen tüm profiller göstermiştir ki, alt kabuğun yüksek hızları basenlere doğru, basenlere şeklini veriyormuş gibi görünen uzantılar yapmıştır. Orta ve Çınarcık basenlerinin kuzeyinin altında, bu basenlerin kuzey sınırlarını taşıyormuş gibi görünen dirençli duvarlara benzeyen yüksek hızlar 5 km ile 15 km arasında tespit edilmiştir. Basenlere doğru bu çıkış yapan yüksek hızlar ortalama 6.3 km/s hızla görülmüştür. Bu uzantılar bölgedeki makaslama geriliminden kaynaklandığı ve hızlardaki baseni şeklini vermiş olabilecek yapıların basenleri oluşumu ile aynı döneme denk gelmiş olabileceği tahmin edilebilir. Yani hem bu yüksek hızların hem de basenlerin Kuzey Anadolu Fay Hattı'nın Marmara Denizi'ne bölgenin kuzeyindeki dirençten kaynaklanan makaslama stresinin hakim olduğu dönemde girmesi ile ilişkili olabileceğini söyleyebiliriz (Yılmaz, 2010). 3D model ile yapılan lokasyonlardan sonra bölgede sismisite 5 km ve 15 km arasında gözlemlenmiş, deprem lokasyonları iyileştirilmiş ve sismojenik zon bu aralıkta belirlenmiştir. Pre-kinematik ve kristalin taban deniz altında değişimler göstermiştir. Deniz ve kara hızların 8 km den sonra uyum gösterdiği görülmüştür.

TABLE OF CONTENT

LIST OF FIGURES

LIST OF TABLES

LIST OF SYMBOLS / ABBREVIATIONS

G   Jacobian matrix vector

ε Damping parameter

I   Identity matrix

H   The matrix of hypocenter parameter

Δh The vector of hypocenter parameter

M   The matrix of velocity parameter

Δm The vector of velocity parameter

R   Resolution matrix

NAF   North Anatolian Fault

KOERI   Kandilli Observatory and Earthquake Research Center

TUBITAK   The Scientific & Technological Research Council of Turkey

Ms   Surface Wave Magnitude

N   North

S   South

E   East

W   West

1-D   One Dimensional Huseybe Method

2-D   Two Dimensional

3-D   Three Dimensional

ART   Algebraic Reconstruction

RMS   Root Mean Square

LET   Local Earthquake Tomography

DWS   Derivative Weighted Sum

RDE   Resolution Diagonal Element

SF   Spread Function

RKP   Runga-Kutta Perturbation

RRT   Restoring Resloution Test

WARR   Wide angle Reflection/Refraction

MSC   Multi-Channel Seismic Experiment

TR   Turkey

FR   France

PB   Pseudo Bending

1. INTRODUCTION

Marmara Region has a significant importance for its being the most complicated region linking Europe and Asia having metropolitan cities under a high risk in the case of a devastating earthquake.   It has the most complex part of the NAFZ set within the deep basins with sediment infill almost down to 6-7 km under the sea, generating large earthquakes which draw attention for the scientists of earth sciences, especially the 17th August 1999 earthquake which caused hundreds of people to die.

NAFZ, which crosses the Marmara Sea toward the Aegean Sea in the lower Pliocene, some 4-5 Myr ago (Armijo *et al.,* 1999; Hubert-Ferrari *et al.,* 2003), straddles Marmara Sea at the north of the Armutlu Peninsula which is described a collisional mountain belt along where the Rhodope-Pontide fragment collided with and was thrust over the Sakarya continent (Yılmaz, 1995). It is a right lateral strike-slip fault with normal component in the sea at both branches (*e.g.* Pondard, 2002). The northern branch of NAFZ in the Marmara Sea is loaded most of the westward movement (20 mm/yr in average) and it turns into a more complex system which is still not revealed completely.

The development of the Marmara region and its sea is mainly controlled by the NAF (Yılmaz, 2009). Before NAF entered the Marmara Sea, the region was being controlled by the N–S extension. This was followed by a right lateral shear regime which captured the existing normal faults by the strike slip faults generated during this period. New strike slip faults also started to occur in the second period. The second period is accepted as the initiation of the development of the NAF (Şengör *et al.,* 1985) and the sub-basins of Marmara Sea (Barka and Kadinsky-Cade, 1988). The Marmara Region has a remarkably flat from which is described as a peneplain surface developed above the Paleozoic, Mesozoic, and Cenozoic rocks including the upper Miocene units that crop out as the major rock units of the region (Yılmaz, 2009). It is suggested that the morphological difference between the north and south of Marmara is related to the NAFZ (Yılmaz, 2009).

Le Pichon *et al.* (2001) suggested a pure strike-slip fault crossing the Marmara Sea until Aegean Sea, by analyzing the results of a deep-towed seismic reflection data set. After their study a contrary fault model was suggested by Armijo *et al.* (2002) as a pull-apart fault system by analyzing the slip partitioning. These contradicted models were followed by micro earthquake study by using OBS stations in the sea (Sato *et al.,* 2004). The results of their study have shown that the western main Marmara Faults appear as a strike-slip regime while the north of the fault is dominated by both normal faulting and strike slip faulting.

Gürbüz *et al.* (2000) computed the 1D velocity structure though 180 events recorded by well distributed land station geometry around the Marmara Sea. It has 3km/s P wave velocity until 4.8 km which is not accurate for the deep sedimentary layers under the sub-basins of Marmara Sea. Another crustal structure study for the whole Marmara Region is a tomographic inversion method by Barış *et al.* (2005) using 3949 earthquakes with the inversion code TOMOG3D (Zhao *et al.,* 1992). They suggested that their results showed a relationship with fast wave velocity and the locations of the earthquakes until 15 km. However, the quality of the S wave readings of their study did not let them to estimate a good Vp/Vs ratio within the study area.

The shallow crustal structure of eastern Marmara was modeled with finite difference algorithm developed by Vidale (1988) and modified by Hole and Zelt (1995) by Karabulut *et al.* (2003). They showed that the velocity under the Çınarcık Basin increases until 4 km with a gradient. The focal mechanisms of earthquakes occurred here observed as normal faulting until 7 km and strike-slip faulting after 7 km (Özalaybey *et al.,* 2002). They also found a relationship with the locations of low velocity zones and strike slip motion of the northern branch of the NAF. A similar study was applied to the same area by Denli (2008). His tomographic results have shown that the low velocity areas seem to match the fault zones.

Zor (2006) revealed that the crustal thins from south to north. The results of this study showed the maximum crust thickness in the Marmara Region is 35 km under the Sakarya Zone. In general he found the average crust thickness as 31 ± 2 km and S wave velocity as 3.65 ± 0.15 km/s.

The most recent offshore crustal structure studies in the Marmara Sea are Becel (2006); Becel (2009) and Bayrakçı (2009). Becel (2006) and Becel, *et al.,* (2009) have revealed that the Moho depth varies horizontally, using WARR and MSC studies. Their results allowed suggesting a negative flower structure related to the consistent model of thinning, extension and transtension at the scale of the lithosphere (Becel *et al.,* 2009). Bayrakçı (2009) estimated the 3D basin structure under the sea by explosion data tomography. Her results let us to see the detailed basin structure and the velocity which has a great importance while locating the earthquakes occurred in the sea.

Kaya *et al.* (2013), revealed the 2D resistivity variation along a profile crossing the Çınarcık Basin. The results of their study from sea bottom receivers showed that there is the existence of a conductor at a depth of~10 km in the middle of both profiles crosses the Çınarcık Basin in NE-SE direction, along with a deeper extension into the upper mantle, implying the presence of fluid in the crust and partial melting in the upper mantle. Moreover, their results indicated that faults seem to be settled at the boundary of the conductive and resistive zones.

The main objective of this study is to obtain a 3D P wave velocity model to locate the earthquakes occurring here better with minimum error.   What makes this study different from previous studies here is that the data set we used is composed of both land and sea bottom stations which results in a quite realistic velocity model representing both land and sea bottom structure at the same time.

Generally, in LET studies rays do not cross the uppermost part of the crust which we do not want to experience for Marmara Region. What we expect and aim to do is creating an initial model that is close to the real structure by joining both a network in sea recorded a series of shots (Seismarmara Survey, 2001). For the sake of having a 1D minimum initial model, we run VELEST code but with a unusual way which I call layer by layer inversion which can be found in the 4th chapter. Another objective is to show that neither a 1D model nor the tomographic inversion result of a 1D initial model can represent the whole medium. Due to high contrast lateral velocity variances in the sea having its origin in the deep sediment infill in the sub-basins sunk in the pre-kinematic basement, we tried a different way of finding an initial model by extracting 1D models which represent different

parts of the medium.

In tomography, there are many challenges, but in the case of Marmara Region there are obstacles which should be taken into account seriously in order to prevent any erroneous results and artifacts. While inverting the model, the code we use asks how fast to change the model. The previous knowledge of the sea bottom studies (2D or 3D models), shows that there is a high contrast between the sediment infill in the sub-basins of Marmara Sea and the surroundings. So, we need a high enough maximum P wave perturbation value to invert completely both the basins and the land. A low one may be enough for the land areas but not enough for the sediment infill areas. On the other hand, a high one would invert the sediments well but this inversion would be very fast for the land areas. Both ways are tried. Another challenge is the iteration number. In order to decide whether a model would be reached a minimum or not we observed the change in the RMS by making a series of iterations. Deciding a grid space is another tackle. Although the land is homogenous within the layers, it is not the same for the medium under the sea which indicates that grid must be designed by taking into account the lateral and vertical changes under the sea. Thanks to the previous studies we had a priory information of the structure in the sea. The last challenge is testing the reliability of the model. Since the P wave perturbation is not same for the whole region for both vertically and horizontally, the classical way of checkerboard test could not be applied.

In our study we have chance to compare the results in terms of the previous studies. Our aim of this study is to derive the 3D P wave velocity variation model which could represent the whole region including not only the sea but also the land. We showed the inability of a 1D model in demonstrating the whole region by both the inversion of VELEST (Kissling, 1988) and Simulps (Thurber, 1983).

In the second chapter we gave brief information about the study region. The geology of the region can be defined in 3 different type of structures which are İstanbul zone, Sakarya Zone and Thrace Basin. The sea area has a more complex structure than in the land. Marmara Sea has 3 basic basins filled with sediment deposits which are Tekirdağ Basin, Central Basin and Çınarcık Basin. These sub-basins has their sediment infills down to 7 km which makes a high velocity contrast with their vicinity. The Western edge of

NAFZ is settled in these basins consisted of fragments. These fragments have different faulting systems. The most significant force in the area is the shear stress that is caused by the twisting of Marmara toward southwest (Yılmaz, 2010).

In the 3rd Chapter, we introduced the objectives of the study and the methodology. The main aim of this study is to obtain a whole crustal structure of Marmara Region in order to make better earthquake locations. We tried to reach a 3D model by the tomographic inversion code Simulps which is a damped-least-squares, full matrix inversion intended for use with natural local earthquakes, with or without shots and blasts (Thurber, 1981, 1983, 1993). We also presented the 1D modeling process in this chapter. The data set is eliminated according to the requirements of Velest code and 648 well located events were chosen to compute the 1D minimum model.

In the 4th Chapter we presented the data set which is composed of 3700 earthquakes recorded at 90 land stations and 30 OBO stations and 650 shots (Seismarmara Survey, 2001) recorded at 35 OBO stations between 39.5-42.5 N and 26-30.5 E. The region that we observe is smaller than the area where the earthquakes occurred so that the resolution around the boundary of the study area is improved.

In the 5th chapter, we explained the details of finding an initial model for the 3D inversion. None of the 1D models we used for the 3D inversion was accurate enough to be inverted. We combined 1D models and showed the differences between the inversion result of the 1D models and combined models. The resulting model and the synthetic tests can be found in this chapter.

Finally, in the 6th Chapter, we discussed the cross sections of the resulting models, that are interpreted according to the threshold values of quality estimators such as RDE, SF and hit count, by comparing them with the previous crustal structure studies in the Marmara Sea (Becel, 2006; Becel *et al.,* 2009; Bayrakçı, 2009, Kaya *et al.,* 2013). Since the main aim of this study is to recover the erroneous locations due to insufficient 1D model used for the location, we made a relocation of a main shock and its after shocks. We also showed the change in the locations of earthquakes > 3.

2. TECTONICS OF THE MARMARA REGION AND PREVIOUS STUDIES

2.1. Tectonics of the Marmara Region

Marmara Region is positioned between Aegean, Balkan, Black Sea, and Anatolian regions on the northwest corner of Anatolian Plateau. As the region covers the intersect of the N-S extension of Aegean Region and the North Anatolian Fault Zone (NAFZ), it is tectonically critical and complex (Figure 2.1). The NAFZ (150 km) as the northern boundary of Anatolian Plateau splays into two main branches in the Marmara Sea which can be accepted as the main feature of the region as it was witnessed many large hazardous earthquakes.
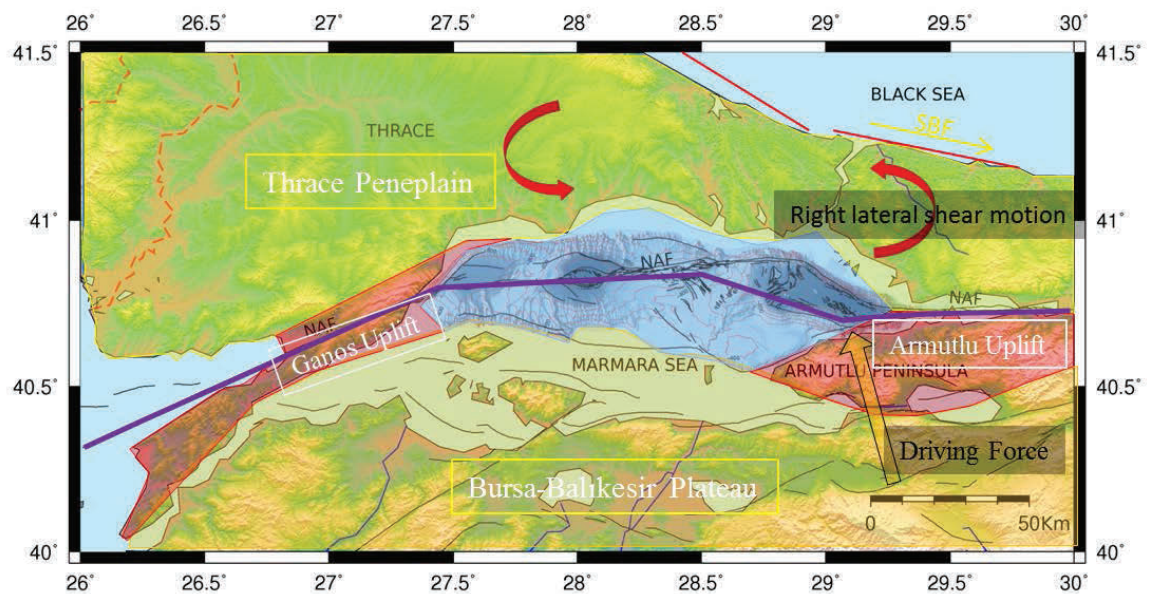
Figure 2. 1. Tectonic Setting of Marmara Region, Red arrows indicate the dextral shear stress in the region caused by two right lateral strike slip faults. (Modified from Prof. Dr. Yücel Yılmaz, Lecture Notes, İTÜ, 2013).

2.1.1. North Anatolian Fault Zone

NAFZ is an intra-continental transform fault zone forming between the Karlıova triple junction in the east and mainland Greece in the west. Even though it has a continuous structure along the Black Sea Region, it starts to behave more complicated when it enters the İzmit Bay. The reason of this switch is the transition between the strike-slip behavior of NAFZ on the east and the extensional behavior of the Aegean Region in the west. Complexity reveals itself with the fault segments which have different fault types and trends (Gürbüz, 2000). It had an important role on the development of Marmara Region Basin which is one of two main sedimentary successions in the study area in the late Pliocene. NAFZ also had a control on the Marmara Sea, Saros, Manyas-Ulubat, Bursa, Yenişehir, İznik and Gönen (Figure 2.1) (Yaltırak, 2002).

The Northern Branch of Marmara which is moving westwards 20mm/year, is composed of 3 segments: Ganos Segment, Central Marmara Fault, North Boundary Fault. Most of the major earthquakes in Marmara Region occurred along the Northern Branch of NAFZ (NNAFZ) (Figure 2.2).

Both branches, the north and the south, are principally Right-lateral strike-slip with a normal component (e.g. Pondard, 2002) and end entering Aegean Sea. The only segment which has not been ruptured since the 18th century earthquake sequence is the fault between the Çınarcık and Central Basins (Armijo *et al.,* 2005). Although there is not a certain information about the age of NAFZ recent studies have shown that the age is nearly 200 ka (İmren *et al.,* 2001; Le Pichon *et al.,* 2001; Gökaşan *et al*., 2001; 2003; Dolu *et al.,* 2007).
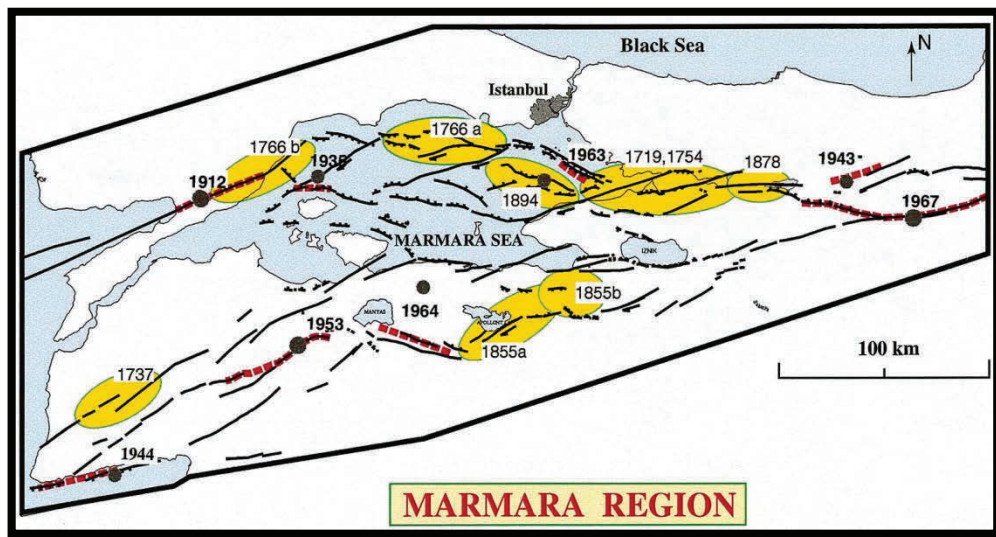
Figure 2. 2. Historical eartquakes occured in Marmara Region (modified after Barka, 1997).

2.1.2. Marmara Sea and It's Sub-basins

Marmara Sea is an intra-continental sea located between Anatolia (Asia) and Thrace (Europe) connecting Black Sea and Aegean Sea with two straits on the northeast and southwest named Bosporus Strait and Dardanelles Strait, respectively.

The period of the opening of Marmara Sea is coincide with the period that the horst-graben structure developed in all Aegean covering also the Bursa-Balıkesir Plateau with a major effect of normal faulting starting from the end of late Miocene. The development of it can be expressed in two tectonic phases (Yılmaz, 2010). The first stage of the development was under the control of normal faulting. It was a wide and shallow basin. The second stage was started with the development of NAFZ under the control of a right-lateral strike-slip shear regime. At this stage the right-lateral strike-slip faults captured the normal faults which already formed at the previous stage. Also new strike-slip fault systems developed at this stage of the evolution of Marmara Sea. This shear regime caused sub-basins to form with a NE trend so this co-evolution of strike-slip shear regime and the sub-basins formed the Marmara Sea as it is now.

The sea now contains shelves, slopes and sub-basins. There are two main shelves in the sea, first is the northern one which is narrower as 3-5 km wide, and the second is the southern one as 30 km width, covering the largest area as 6077km^2 of the sea (Gazioğlu *et. al.,* 2002). The main features of these shelves are Prince Islands and Marmara, Imralı, Turkeli, Paşalimalı Islands and Kapıdağ Peninsula, respectively.

Armutlu and Ganos Mountains, being risen steeply, limits the sea from east and west ,respectively so there are no shelves along them.

The sub-basins which formed primarily under the control of NAFZ (Yılmaz, 2010) are Çınarcık, Central and Tekirdağ Basins from east to west. The deepest one is Çınarcık Basin as 1270 m and it contains 3 km young Plio-Quaternary sedimentary infill (Carton, 2003). The depths of Central and Tekirdağ Basins are 1250 m and 1120 m, respectively. There is also a shallower basin right at the top of the Eastern Ridge with a depth of 830 m called Silivri Basin (Yılmaz, 2010).

2.1.3. Land Areas in the Marmara Region

The two sides of the Marmara Sea, the north and the south parts, have different high elevation rates. The north land is 40-300 m high whereas the south is 500-1000 m high. The north part which is called the İstanbul Plateau is a horst structure which elevated like a horst but also was exposed to the shear regime two right-lateral strike-slip faults which are the boundary faults of two adjacent sea basins (Yılmaz, 2007). The differences of the stabilities of the faults here, the horst rotated. The other side, southern of Marmara Region is called Bursa-Bilecik Plateau. The western motion of Anatolia causes this part of the land in Marmara Region to form a tectonic bend and so have different elevation rate, 300-350 m and 800m, respectively. This prevented the further movement to west and the anticlockwise rotation towards the Hellenic arc. A recent study suggests that this period of the development of Bursa-Balıkesir Plateau is a young event (2-3 ma) which is proved by the paleomagnetic data (Piper, 2010).

2.2. Geological Characterization

The region can be expressed in three geological structures (Figure 2.3). İstanbul zone which covers the north part of the region mostly comprises Precambrian crystalline basement overlain by a continuous transgressive sedimentary succession also overlain by a unconformity of Mesozoic succession (Dean *et al.*, 1997; Görür *et al.*, 1997). There are widely Senonian andesites and small acidic intrusion caused by the northward subduction of the İzmir-Ankara ocean (Okay and Tüysüz, 1999).
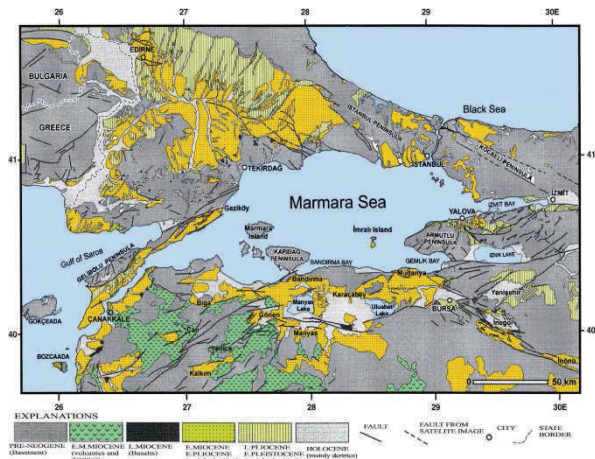
Figure 2. 4. Simplified geology map of the Marmara Region (Modfied after Yaltırak, 2002, Yılmaz, 2010).

Figure 2. 3. General geological structure of the Marmara Region and its surrounding areas (Okay, 2008).

The Strandja Zone forming the easternmost part of the crystalline basement is made of metamorphic rocks interrupted by Permian granites. The structure overlain by a Triassic succession (Aydın, 1974; Okay and Tüysüz, 1999) which were metamorphosed and overlain by Cenomanian conglomerates, shallow marine limestone. As in the case of the Istanbul Zone, these are covered by Senonian andesites and intruded by associated granodiorites (Moore *et al.,* 1980).

The Sakarya Zone composed of a strongly deformed and partly metamorphosed basement named Karakaya Complex as a subduction-accretion complex. The deformation was completed with the Senonian andesites (Altıner *et al.,* 1991; Tüysüz, 1993).

The northwestern shore of Marmara Sea covers Thrace Basin. The crystalline rocks constitutes basement like the Strandja-Rhodope basement (Görür and Okay, 1996). This formation can be expressed by tuffaceous siliciclastic turbidites (Sonel, 1998). Also continental to shallow-marine clastics and carbonates with subordinate volcanoclastics were laid along the margins and on elongate bathymetric highs (Zattin *et al.,* 2010).

2.3.   Seismicity

Marmara Region where NAFZ splays into two main branches in the sea is tectonically active and has a dense seismicity. Here, NAFZ has the primary role controlling the seismic activity in the region. The zone both comprises normal faulting and strike-slip faulting (Gürbüz, 2000; Altunel *et al.,* 2000; Taymaz, 1990, 2001; Altınok *et al.,* 2001; Yaltırak and Alpar, 2002). In the region both extension and shear regime show appears. A recent study of Karabulut *et al.* (2011) has shown that although one of the largest earthquakes in Marmara Region (17 August 1999) occurred on a strike-slip fault and affect the seismicity of the region actually the extension regime affects here more.

The region has witnessed some of the most devastating earthquakes occurred in Turkey. Two of them are the 17 August 1999 İzmit Earthquake with a magnitude of 7.4 Mw and 12 November 1999, Düzce Earthquake with a magnitude of 7.2 Mw. Studies related to these earthquakes show that around İzmit bay where NAFZ enters the sea, strike-slip faulting appears, near Armutlu Peninsula strike-slip and normal faulting were observed and around Tuzla Peninsula normal and strike-slip faulting comprises the region at shallow and deeper parts (Karabulut *et al.,* 2002). On the Eastern Marmara Trough there have been East-West trending strike-slip faults which created large earthquakes between 6.6 Ms and 7.4 Ms at an average depth of 10 km. These were from east to west: 1943 Hendek, 1951 Kurşunlu, 1957 Abant, 1967 Mudurnu, 1999 İzmit and Düzce earthquakes (Mc Kenzie, 1972; Ambraseys and Jackson, 1998; Taymaz *et al.,* 1991, 2001; Taymaz, 1999, 2000). Yaltırak (2002) claimed that the behavior of the faults turn into normal faulting when an earthquake occurred under the magnitude of 6.4 Ms. There have been also observed trust fault and right-lateral offset with normal component around Ganos Mountain and Saros Trough , respectively (Kalafat, 1995; Taymaz, 1990, 2000) .

On the middle branch of NAFZ there are Northwest-Southeast-trending extension along normal faults. On the other hand around Armutlu Peninsula Northeast-Southwest dextral strike-slip faulting was observed (Gürbüz *et al.,* 2000). Oblique normal faults were also observed around Gemlik Bay (Gürbüz *et al.,* 2000). It was also observed that other two earthquakes occurred on the eastern part of the middle branch in Marmara Sea (1953 and 1969 Yenice) gave Northeast-southwest trending thrust faults with right-lateral component and pure dextral strike-slip faults, respectively (Taymaz, 1990, 2000) which can be accepted as an evidence for the southward bending of the middle stand and westward escape of Anatolian Block (Yaltırak, 2002).

2.4.   Previous Studies

Marmara as a tectonically active region on the northern corner of Anatolia has been subjected to many geophysical and geodesic studies yet most of them were implemented after 17 August 1999 İzmit and 12 November 1999 Düzce earthquakes. These studies including the multidisciplinary ones have lighted up most of the answers of unclear subjects of geophysical, tectonic, geological questions.

One effective way to understand the behavior of the crust is to identify the layers with respect to velocities of seismic waves. Until the sea bottom observatory stations were deployed in Marmara Sea the studies were only on-shore. So the crustal structure belonging to this region could only represent the velocities of land. There are several on-shore studies that takes place in the literature Gürbüz *et al.* (2000), Karabulut *et al.* (2003), Denli (2008) , Barış *et al.*(2005), Zor (2006). Gürbüz *et al.* (2000) has run VELEST code and find a minimum 1D model representing the area. The velocity model is given below.

Table 2.1. Minimum 1D model for Marmara Region (Gürbüz *et al.,* 2000)

P Wave Velocity	Depth
3.0	0.0
5.3	4.8
5.9	9.5
6.2	12.5
6.5	17.0
7.3	24.0
7.9	29.0

In this model we see that there are no layers that could represent the low velocity zones in the sea but this model could be one of the initial model that is available for LET studies in the region. Another study is a receiver function study which lights up crustal thickness of eastern Marmara Region. Zor (2006), has shown that the average crustal thickness and S-wave velocity for the eastern Marmara Region are 31 ± 2 km and 3.64 ± 0.15 km s^{-1}, respectively. Karabulut *et al.* (2003) also find the average P wave velocity for the upper crust in the same region (5.7-5.9 km/s). They related the results with the complex geology. Denli (2008) in his study, find similar results as the study of Karabulut and Zor. His study also matches the study of Nakamura (2002). They all reach the idea that there are low velocity zones under the southern and northern branches of NAFZ in Marmara Region between 2 and 15 km depths. With these studies it is seen that there are higher velocities under the İstanbul Zone especially under the Armutlu Peninsula which is due to the granitic intrusions within the metamorphic body (Karabulut *et al.,* 2003).

As the large area of Marmara Region the Marmara Sea with its sediment filled deep basins has an important role when estimating crustal structure because of its low velocities. The studies made to understand the crust under the sea is not only important to understand the evolution of NAFZ in the Marmara Sea but also has a critical effect on the location of the earthquakes occurred on the fault zone. As long as a model that represents the land is used to locate the earthquakes occurred in the sea, the reliability of the locations is

questionable. Some of the off-shore studies implemented in Marmara Sea Region are Kaşlılar-Özcan (2001), Bécel *et al.* (2008), Laigle *et al.* (2008), Bayrakçı (2009), Bécel *et al.,* (2010), Sorlien *et al.* (2011), Zitter *et al.* (2011), Faridfathi (2011).

Ateş (2003) observed that the Curie isotherm level lies between 6-8 km and it is shallower than on the continent which can be a precursor of the crustal thinning in the region. He also provided that although sedimentary units show no magnetism which can be explained by the low P wave seismic velocity (2.8 km/s), under 6.5 km magnetic rocks observed. Tank *et al.* (2005) showed that there is a relation between high resistivity area underlain by a low resistivity zone and the occurrence of an earthquake on the northern branch of the NAF. They also interpreted that the fluid rich region triggers the earthquake generation and responsible for post seismic creeping. Same is suggested by Kaya *et al.* (2013) for the Çınarcık Basin area.

3. METHODOLOGY

As long as the structure lets us we can work with a 1D model in LET studies. However, in the case of our study where the strong lateral velocity variations are dominant in a large part of the study area. Thus we need a code which would calculate the ray paths in 3D. Since our data set is composed of both shots and earthquakes, we have chosen the code SIMULPS (Thurber, 1983) which can make a joint inversion of both. The code is generally used for developing P and S velocity structure by inverting P and S first arrival times. The advantage that we made use of the code is that the possibility to invert earthquakes and shots at the same time.

SIMULPS (Thurber, 1983) provided us with a 3D model, which is quite realistic due to the inversion made with a series of shots in the sea where normally we would not expect a dense ray sampling in shallow depth and also with the earthquakes located on land, surrounding the study area. This joint inversion is very important because we wished to ensure about completeness of the ray sampling in the medium of study for the sake of creating a model that would represent both land and sea at the same time.

3.1 Principle of Tomography

Seismic tomography is a data interpretation technique that uses information in seismic records to constrain 2D or 3D models of the Earth's interior. It generally requires the solution of a large inverse problem to obtain a heterogeneous seismic model that is consistent with observations (Rawlinson, 2009).

In seismic tomography, either in a known (artificial) or in an unknown (natural earthquakes) location, a seismic source is activated at an origin time "t_j^0". In our study the both cases are handled so both of them will be explain in terms of seismic tomography. In the case of artifical source, we do not need an inital guess for the hypocenter because it is already known. So the unknown is only the model. However, in the case of LET studies both the model parameters and the origin times with the locations are unknowns.

Due to the strong non-linearity of a tomographic problem, the direct approach is not possible. Instead, we have a chance to make a good guess of the model parameters and linearize the problem. If we consider the problem as a function of the model parameters it can be simplified as below:

$$g(m)=d \qquad (3.1)$$

Where d contains the travel times of the wave readings, m is the model parameter and g is the function which represent the relation between m and d. If m_0 is an estimation of the model parameters, we can assume that the real model parameters are :

$$m = m^0_{est} + \Delta_m \qquad (3.2)$$

where the Δm contains the model corrections. Thanks to initial estimation of the model parameters the 3.1 can be linearized as :

$$g(m) \cong g(m^0_{est}) + G_0 (\Delta_m) \qquad (3.3)$$

where $g(m)$ represents the observed data T^{obs} and $g(m^0_{est})$ represents the predicted ones T^{est} . The Jackobi-matrix G_0 contains all the derivatives evaluated at m^0_{est}. Thus 3.1 can be written as :

$$\Delta d \cong G \Delta m \qquad (3.4)$$

where Δd contains all travel time residuals ΔT_{ij} which are the misfits between the observed T^{obs}_{ij} and calculated T^{est}_{ij} travel times,

$$\Delta T_{ij} = T^{obs}_{ij} - T^{est}_{ij} \qquad (3.5)$$

where the ij denotes i^{th} observation of j_{th} event. The arrival time T_{ij} is a sum of the origin time t^0_j of the event and its travel time t^s_{ij} along the path s, from the source (x^0_j, y^0_j, z^0_j) to the receiver (x, y, z).

$$T_{ij} = t^0_j + t^s_{ij}(x^0_j + y^0_j + z^0_j, v(s), x, y, z) \qquad (3.6)$$

where $v(s)$ is the velocity along the path s. Thus ΔT_{ij} can be written as;

$$\Delta T_{ij} \cong \Delta t_j^0 + \sum_{k=1}^3 \frac{\delta t_{ij}^s}{\delta x_{kj}^0} \Delta x_{kj}^0 + \sum_{l=1}^L \frac{\delta t_{ij}^s}{\delta v_l} \Delta v_l \qquad (3.7)$$

This equation implies a discrete parameterization of the velocity model with L model parameters. Therefore the velocities of the medium are defined on a grid of nodes. In the Equation 3.3, G contains the partial derivates and the Δm contains the model corrections Δt_j^0, Δx_j^0 and Δv_l. In the actual inversionstudy since the inverted data set consist only in shots with known origin times and locations, the vector of model corrections contains only the velocity perturbations Δv_l. They can be calculated with respectto the initial estimation of the model parameters m_{est}^0 , thus with respect of a initial velocity model by solving the Equation 3.3 in a least square sense, by minimizing the Δd which are the travel time residuals in our case.

The model corrections are calculated with respect to the initial estimation of model parameters. So, the result is highly dependent to the initial velocity model.

Due to the linearization, model parameterization and data error, it is not possible to fit perfectly T^{est} to T_{obs}. That is why an approximately equal sign is used in the Equation 3.3 and Equation 3.4. The uncertainties of observations and of station or shot coordinates affect the observed travel times consequently travel time residuals. Moreover, the discrete parameterization of the medium by an inversion grid, the way how the ray paths and travel times along them are calculated has an influence on the predicted travel times. Thus, they also affect the travel time residuals. Those uncertainties of the travel time residuals together with the resolution which is limited by the finite data set and the distribution of rays in the targeted volume, make that the result of the tomography is not a final image in which every anomaly can be interpreted. Some of the model corrections cannot be resolved independently or some of them will not be resolved at all. In order to obtain a meaningful solution despite these shortcomings, in code Simulps the damped least squares method (Crosson, 1976) method is applied. Without going into mathematical details, the damped least square solution is

$$\Delta m = (G^T G + \varepsilon^2 I)^{-1} G^T \Delta d \qquad (3.8)$$

where I is the unity matrix and ε is the damping parameter.

In order to decrees the computational coast Thurber (1983) incorporated a parameter separation where the $G\Delta m$ split into two parts: one containing the velocity model parameters and the other one the hypocentral parameters.

$$\Delta d = H \Delta h + V \Delta v \qquad (3.9)$$

where $H\Delta h$ contains the hypocentral part and $V\Delta v$ the velocity part.

3.2. Grid Space

Decision of an inversion grid is related to the distribution of receivers and the sources in our case both shots and earthquakes. If the node spacing is smaller than the average distance between source and the receiver, the result would not be a realistic velocity model. In that case the only the nodes close to the source would be inverted and the other would be fixed which would cause artificial velocity changes. The shallow artificial velocities also would bias the deeper part of the model. In the case of Simulps, the vertical node spacing needs to be small enough to provide a good ray sampling in a node.

In our study the source and receiver distribution is quite dense in the western and eastern Marmara Sea. The source information from the land is remarkably coarse because of the seismicity. This made us to add extra earthquakes which surround the outer part of the study area. By adding earthquakes located outside of the study area, we tried to strengthen the information on the boundaries.

Considering the previous knowledge from a WARR study we can understand the expected vertical and horizontal velocity variation, at least in the sea.
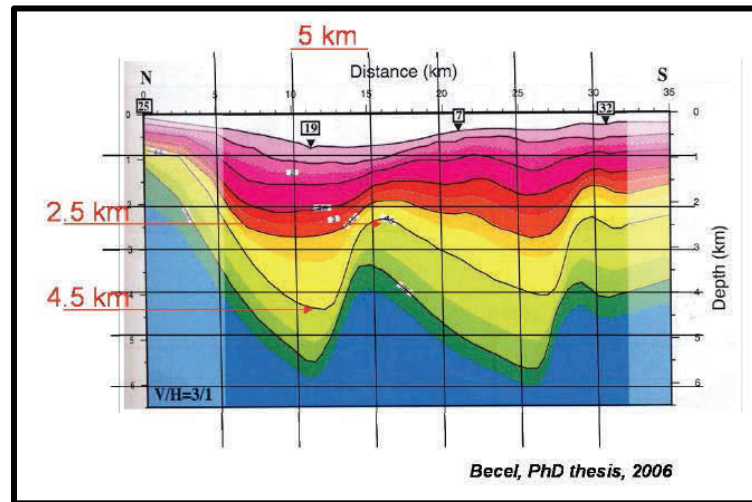
Figure 3. 1**.** The final velocity depth model obtained by wide-angle reflection, refraction modeling along N-S profile, Profile 5, by Bécel (2006). The WARR result allows quantifying sizes of vertical and horizontal velocity heterogeneity that we can expect to find within the Marmara Sea.

In Figure 3.1 we can see the vertical and horizontal velocity change along a profile cutting across the Central High. Although the both the receiver and source distribution let us to work with a 5 or 6 km grid we should take into account that the distribution is not the same for the land area. So rather than creating a grid which is finer type we preferred to enlarge the node spacing in order to compensate the ray sampling in land and we created a grid of 9*9*3 km.

3.1.1 Ray Tracing

In the code SIMULPS (Thurber, 1983) the computation of the forward solution, so the computation of theoretical traveltimes is done with the ray theory. A ray tracer is used for the determination of the ray paths which reach the source to the receivers by propagating the wave through the initial model, then by calculating the travel time along the path.
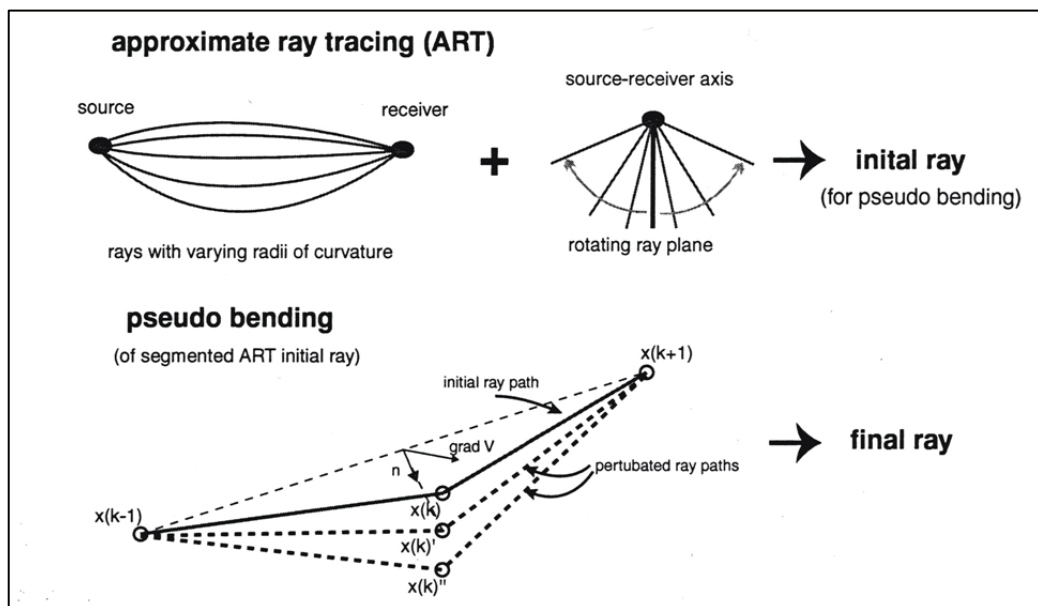
Figure 3. 2. The illustration of the 3D approximate ray tracing (ART) and pseudo bending (PB).

In Figure 3.2, first, with ART, the ray path is approximated by arcs of varying curvatures along the source receiver axis. In a second step, the arc with the smallest travel time is adjusted to the velocity gradient by PB (Husen *et al.*, 2000).

Ray tracing techniques can be categorized as exact or approximate techniques (Thurber, 1993). The ray equation can numerically be solved as initial value problem, where the ray direction at a starting point is given (shooting), or as boundary value, where the ray starting point and end point are given (bending). In both case the solution will yield a ray path and integrating over this path will give the travel time for this path (Haslinger *et al.*, 1999). Both methods suffer from the same disturbing possibilities of convergence to a

local rather than global travel time minimum. The use of approximate ray-tracing methods has the advantage of the computation speed but may introduce some residuals, hypocenter or velocity errors due to the wrong calculation of the travel time or wrong choice of the direction of the ray path. One way to determine the influence of ray tracing on the tomographic image is to use different forward solving schemes and to compare the results. Thanks to the previous comparison results of ART-PB and RKP made in the same study area but only with shot data, we will only present the results from ART_PB method which was preferred according to the result of the previous test runs because of its speed (Bayrakçı, 2009).

With the code Simulps, it is possible to solve the forward problem either with approximate ray tracer (ART) (Thurber, 1983) and pseudo-bending (PB) method (Um & Thurber, 1987) or with Runge Kutta and perturbation (RKP) method which is described by Virieux *et al.* (1988), Virieux (1991), Virieux &Farra (1991).

In order to test the accuracy of a ray tracing scheme in the present study, the ART-PB method and the RKP methods have been compared. The ART-PB method is an approximate ray tracer. First, rays between source and receivers are approximated by circular arcs of different radii and are rotated along the source receiver axis. The ray corresponding to the smallest travel time is taken as the initial ray for the pseudo bending. Then, the initial path is adjusted according to the velocity field gradient along the ray path (Husen *et al.,* 2000) with the pseudo bending.

The RKP ray tracing scheme connects the source to the receiver by shooting method. The ray equation is solved as an initial value problem. The smallest travel time is found by varying the initial azimuth and take-off angle at the source according to the velocity field. For numerical reasons, the RKP ray tracing scheme requires to represent the velocity filed as squared slowness on a evenly distributed grid (Haslinger & Kissling, 2001; Virieux, Farra, & Madariaga, 1988; Virieux, 1991; Virieux & Farra, 1991).

4. DATA ANALYSIS

4.1 Data Set

The study includes two data sets. On is the small data set with 1300 earthquakes (TR) and 650 shots (FR) and the other is a large data set with 3700 eartquakes (TR) and 650 shots (FR). These are recorded at 156 stations in different time periods. There are 12 temporary stations operated from 1st October 2009 to 15th March 2010 and 10 other temporary stations operated from 15th April 2011 to 31st July 2011. This part of the seismic data was obtained from IFREMER in 12 hours sac format. Since these stations were temporary they had a time shift. This time shift was assumed as linear and then eliminated from the data to avoid uncertainties. The stations include also 5 broadband OBO stations which have been operating by KOERI. We also add the shot data in the sea, surrounding all the basin and fault area, recorded at 37 well located stations operated by IFREMER (Seismarmara Survey, 2001). One part of the rest is operated by TUBITAK and others by KOERİ on land.
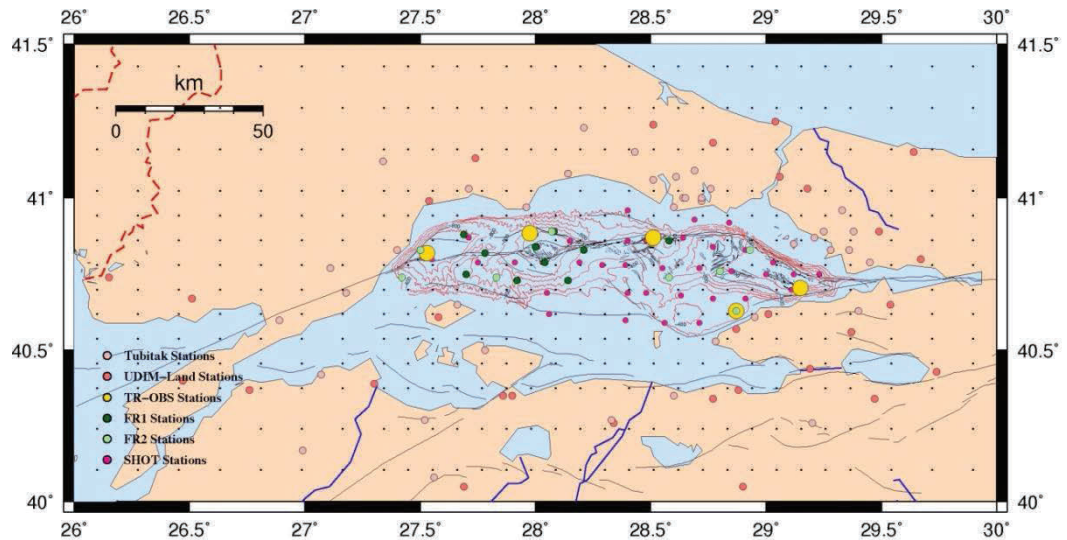
Figure 4. 1. Station distribution used in the study

The first time arrivals of the earthquakes recorded at land stations were joined together with the first time arrivals of the same events recorded at stations in the sea by the time periods 1st October 2009-15th March 2010 and 15th April 2010-31st July 2010. The

rest of the data combined with only the OBO stations operated by KOERI.

The data until 31st July 2011 consists of 1320 earthquakes. These were located with hypocenter program and eliminated considering the quality factors such as the gap, latitude error, longitude error and number of stations recorded the earthquakes. After the elimination 620 earthquakes were left. These were then used for deriving a minimum 1D model and a 3D model. After deriving the 1D minimum model a second part of land data from 31st July 2011 to 31st December 2012 was added to the data set in order to improve the resolution within the land area. Second part of the data was not included in the 1D minimum model deriving process and consist of 738 well located earthquakes. The second part of the data was combined with OBO stations. In total the tomography process was carried out with 1358 earthquakes and 650 shots. First time arrival picking and 1D minimum model deriving steps were made through out SEISAN.
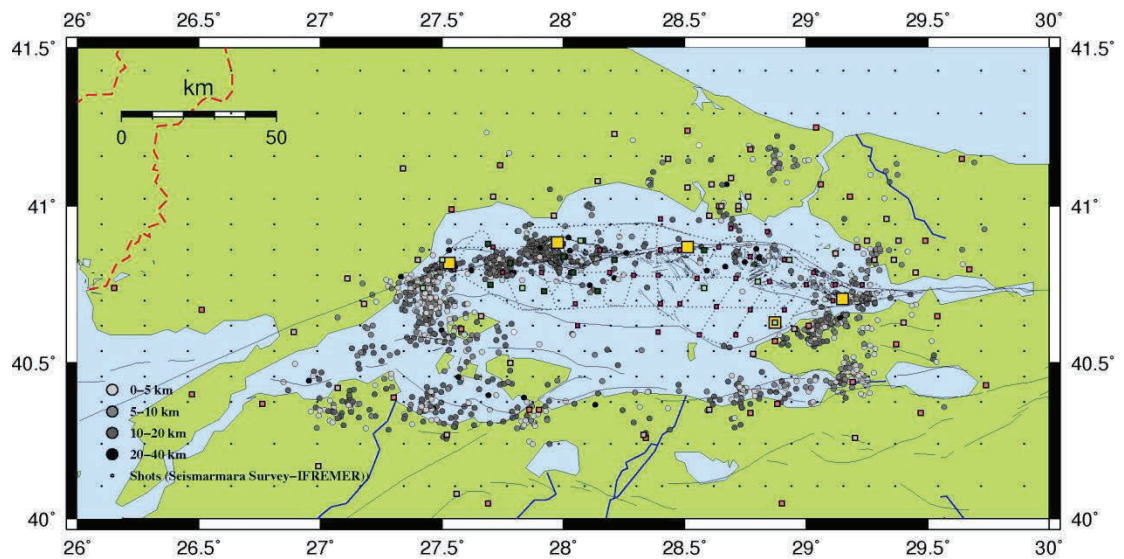
Figure 4. 2. Small data set.
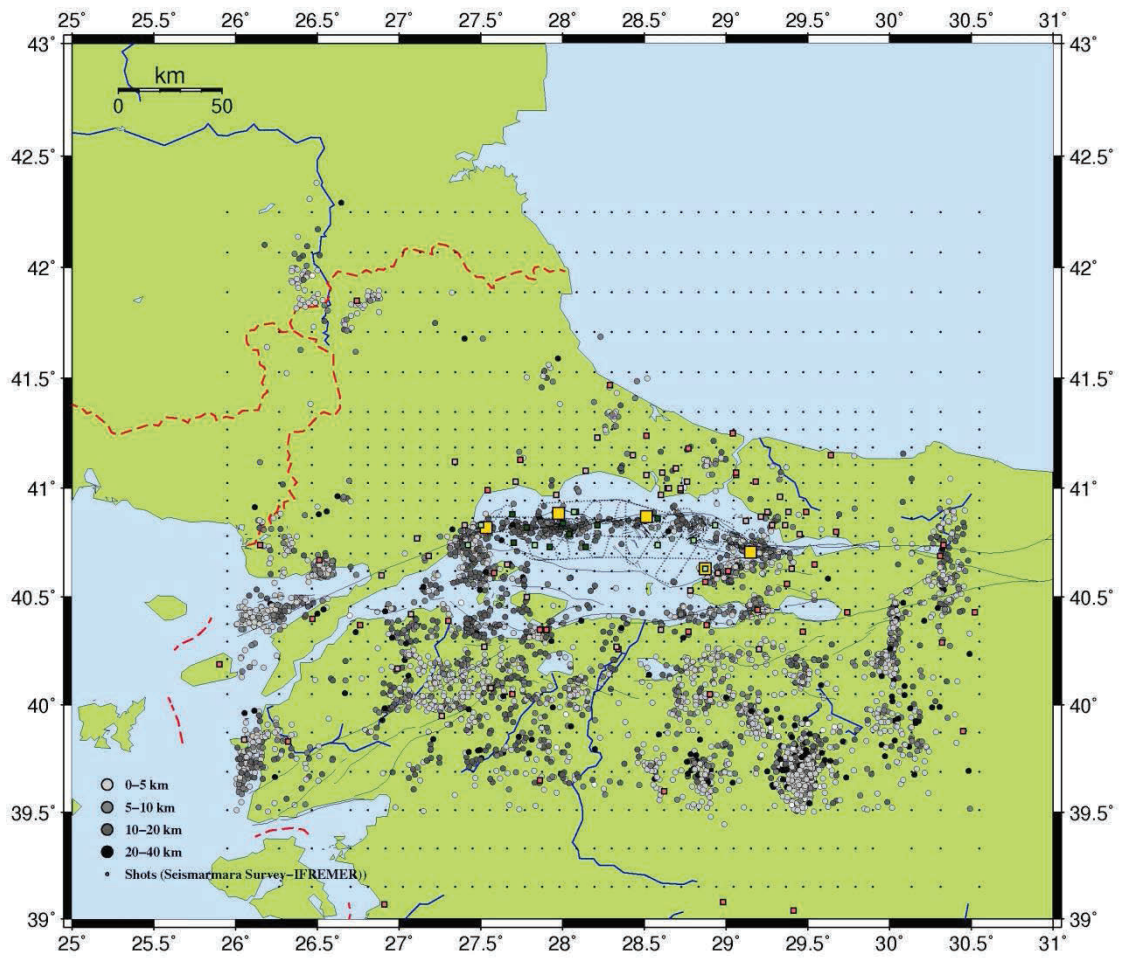
Figure 4. 3. Large data set
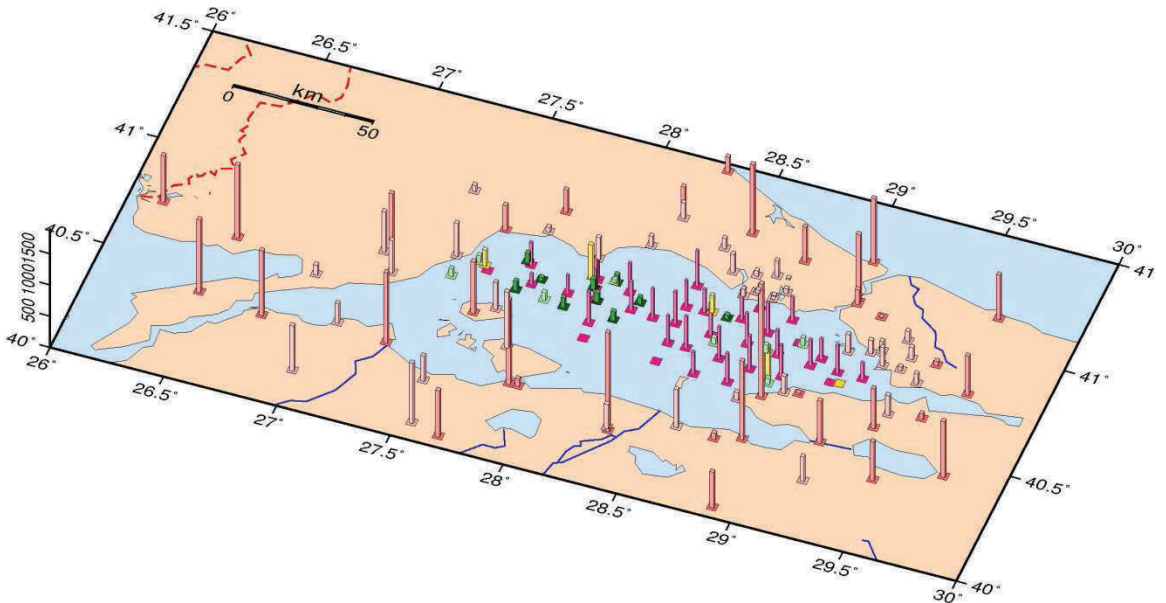
Figure 4. 4. Recordings at stations.

In Figure 4.4, we see that the recording number at stations located north of the Marmara Sea is remarkably less than the others on land. Also the recordings of light green (FR) and dark green stations (FR) have less recording compared to others on land. However, the pink stations which recorded the shots provide a good ray coverage with dense data. The light pink stations of TUBITAK fill the gap around the Marmara Sea but with less data then KOERI stations on land. Light orange stations of KOERI strengthen the boundary of the study are with the largest amount of recordings.

4.2   1D Model Calculation with VELEST Code

Program VELEST is a FORTRAN77 routine that has been designed to derive 1-D velocity models for earthquake location procedures and as initial reference models for seismic tomography (Kissling 1988; Kissling *et al.,* 1994).

The code solves a coupled hypocenter-velocity model problem. The RMS which is the difference between calculated and observed travel times gives an idea how good is the model. To find a minimum RMS we used a two step test. The first one is to try different

initial models which could represent the study area. The other is to make many iterations to find at which iteration the solution reaches a minimum RMS. In this coupled hypocenter-velocity problem, the resulting velocity model strongly depends on the initial model and the initial hypocenter locations. After deciding initial model and the iteration number the control parameters should be adjusted to obtain a minimum model which fits the data set best. This final model called the 1D minimum model.

Due to the lack of information about thickness in the resulting 1D model, we need to create an inital model which has many layers so that the thicknesses would be adjusted.

The advantage of VELEST code in the present study is that we have chance to solve the deeper layers better than Simulps. The 3D modelling code Simulps has a disadvantage due to its model parameterization which is limitted to data in each grid. On the other side the VELEST code uses a model parameterization as vertical layers which lets the result to include deep layer information. The details about the VELEST processing will presented in the next part.

4.3   Deciding Initial Parameters for VELEST Process

To start velest process, a priori velocity model belonging to the study area should be determined. After deciding the most appropriate initial model, Velest is run until finding a minimum model. Since Velest is an algorithm that runs in terms of its control parameters such as, damping for the velocity iterations, damping for the station corrections, damping for the hypocenter parameters, the code should be run several times for both catching the correct parameters and designing the best velocity model that fits the data set.

The study area is known with its lateral velocity variations under the Marmara Sea because of thick sedimentary layers beneath the main basins. It is known that under these deep basins the velocity of P wave is very low compared to which of basin rims and land so it is not possible for a 1D model to represent this area.

According to the study of Becel (2006) an initial model representing the average velocity under the Marmara Sea is used for an initial model which is the P wave velocity beneath the middle of the sea between the Central Basin and the Çınarcık Basin. In a

general sense there are areas that have very low velocities and also there are areas with high velocities. These shallow sudden velocity changes lead us to the idea that the 1D model should change -while inverting- suddenly. To avoid that we kept the control parameter that is the maximum velocity adjustment low so that these sudden changes would not affect the final velocity model. When tried to introduce a high velocity adjustment the model ended up with unrealistic velocities.

When we consider the whole inversion process, it is seen that velocities tend to change rapidly in the shallower parts .The reference station is OBO3 since it is the closest station to the center or the study area (40.8N 28.3E). Even though it is not the station that recorded the largest amount of events, the velocity model is the closest model to the initial model. Before accepting it as reference station we tried OBO3 and a land station ARMT. The results showed that changing the reference model changed not only the station corrections but also the velocity model itself. On the other hand, since the actual model under the ARMT is very high from initial model the resulting model was not realistic for an average model for the study area. Also OBO2 did not show a more realistic model compared to the OBO3.

The aim of the Velest is to compute an average velocity for a layer so before deciding the 1D minimum model we expected to end up with an average model of the initial model since it already represents the velocity model under the Marmara Sea. We paid attention being aware of the RMS that shows the average difference between the computed and observed travel times. We stopped running the program when model showed very little variance and the RMS reduced to a minimum after fifth run.

4.4   LAYER BY LAYER INVERSION

RUN 1: After locating all 1340 events with HYPOCENTER program an elimination is done in respect to the these criteria as: observations more than 10 stations, RMS between -1s and 1s and without considering the gap to see if the gap would reduce. After running VELEST the events were eliminated in terms of gap < 180 degree and 765 events were left. The reason to eliminate these events is to invert the well located events and also to prevent possible artifacts in the future process due to large. So, after the 1st run the average gap was 115 degree and the RMS was reduced from 0.78s to 0.49s after 9 iterations.
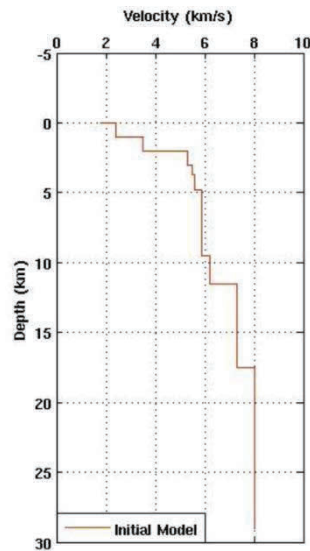
Figure 4. 5. 1D initial model extracted from
the WARR study (Becel, 2006).

RUN 2: The outputs of the 1st run are used as initial data for the 2nd run. The model has changed significantly about 4km below the sea level. The rest stayed closest to the initial model of the 2nd run.
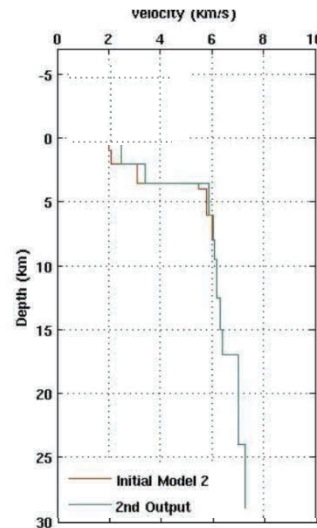
Figure 4. 6. Result of 2nd run.

For the second run additional layers whose velocities increased linearly are inserted to the model to see if there is a strong change between these layers. The aim at this point was to identify the layers showing very low or very high velocities. No significant changes have seen above about 8 km. The result of this inversion indicated that only the shallow part of the crust under Marmara Sea shows significant lateral velocity variations. The average gap was reduced to 102 degree and also the RMS was reduced from 0.79s to 0.49 after 9 additional iterations. Although the initial model was lower than its output still the output was not what I expect considering the previous a priory model for the region.

RUN 3: Because some shallow layers show similar velocities after 2nd run. I mixed them and reduced the number of layers to avoid miscalculations. The thickness of the layers in the shallow part of the crust became thicker and additionally I introduced a little higher velocities in these layers than the previous output to see if the velocities would come to their original place. This let me to be sure of some velocities of shallow layers. And indeed, they turned back nearly to their original place. The average gap was 102 and the RMS was reduced from 0.66s to 0.46s. Still the very shallow part of the area did not

showed what we would expect. The model says that the velocity is 2.22 km/s under the study region but when we consider the average of first 4 km or 4.5 km it was higher than expected. Again model did not showed significant changes below 4 km.
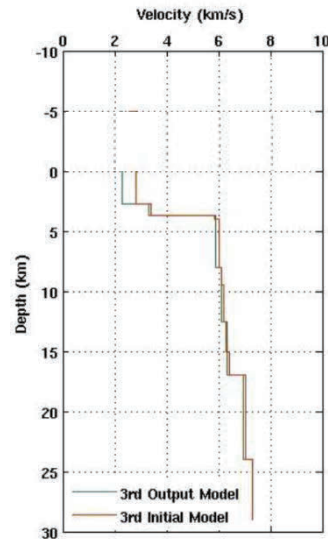
Figure 4. 7. Result of 3rd run

RUN 4: To check if the shallow part is represented correctly or not I made the same thing in the 3rd run. This time I introduced a sudden increase after 2.70 km and for the other layers an average of lower and higher layers. This would also help me to find the average velocity for the all depths. The result indeed showed a nice consistence with the previous output model. The gap was again 102 degree and the RMS was reduced from 1.03s to 0.49s. This increase in the RMS might be the result of the high velocity layer that was introduced after 2.70km. But it proved that the layer velocity here is not as high as about 5km/s since it lead to 3.50 km/s and the decrease in the RMS also supported that idea.
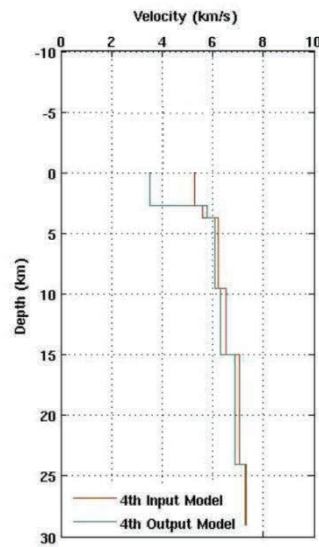
Figure 4. 8. Result of 4th run.

RUN 5 : Finally 5 iterations were made to check if the RMS is the minimum. After five routine iterations with velocity damping 0.01 and station damping 0.01 the model has reached fine average velocities for the first 4 km. The RMS was reduced from 0.48s to 0.45s and the average gap was 102 degree again. According to the Velest User's Manuel, the velocity damping was taken as 1 and the station damping was taken 0.1. The aim of the change is to see how the model changes when the damping for velocity is increased. The result was what I expected according to the previous studies. The average of the first 4 km was a little bit lower than before and average gap was between 27 and 179 with an average of 99 degree. The RMS was reduced from 0.46s to 0.45s and this showed that the RMS was no more changing. This model is called according to Velest Uses's Manuel the Updated A Priory Model. After deciding the Updated A Priory Model, some events were eleminated again with respect to the criteria that the RMS is between -0.6 and 0.6. So the best well located 648 events were left.
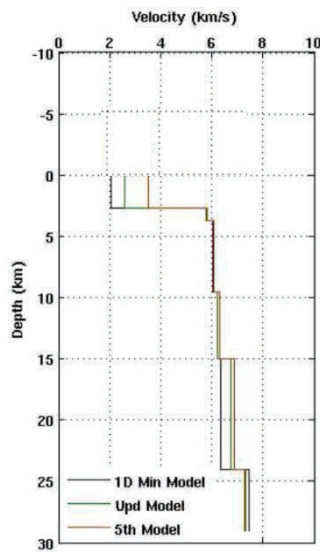
Figure 4. 9. Result of 5th run.
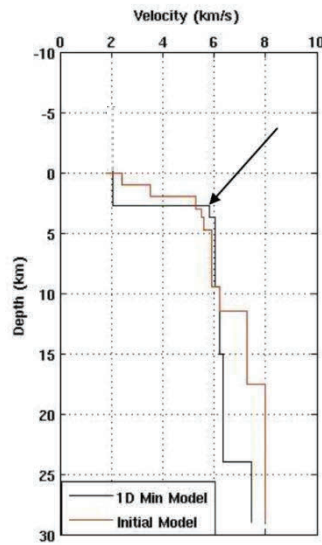
Figure 4. 10. Final 1D minimum model and the inital model.

When we compare the initial and final models (Figure 4.10) we see that in the initial model the velocity increases with depth, while in the final model, it seems like a representative of an average of the first 4 km. The resulting 1D minimum model shows a remarkable difference from the initial model at layers deeper than 5 km. However, the shallow layers of the model seem like an average of the layers of the initial model. At deep layers, we see that final model has slower velocities compared to the initial model. This might be related to the varying Moho depth under Marmara Sea (Becel *et al.,* 2009). Thanks to the previous studies implemented in the same region, we have an idea of average velocity at Conrad as about 6.2 km/s changing between 15 and 22 km and at Moho as about 8km/s changing between 27 and 35 km (Becel *et al.,* 2008). The resulting 1D minimum model has 6.2 km/s between 15 and 25 km. However, the model does not include the Moho depth because of the decreasing number of rays at deeper layers.

4.5   Testing Minimum 1D modeL

There are fewer events in the systematic shifting test which were shifted after the test. About 85% of the data turned back to their original place. Most of them show no change in hypocenter. One thing that is obvious is that in the systematic test depth variations showed a direction towards the shifted values. This shows that the depth is not

being reversed after shifting which is what we expect. In general when compared to the previous Velest runs with different initial models shifting test showed much better results.
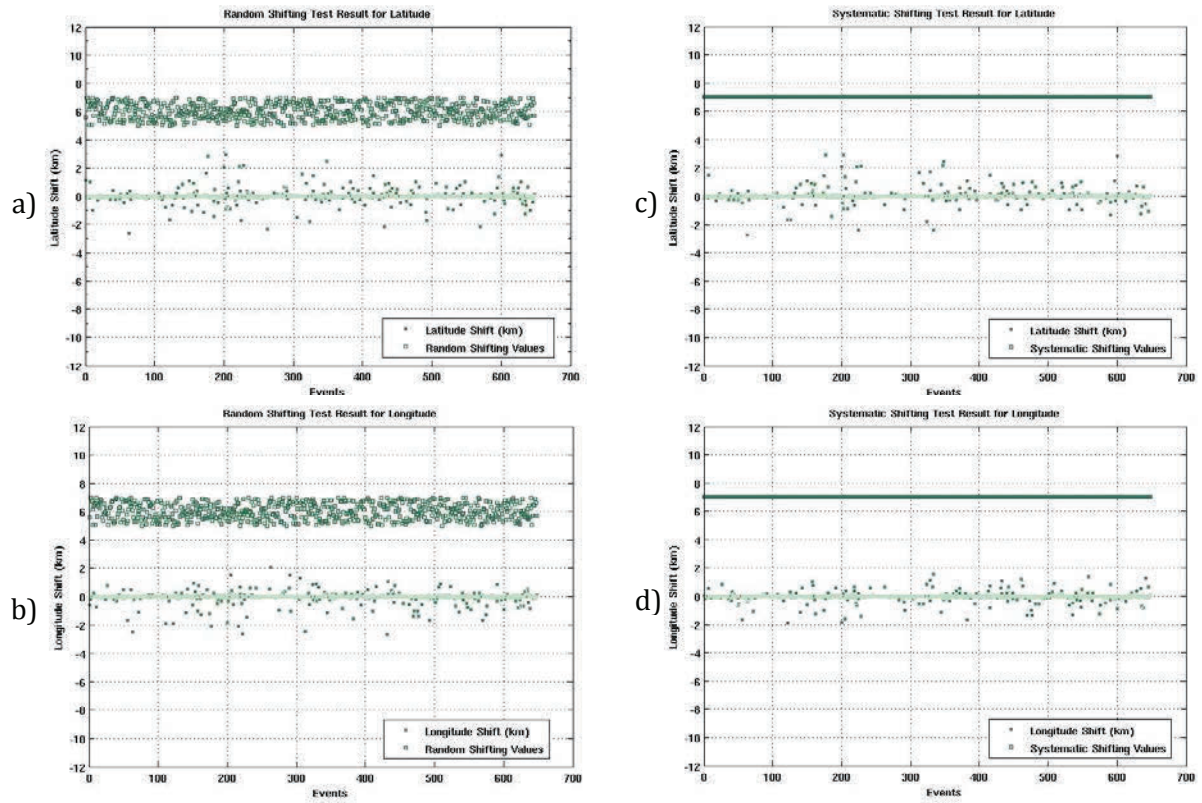
Figure 4. 9. 1D minimum model shifting test

Figure 4.11-a and Figure 4.11-b. show the random shifting test results for latitude and longitude, respectively. Figure 4.11-c and Figure 4.11-d show the systematic shifting test results for latitude and longitude, respectively.

5. 3D MODELLING

5.1 Introduction

Although we already have a priori velocity information belonging to different parts of the study area, we have chosen to use the 1D minimum model that we developed. Another 1D model that was derived by the use of only land stations surrounding Marmara region (Gürbüz *et al.,* 2000). What makes this study different from other tomography studies in the region is that we joined the data from a dense network in sea and land stations covering the land. Here our aim is to create a model which would represent both the land and sea. Due to the low sedimentary velocities in the sub-basins of Marmara Sea which makes a sudden contrast with the basin rims and land, a 1D model is insufficient. So as to understand how satisfying a 1D model, in the case of an inversion for a 3D model, we made an inversion with 1D minimum model. After deciding the model is not well enough to represent the area, we made an approach. The aim of this approach is to find the a 1D model for the area that is extracted from a 3D model which is not completely represent the area but at least a similar model of the real structure except its incapability. The details about this new approach will be presented in the next part. All the inversions to understand how to choose an initial model was made with the small data set.

5.2 Choosing an Initial Model (1D or 3D), Why It Is So Important?

The initial model has a considerable weight at the final 3D model, especially in the case of Marmara region where strong horizontal velocity contrast is dominated in a large part of the study area. After making an inversion with the 1D minimum model, we saw that certain parts of the inversion result show erroneous velocities. Thanks to the previous studies and the geology in the region, we had an expectation of a final model in the sea. These unrealistic parts of the result appeared especially on the border of Prince Islands with 7-7.5 km/s at 4 km and with the high velocities than expected at Kumburgaz Basin. However, most of the model is similar to what we expected. The insufficiency of the model is the cause of incapability of inverting the very low velocities in the basins. This

result made us to find a more realistic 1D model and convert it to a realistic 3D initial model.

5.3   Optimum Value for Damping

Damping is an important parameter by which the data residuals and the model perturbations are weighed. The damping value strongly depends on the spacing of nodes and the number of the data (Eberhart-Phillips, 1993). The optimum damping could be obtained by running a series of single-iterations inversion with different damping values. The plot of data misfit versus the model variance is generally is a trade-off curve, minimum of which corresponds to the optimum damping value. With the optimum damping value, the increase of the model variance is justified by the data fit. A wrong choice of a damping value might result in artifacts in the model.

5.4   Deciding the Iteration Number and the Maximum Allowed P Wave Perturbation

The iteration number is important because of its effect on the resulting velocity model. As we see on the damping curves of test runs most of the velocity change appears after the very first iterations. Rest of the iterations has a little influence on the final model compared to first ones. Simulps has a subroutine called f-test which controls the termination point (Thurber, 1981, 1983). In order to understand how many iterations is ideal for a final model, we made 20 iterations. Where the curve of data variance versus model variance reaches a minimum can be accepted as the ideal iteration number.

Another important parameter is maximum allowed P wave perturbation. In the present study area there is strong horizontal velocity contrast in the sub-basins of Marmara Sea. The maximum allowed velocity perturbation was chosen by making several runs and observing the data variance.
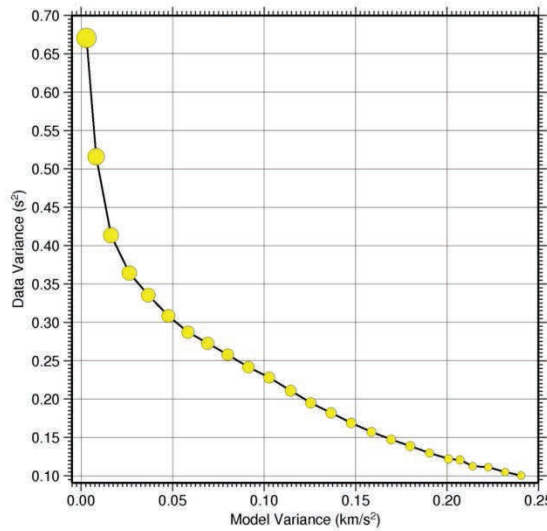
Figure 5. 1 Data Variance Reduction
with damping 0.1 km/s
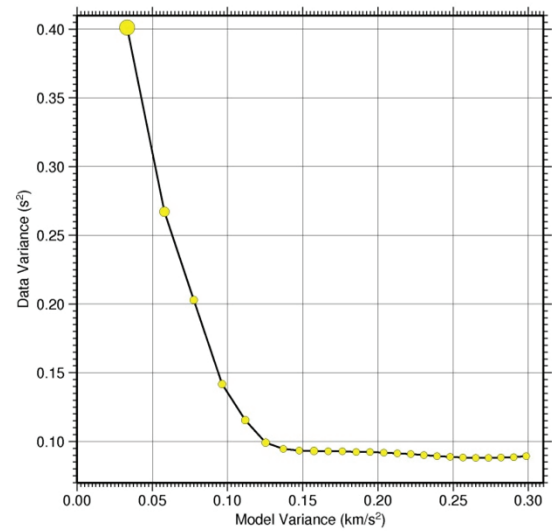
Figure 5. 2 . Data Variance Reduction
with damping 1 km/s
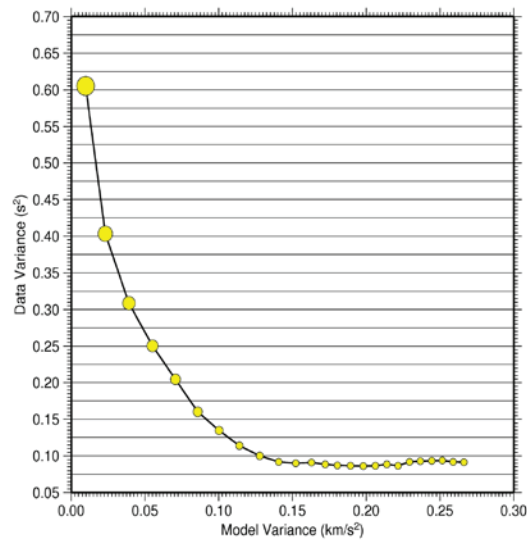
Figure 5. 3 Data Variance
Reduction with damping 0.25 km/s

In Figure 5.1, (yellow circles correspond to the RMS) with 0.1km/s P wave perturbation the model cannot reach to a minimum. The other test done with 1 km/s (Figure 5.2) P wave perturbation reaches to a minimum model very quickly. This indicates, an inversion with 1km/s perturbation would result in the first iterations unrealistic model so the final model would contain unrealistic velocities. Different than other tests, in Figure

5.3, the data variance reduction curve reaches a minimum. Although the idea of reaching the low velocities in the sub-basins of Marmara Sea would be possible with a high perturbation, it would also disturb a realistic final model. Rather than reaching a minimum model with less iterations or lots of iterations, we have chosen 0.25 km/s so as to reach a realistic model with ideal iteration number which would both invert the basins and the land at the same time. In Table 5.1, we see that the inversion needs at least 9 iterations.

Table 5.1. 0.25 maximum allowed P wave perturbation 9*9 model.

Iteration number	Data Variance (s²)	% Change Between Iteration Steps	% Change in Total
0	1.077076		
1	0.605139	43.816	43.816
2	0.403559	33.3114	56.2633
3	0.308702	23.5051	66.5437
4	0.250083	18.9889	72.8967
5	0.204320	18.2991	77.8563
6	0.160493	21.4502	82.6062
7	0.134569	16.1527	85.4158
8	0.113966	15.3104	87.6487
9	0.100013	12.2431	89.1609
10	0.092023	7.9889	90.0268
11	0.089958	2.244	90.2506

5.5 TOMOGRAPHIC RESULTS OF 1D MODEL

On Table 1, we showed, an inversion with 1D minimum model needs at least 9 iterations. We decided the maximum allowed P wave perturbation as 0.25 km/s (Figure 5.1). Another parameter that affects the solution, the damping is obtained by making a series of trial single-iteration inversions with varying damping. The corresponding damping value can be found on the damping curve as 95 (Figure 5.4).
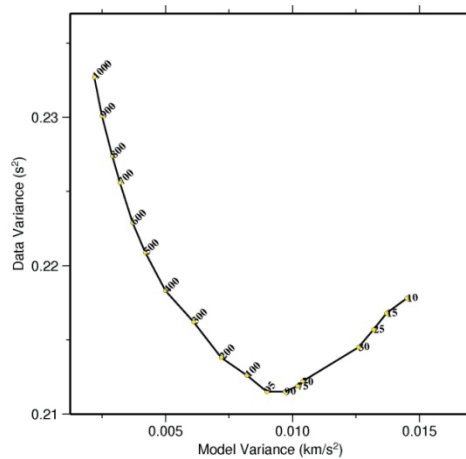
Figure 5. 4. The damping curve for 9*9
grid, 1D minimum model

At the 0 km the basin area satisfies our water velocity expectation. However, near Küçükçekmece and Büyükçekmece we see a high velocity area which is not realistic. At 2 km the 7-7,5 km/s velocities appear near the same area at 0 km. This unrealistic high velocity expands to the Prince Islands at 4 km depth. We see at 8-10 km another high velocity appearance around Çanakkale and at 8-10-14 km near the north of the Marmara Island expanding downwards to the north of the Kapıdağ Peninsula. These high velocities could be related to the Ganos High. The land area of the model seems more realistic than the sea velocities in the sea. Except the basin rims and the shallow basin of Marmara Sea, Kumurgaz Basin. With the purpose of estimating a completely realistic model than the inversion result of 1D minimum model, we extracted six 1D models from the 3D results and decided which one inverted the whole medium best.
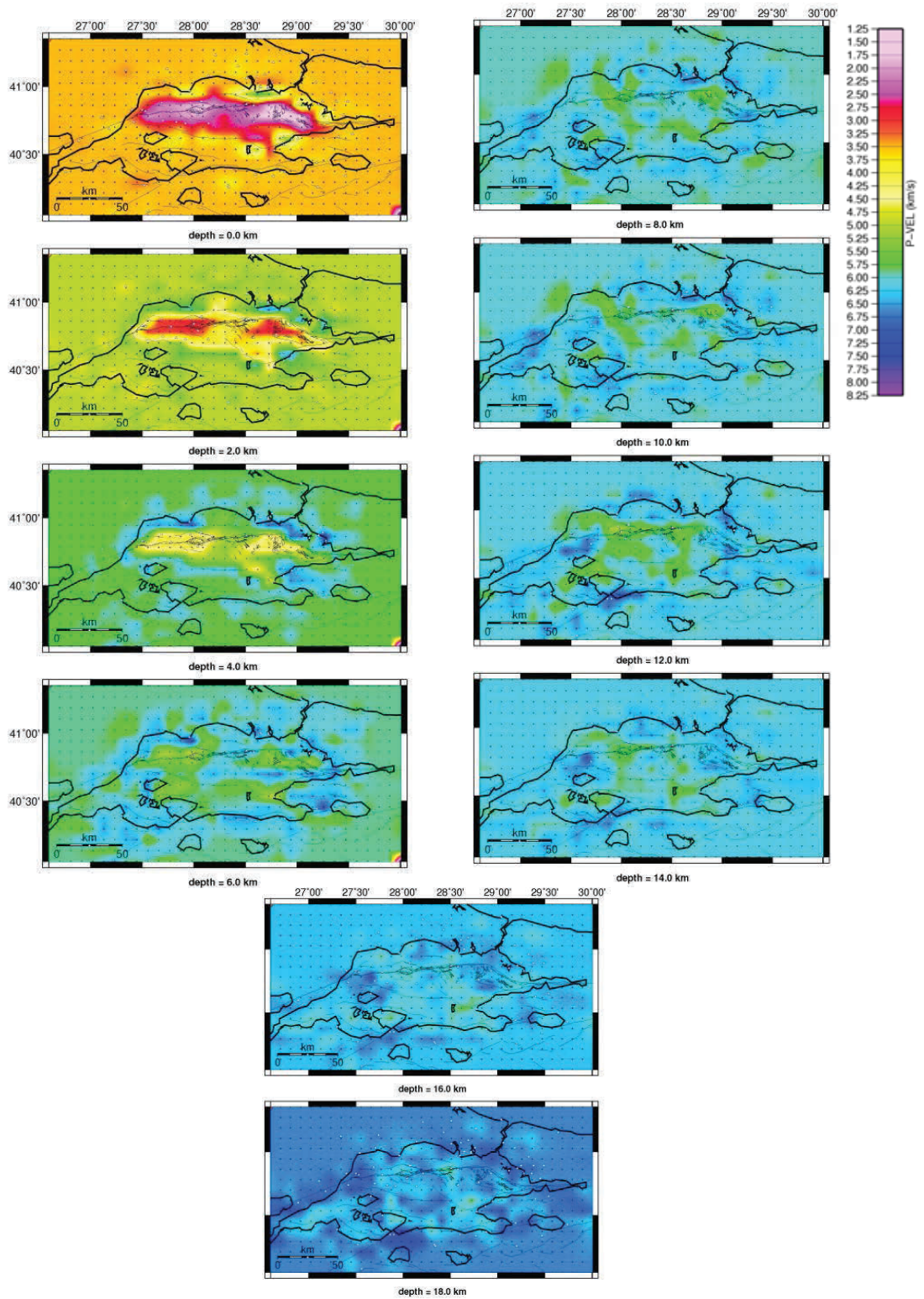
Figure 5. 5. 9 iteration inversion with a damping of 95.

5.6 Deciding Initial Model

5.6.1   Two Different Grid

A coarse grid was tested in order to make sure that the grid we chose is dense enough to show the details of the model. The simplest way to understand how the rays cover the medium is to make a checkerboard test. After making two different checkerboard tests, we made a run with obtained damping of 200 (See Figure 5.6) and plotted the priory and posteriori residuals before and after inversion.
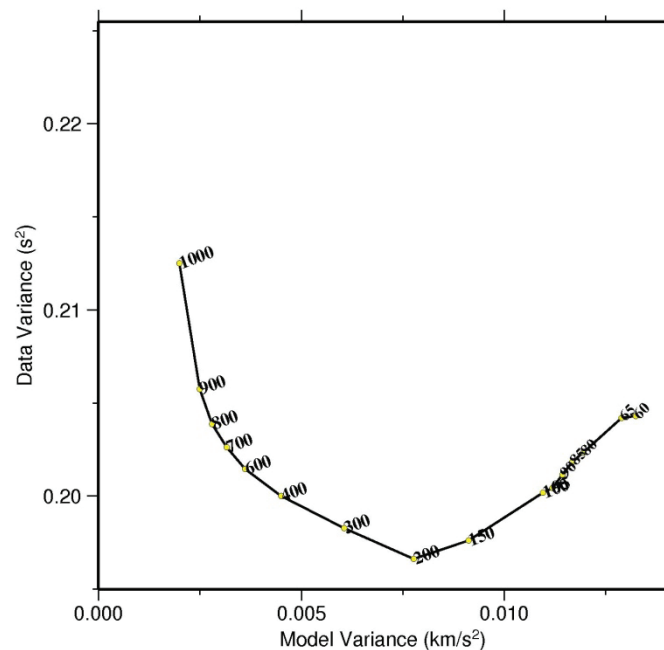
Figure 5. 6. The damping curve for 15*15 grid size

The first checkerboard pattern was designed to test how the initial 15*15 grid would retrieve itself if it were injected a 30*30, ±20% perturbed model into all layers. (Figures 5.7 and 5.8). The second checkerboard pattern was designed to understand how much the layers would retrieve themselves if they were injected a 15*15 km model according to the expected average final perturbation of the real inversion until 6 km (Figure 5.9 and Figure 5.10).

The result of the first test shows a very rough idea of the ray coverage. According to the result the ray coverage continues until 24 km, which is not what we expect because most of the rays in the small data set are received directly from upper crust. So the result is not realistic.

The second test was designed more realistically as a 15*15 grid. What makes this test different from the previous one is that it includes the effect of the deep sedimentary basin infill that would supposed to have a large perturbation compared to land area. We injected ±30% perturbed model until 5 km. After 5 km we injected ±10% perturbed model. This dense more realistic checkerboard pattern gave a more reasonable result about how is the ray coverage. Because the first 5 km was perturbed ±30%, only the sea area retrieved itself. The land showed very little change because the 30% perturbation was very high for land. Until 16 km we see a nice coverage on the borders of land area. After 16 km we see that the model has difficulty to retrieve itself. After 12 km there is no good resolution on land.

According to the test results we should keep in mind that the size of the real grid and the injected grid has a significant importance when making a resolution estimate. An unrealistic checkerboard pattern would affect the ray paths so that the distribution of them would be wrong. In order to prevent this confusion we added also a Gaussian noise which makes the injected checkerboard pattern more realistic.
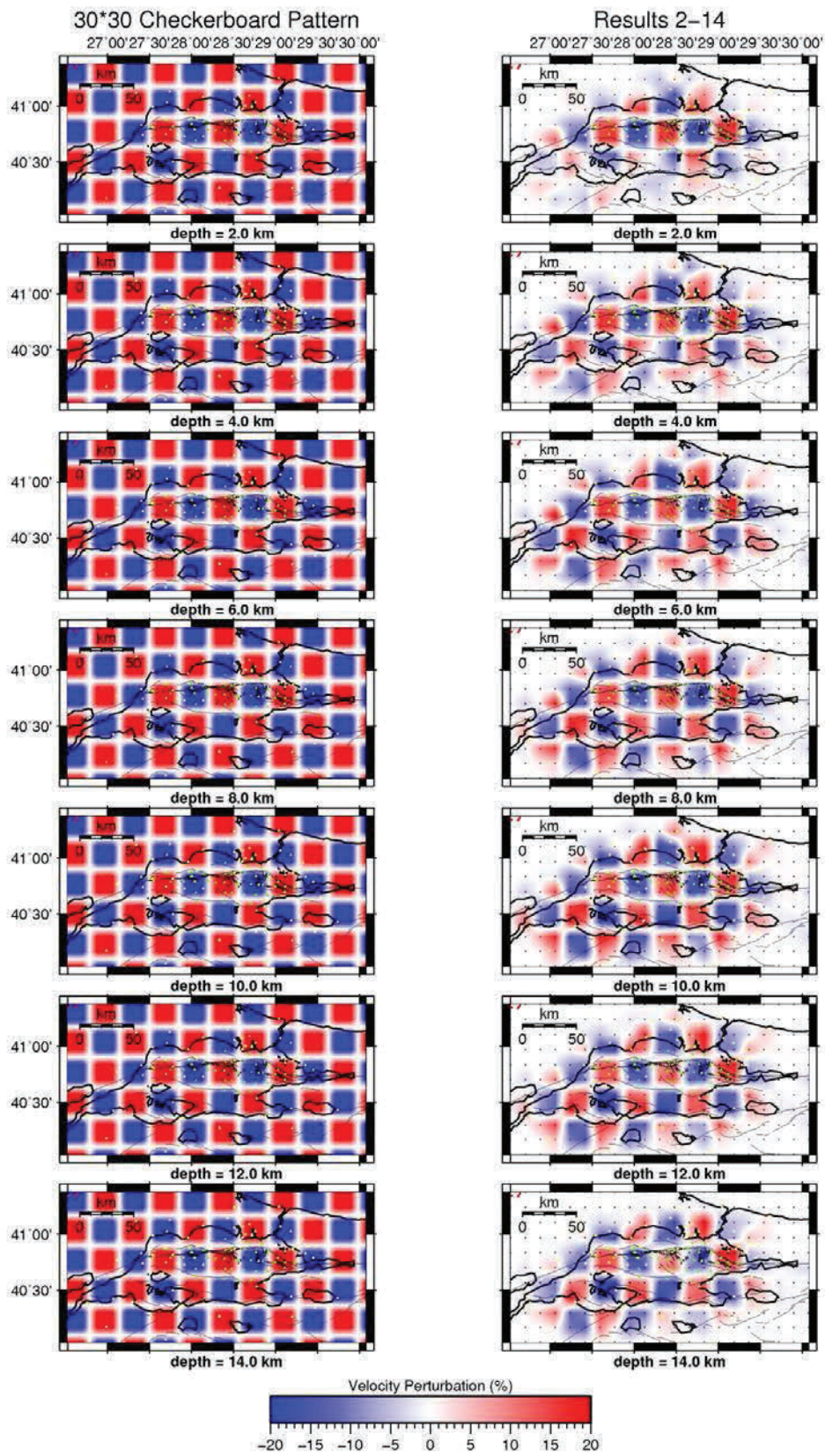
Figure 5. 7. Systematic Checkerboard Pattern (±20%) between 2 and14 km
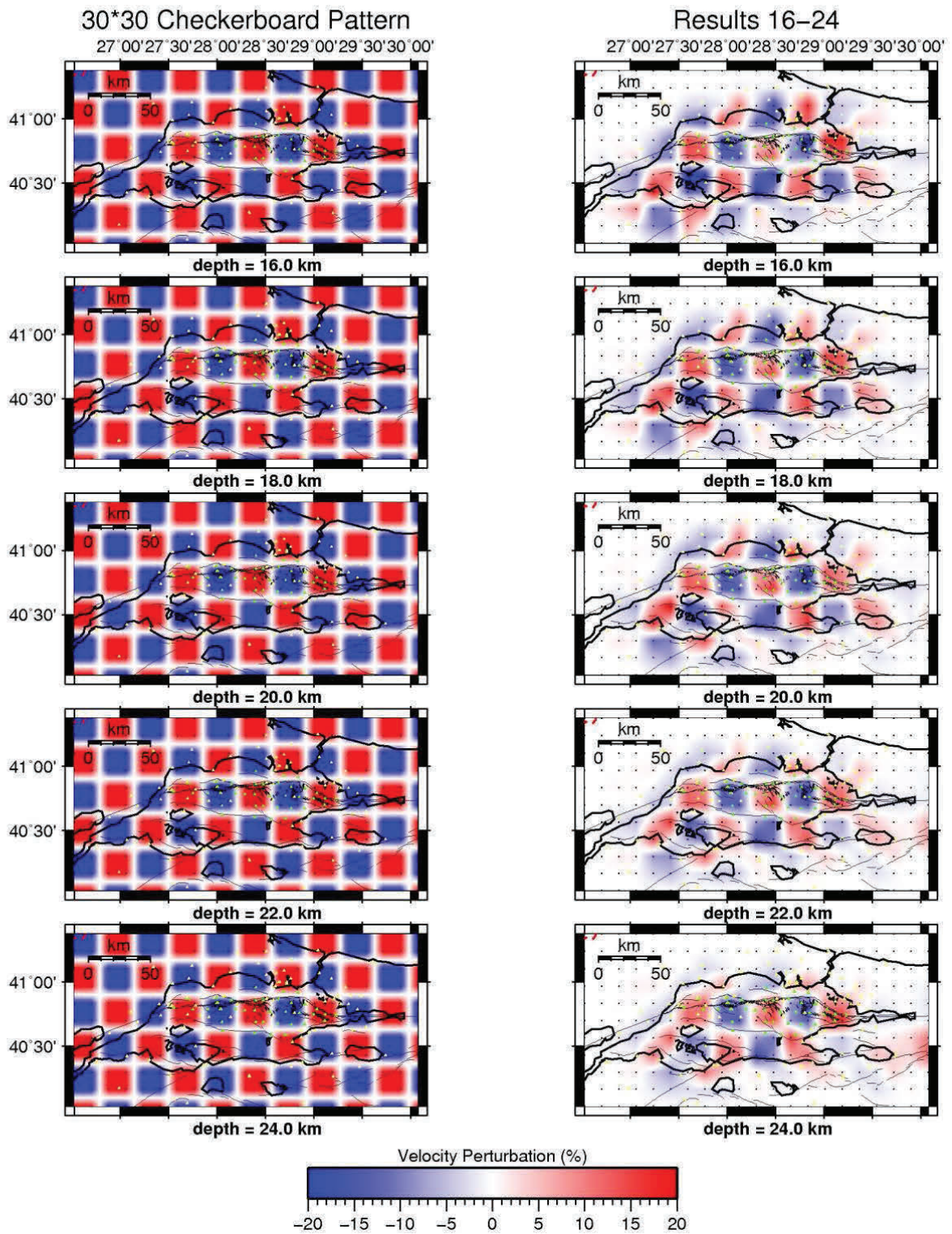
Figure 5. 8. Systematic Checkerboard Pattern (±20%) 16-24 km
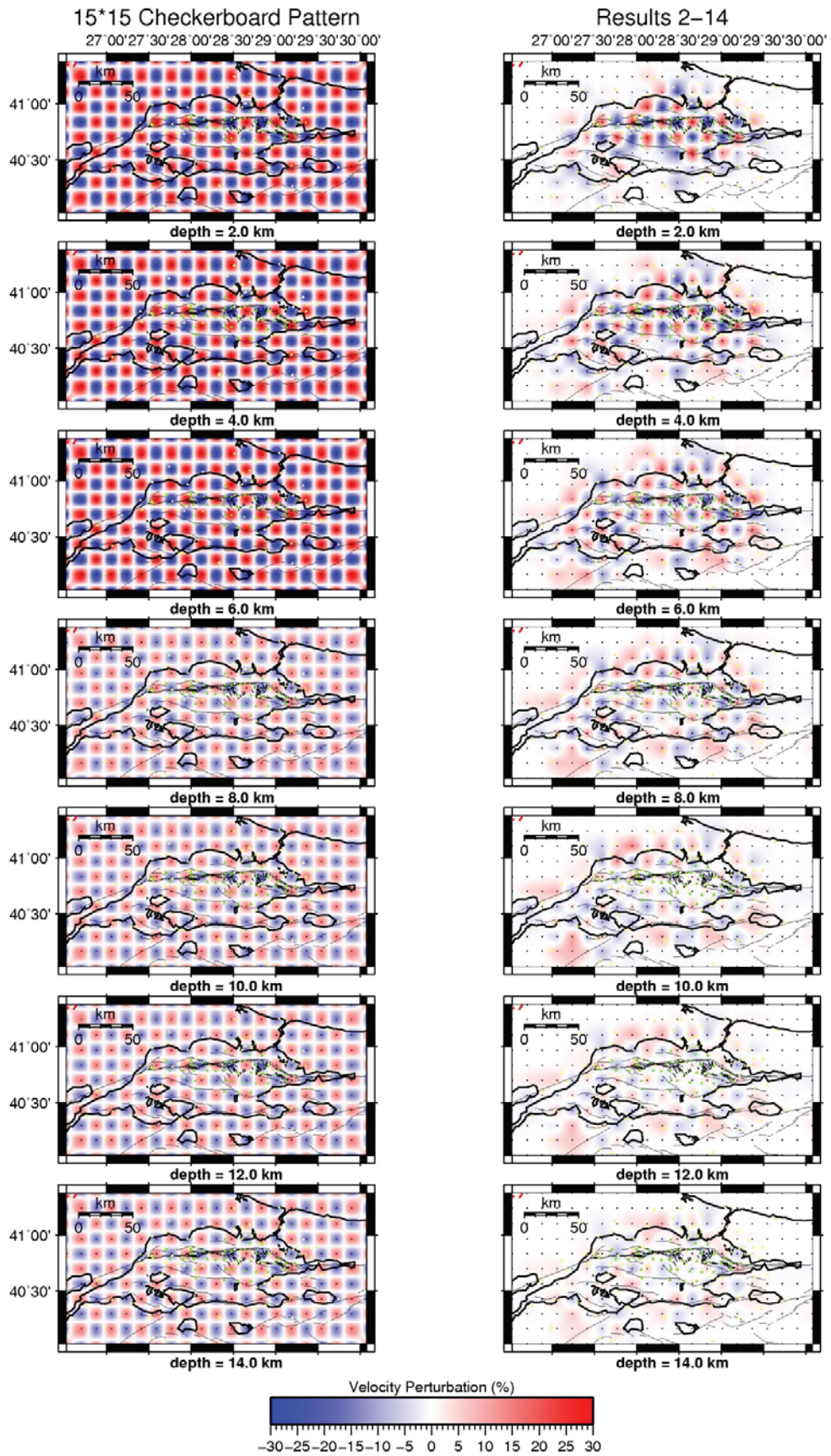
Figure 5. 9 Random checkerboard pattern (Until 5 km ± 30%, After 5 km ±10%) between 2 and 14 km

15*15 Checkerboard Pattern

27˚00'27˚30'28˚00'28˚30'29˚00'29˚30'30˚00'

Results 16–24

27˚00'27˚30'28˚00'28˚30'29˚00'29˚30'30˚00'

depth = 16.0 km

depth = 16.0 km

depth = 18.0 km

depth = 18.0 km

depth = 20.0 km

depth = 20.0 km

depth = 22.0 km

depth = 22.0 km

depth = 24.0 km

depth = 24.0 km

Velocity Perturbation (%)

−30 −25 −20 −15 −10 −5 0 5 10 15 20 25 30
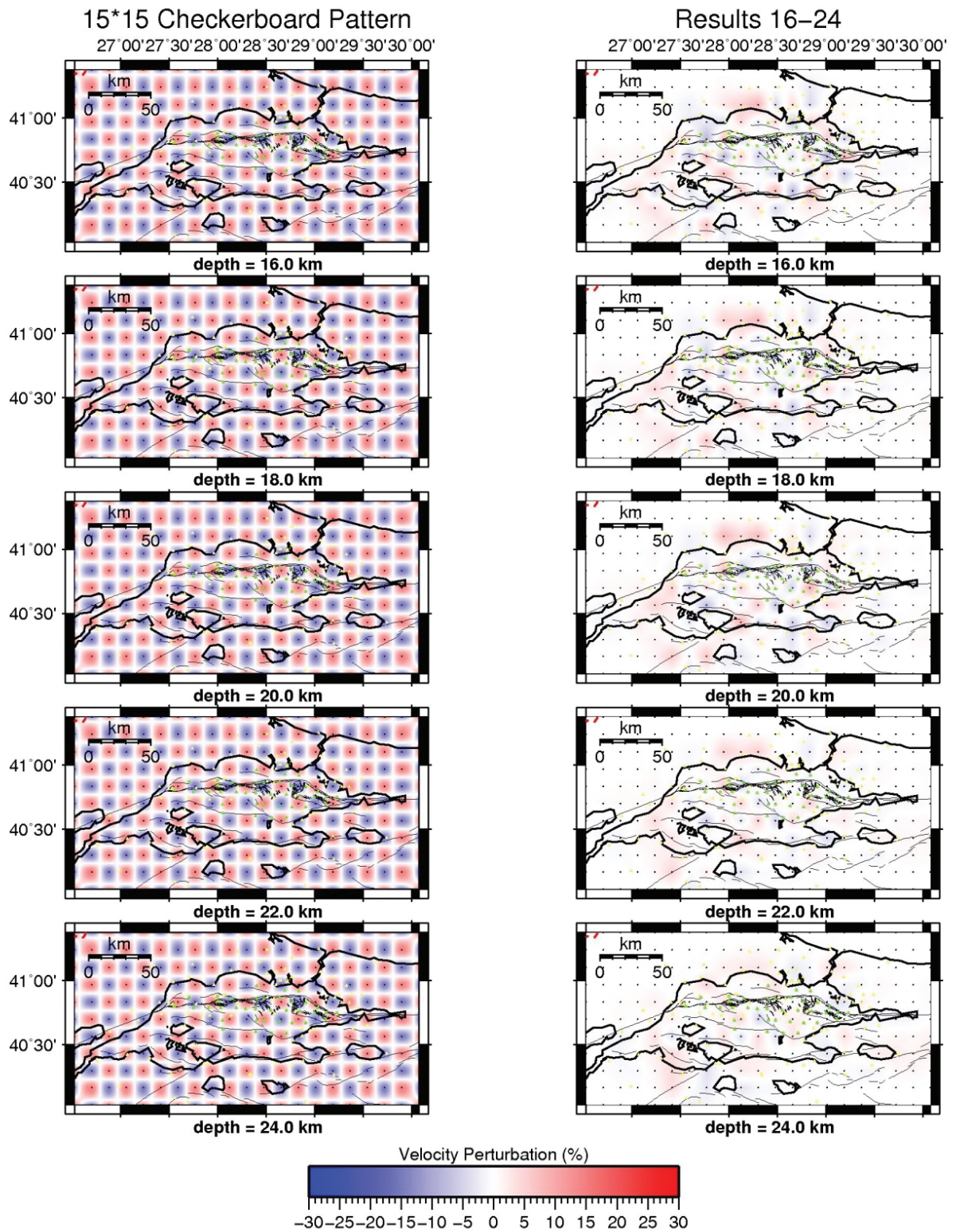
Figure 5. 10 Random checkerboard pattern (Until 5 km ± 30%, After 5 km ±10%)
between16 km and 24 km.
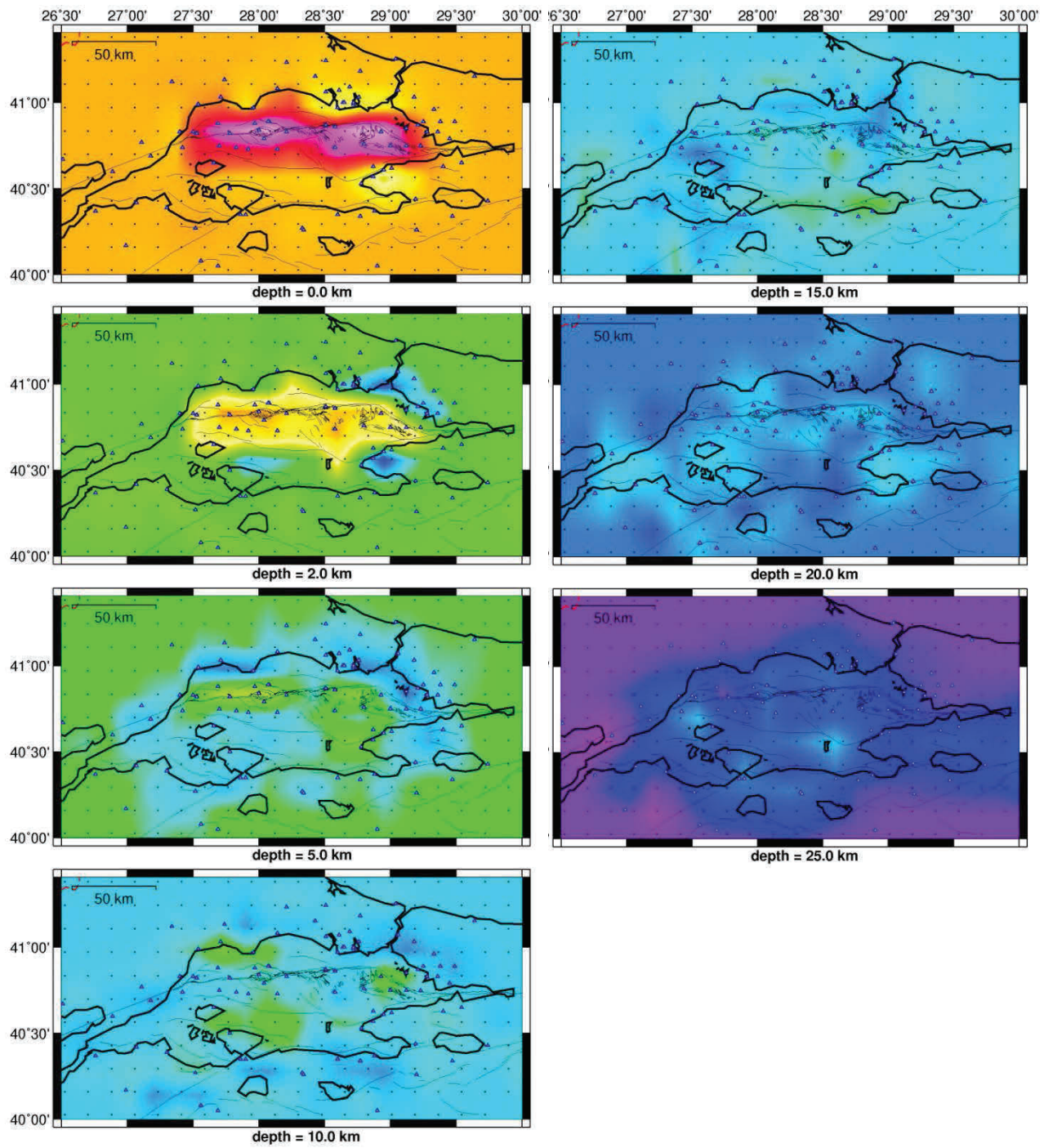
Figure 5. 11. The 3D tomographic result fo 15*15 grid with 1D initial model.

Figure 5.11 shows how much a coarse grid affects the result of the same data set. Although both the 9*9 gird and the 15*15 grid were used with the same data set, the results are quite different. The basin area is not inverted fully even though the resolution test showed the ray coverage is good here. The land area is not inverted properly which we understand from the previous result of the 9*9 inversion. Another disadvantage of a coarse grid is the vertical node interval. Because of the large width of the horizontal node internal according to the Simulps code we have to take the minimum vertical node interval as the $1/3^{rd}$ the horizontal node interval. In the case of a complex medium like the Marmara Region this would let an inversion with erroneous result of inversion.

The comparison of a priori and a posteriori residuals show that there is no remarkable and considerable change (Figure 5.12).
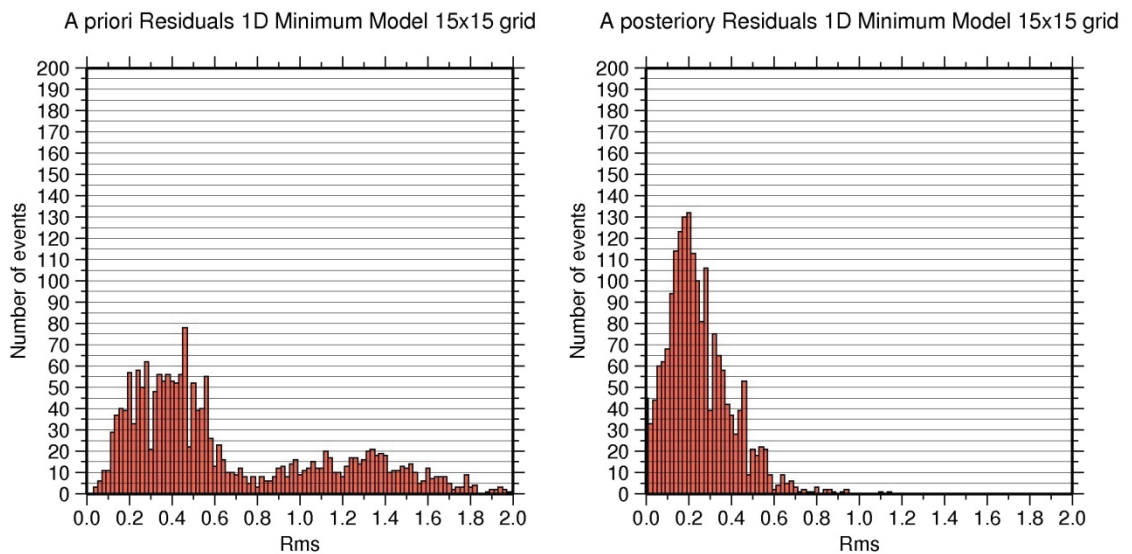
Figure 5. 12 The comparison of a priori and a posteriosi residuals of the inversion with 15*15 grid

5.7 Digging for a 1D Model That Could Represent Study Region the Best, Extracting 1D Models from Preliminary 3D Model

We have mentioned that a 1D initial model is not capable of inverting the whole medium properly. To estimate a more realistic 1D model we extracted 1D vertical cross section from the preliminary 3D model from the points which have velocities similar to what we expect when the geology and the previous studies considered.
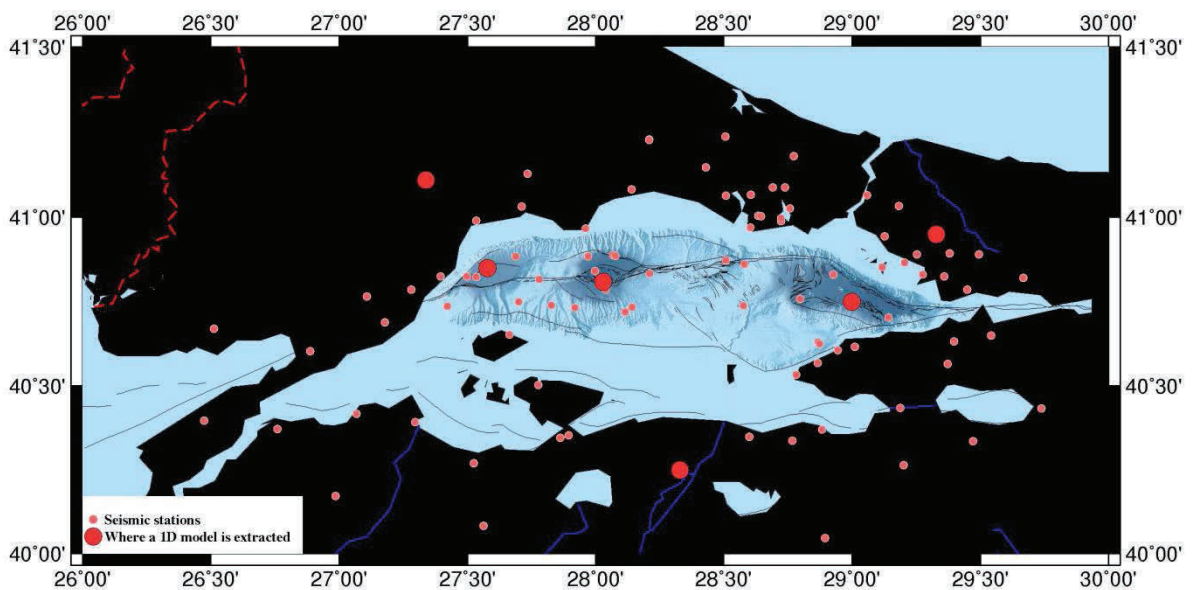
Figure 5. 13. Points where 1D models extracted from the preliminary 3D model.

These points were chosen according to the previous geologic information around them. Three of them were chosen where they represent the low velocity basin infill (from west to east, Tekirdağ Basin, Central Basin and Çınarcık Basin). The other three points were chosen from land. The northwestern point represents the Thrace Basin. It has a very similar 1D model to the 1D minimum model because of the event distribution was coarse in this area in the small data set. The second land point is the northeastern point which represents the İstanbul Zone. The last land point is the southern one which was chosen to represent the Sakarya Zone. The 1D models can be seen on Figure 5.14.
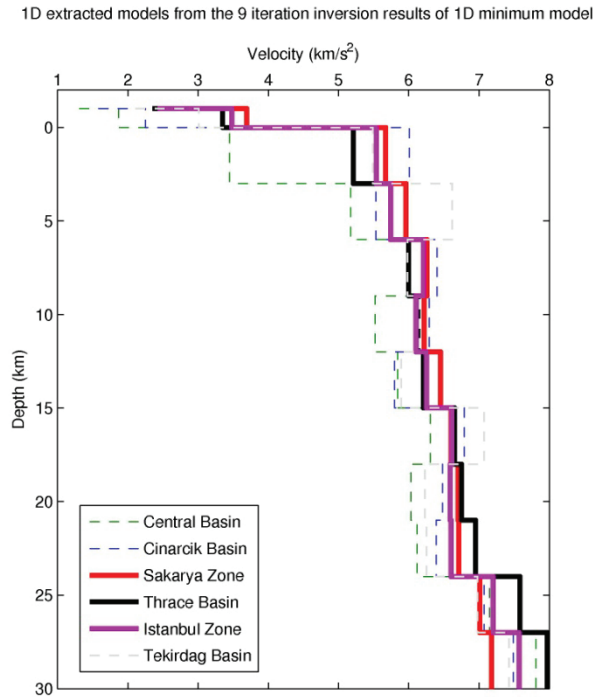
Figure 5. 24. Comparison of 1D models extracted from
preliminary 3D model (9 iteration-damping 95).

The 1D models extracted from the sea has low velocities than the 1D models
extracted from land and land models are similar while the sea models show differences. So
as to understand which one of these models has the best ability of inverting the study area
more realistic, we made 3D inversions for all of them.

5.8 Comparing the Result of 3D Inversion of 1D Extracted Models

We determined damping parameters for each of them and inverted them with ideal
iteration number (Figure 5.15). After mapping each of them and checking a priory and a
posteriori residuals we decided the best 1D model. The numerical test results for the
iteration number can be found in appendix A (Table A-1-6). The iteration number is
obtained as 7, 8 or 9 for inversions (Figure 5.13).
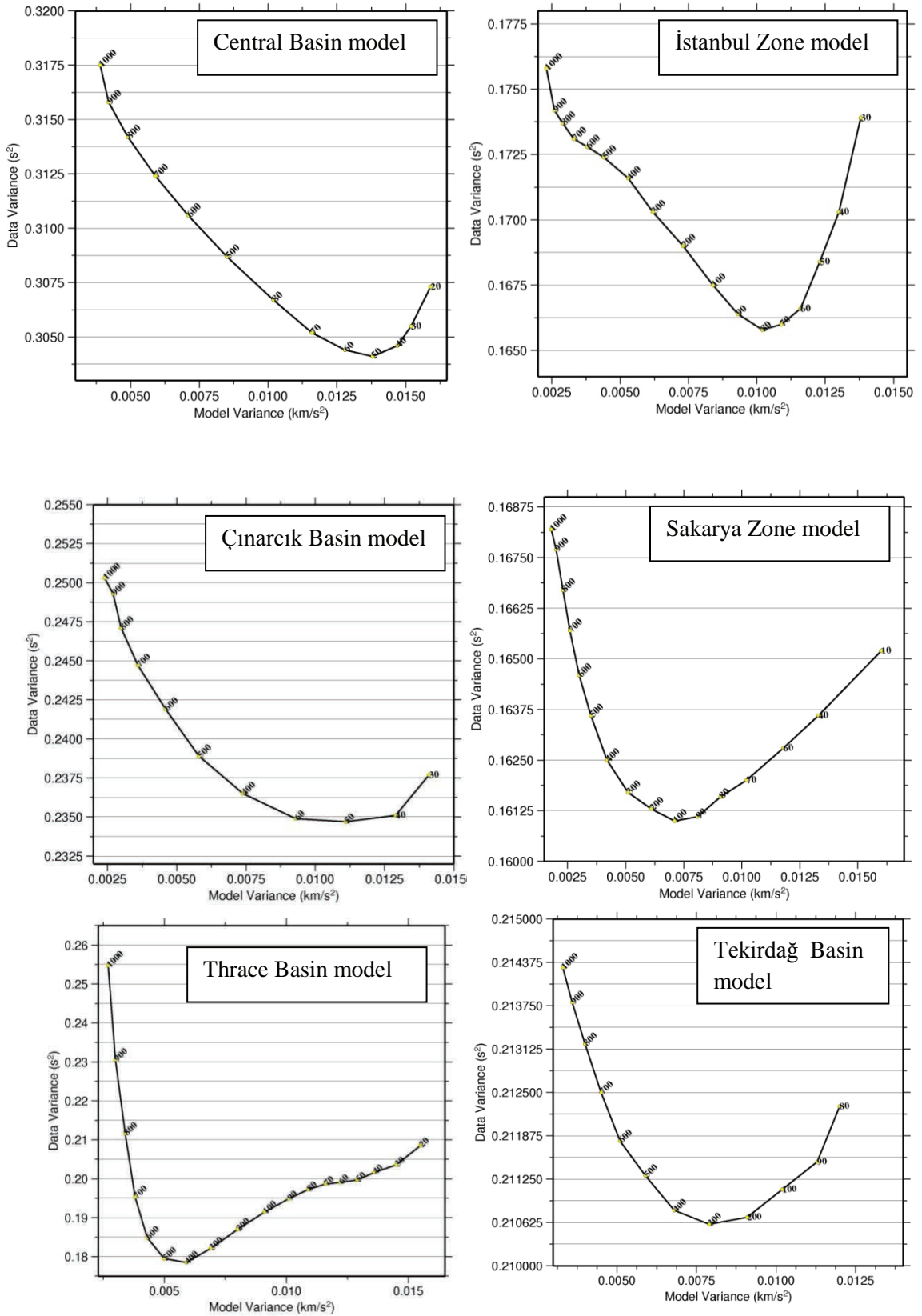
Figure 5. 35 . Damping curves of extracted 1D models.
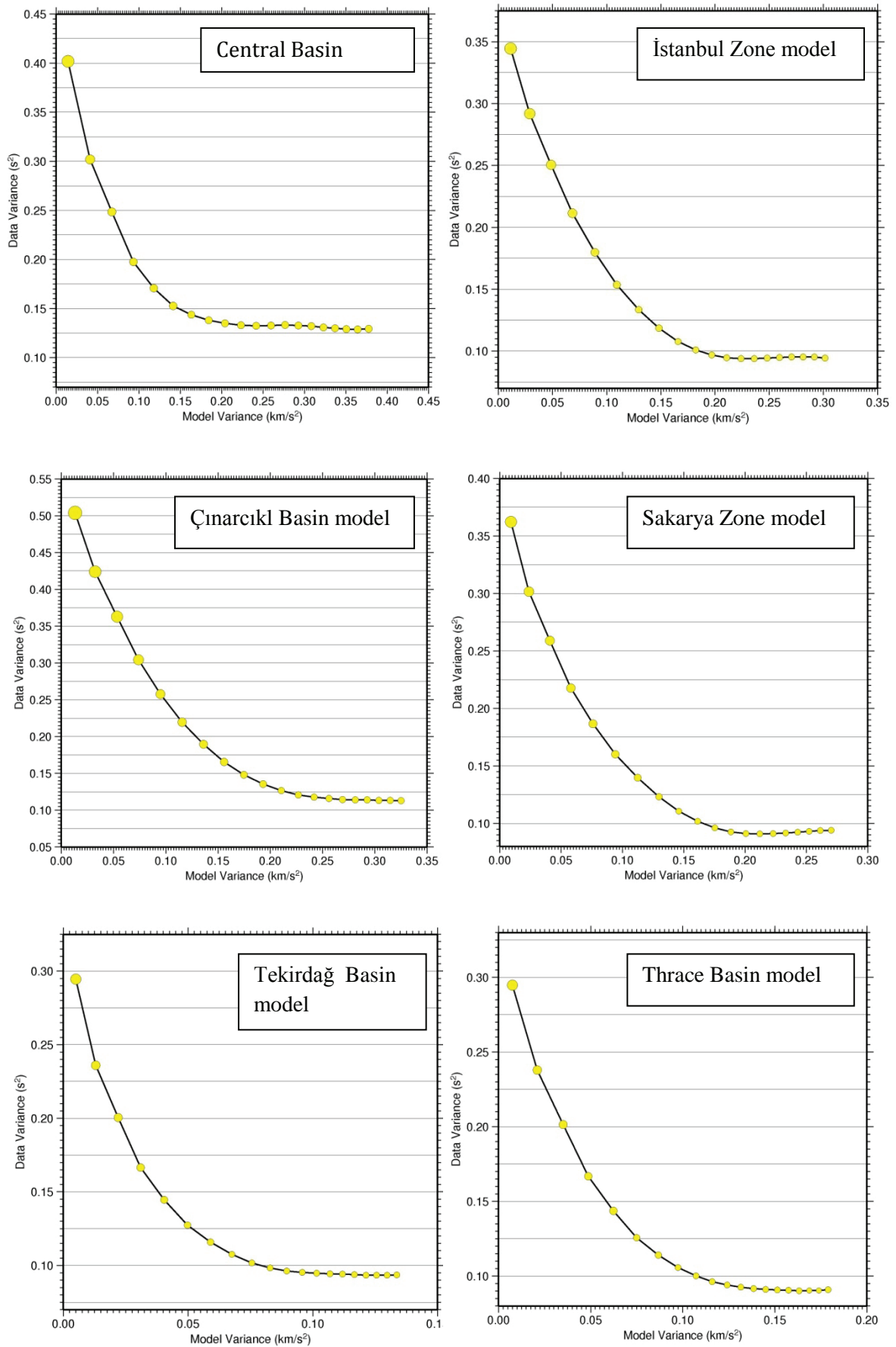
Figure 5. 46. Iteration number determination of the 1D extracted models.
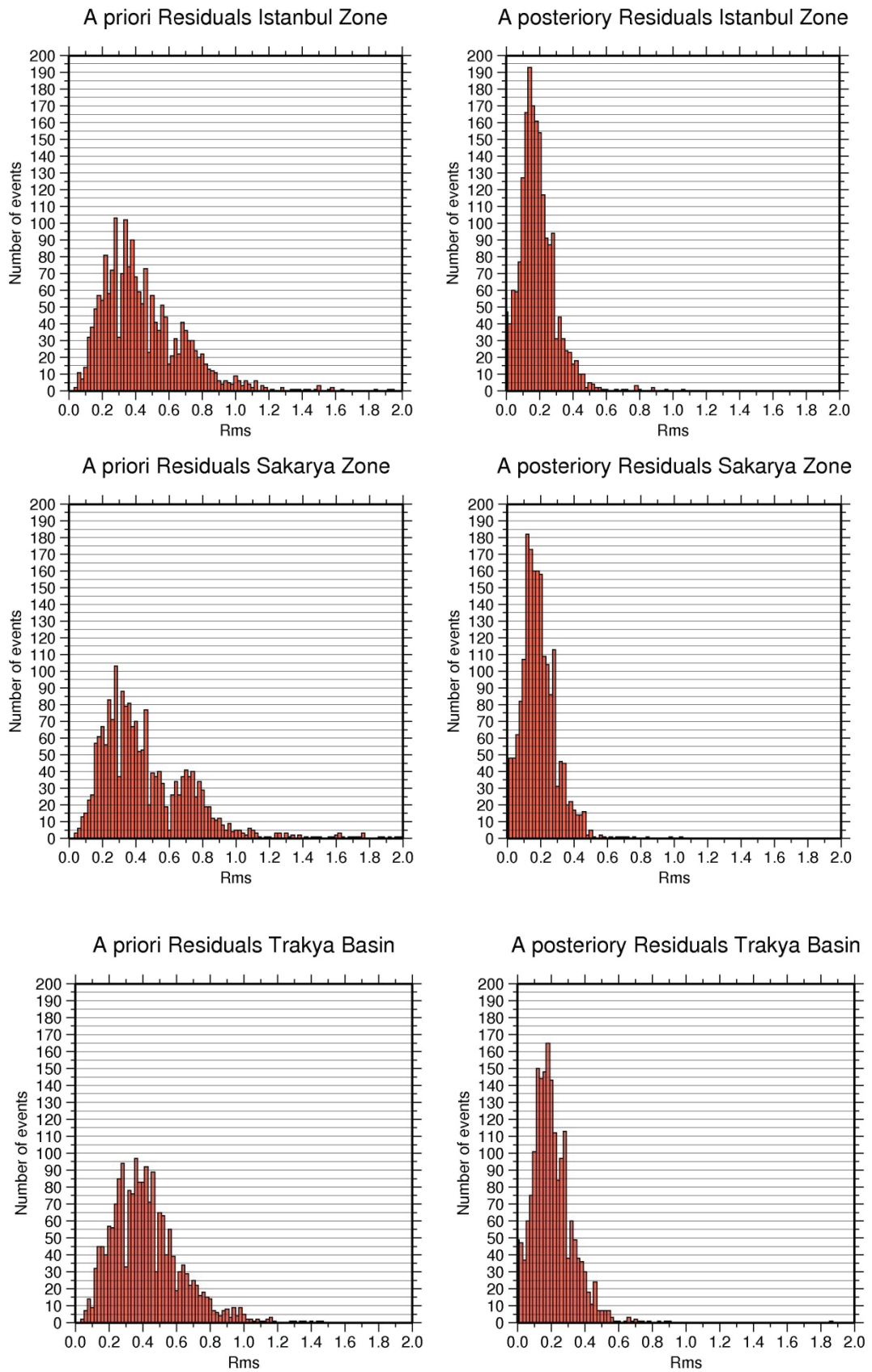
Figure 5. 17. Comparision of a priori and a posteriori residuals of 3D inversions of 1D extracted models (Land).
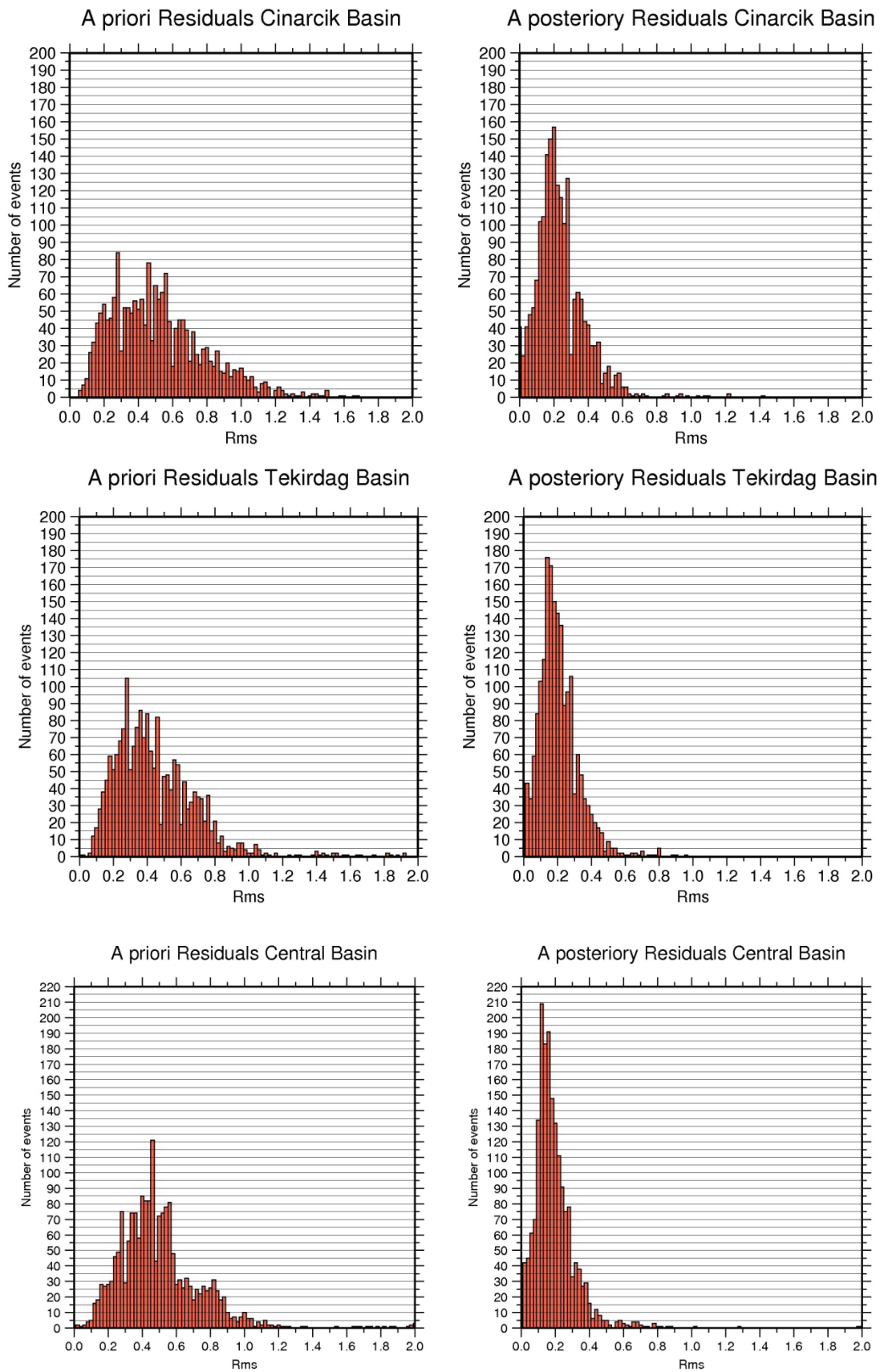
Figure 5. 58. Comparision of a priori and a posteriori residuals of 3D inversions of 1D extracted models (Sea).
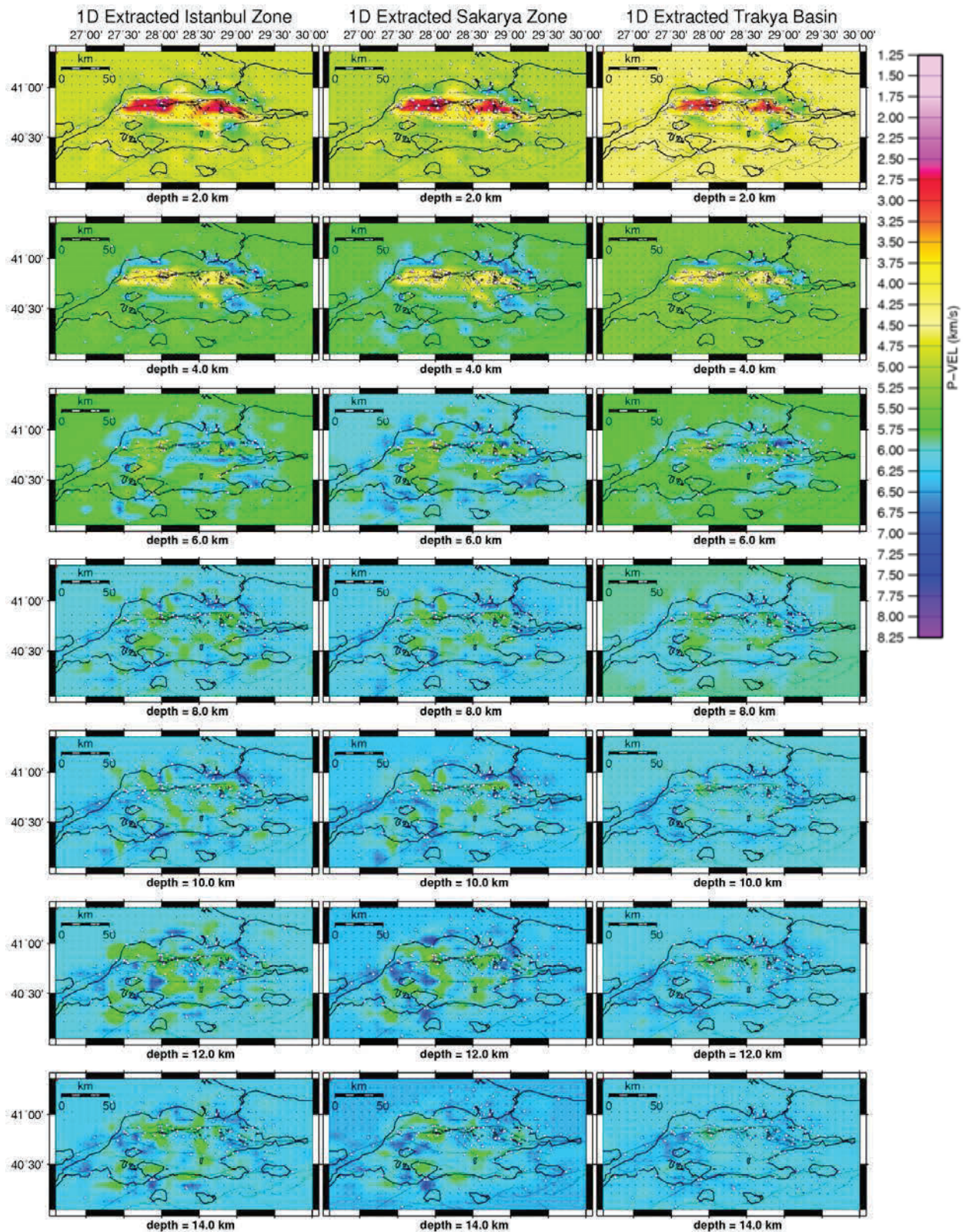
Figure 5. 19. Comparison of land inversion results of 1D extracted models.
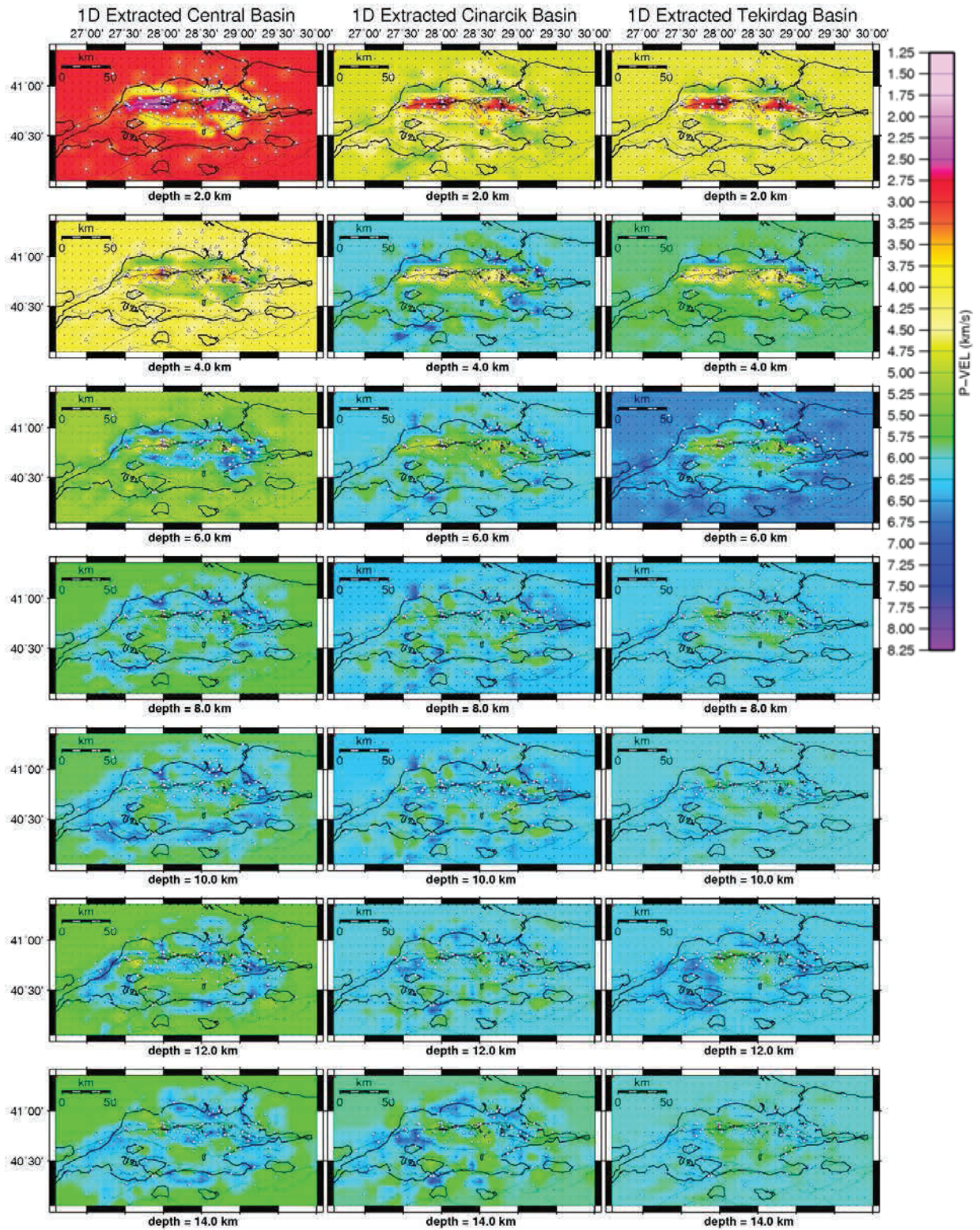
Figure 5.20. Comparison of sea inversion results of 1D extracted models.

After inverting the 6 1D models, the model that was extracted under Central Basin and the model extracted from the İstanbul Zone (station KURN) showed the maximum change. Although two models are completely different from each other the residual distribution showed similar improvement (Figure 5.18). However, the model under the Central Basin has very low velocities which are not acceptable for the deep layers. Because of this bias of this model we have chosen the Istanbul Zone model as the initial model for the real inversion and observed every second iteration result to understand how fast the model changes and at which iteration the model changes abruptly on certain parts of the model (Prince Island, Northwestern part of Marmara Sea). Figure 5.21 and Figure 5.22 show the change after every second iteration.
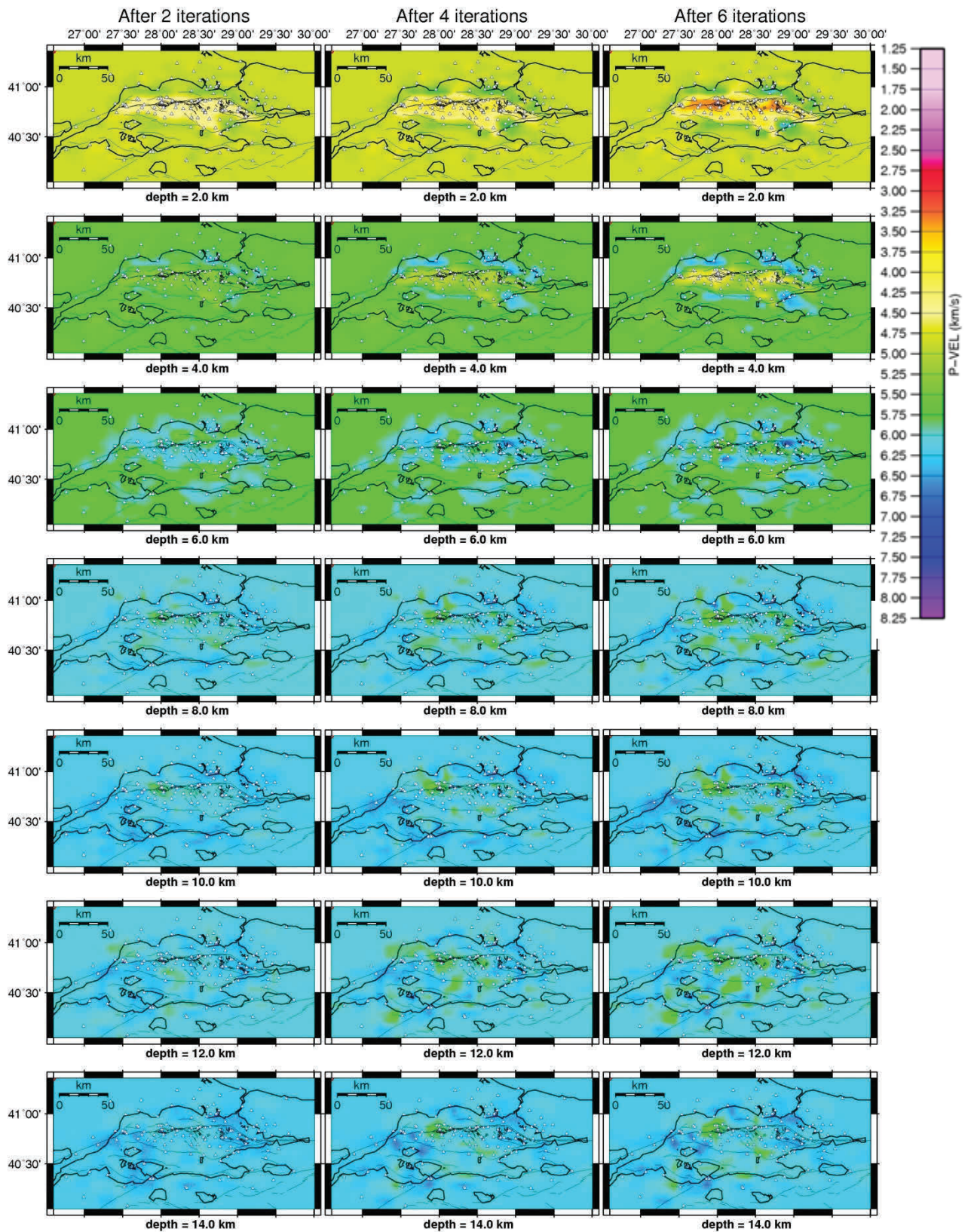
Figure 5. 21. The inversion results of the model extracted under KURN, representing İstanbul Zone- 2nd, 4th, 6th iterations.
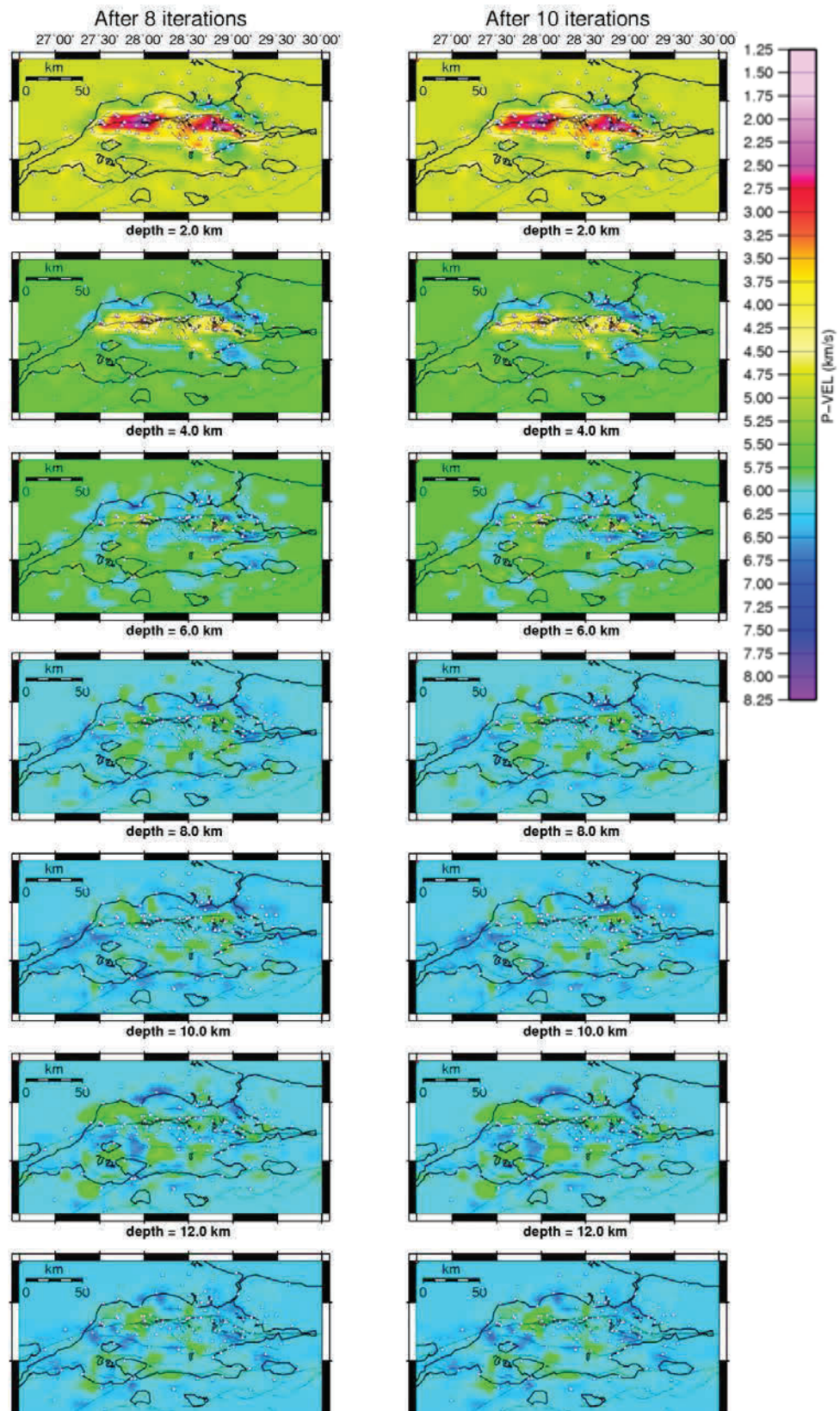
Figure 5. 22. The inversion results of the model extracted under KURN, representing İstanbul Zone- 8th, 10th iterations.

Although the basins inverted as expected after 8 iterations the velocities of basin rims and south of Prince Islands gets worse and appears as unrealistic velocities with 7-7.5 km/s.
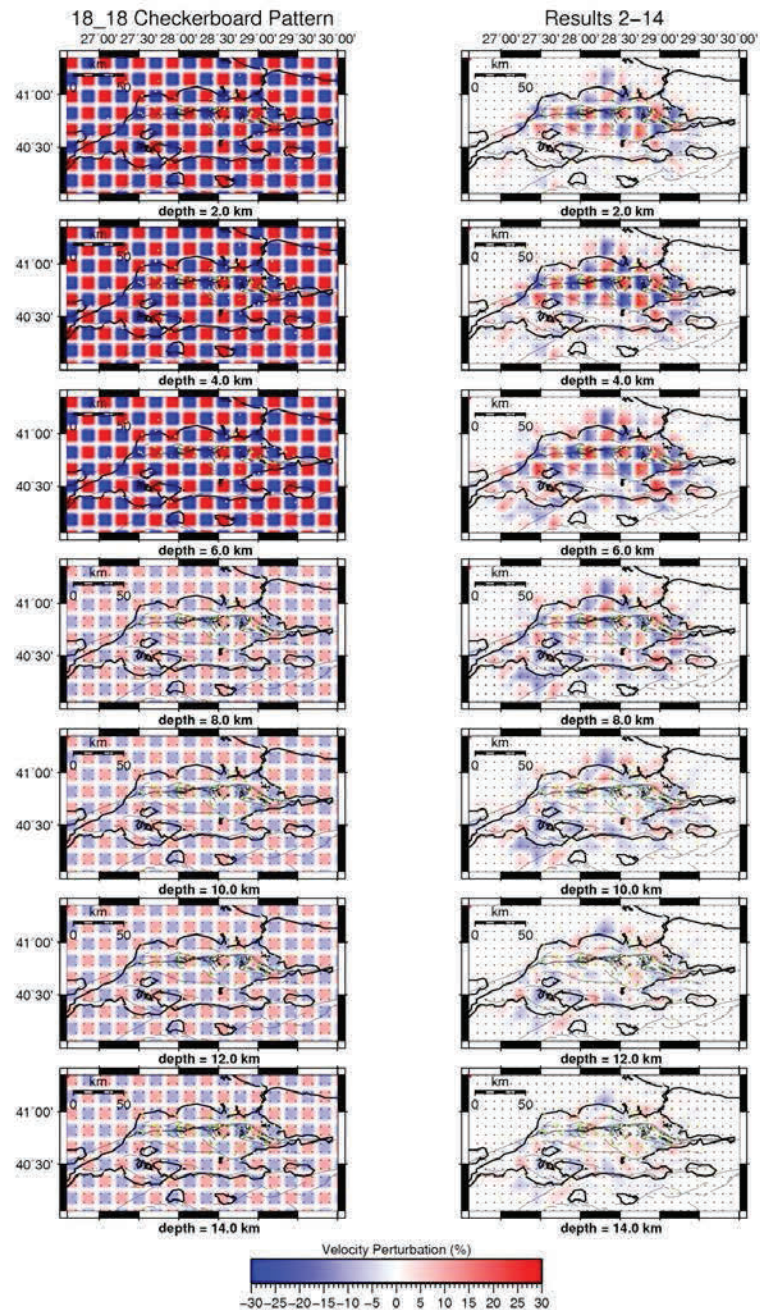
Figure 5. 236. Checkerboard test result of the Istanbul Zone Model (2-14 km).

,
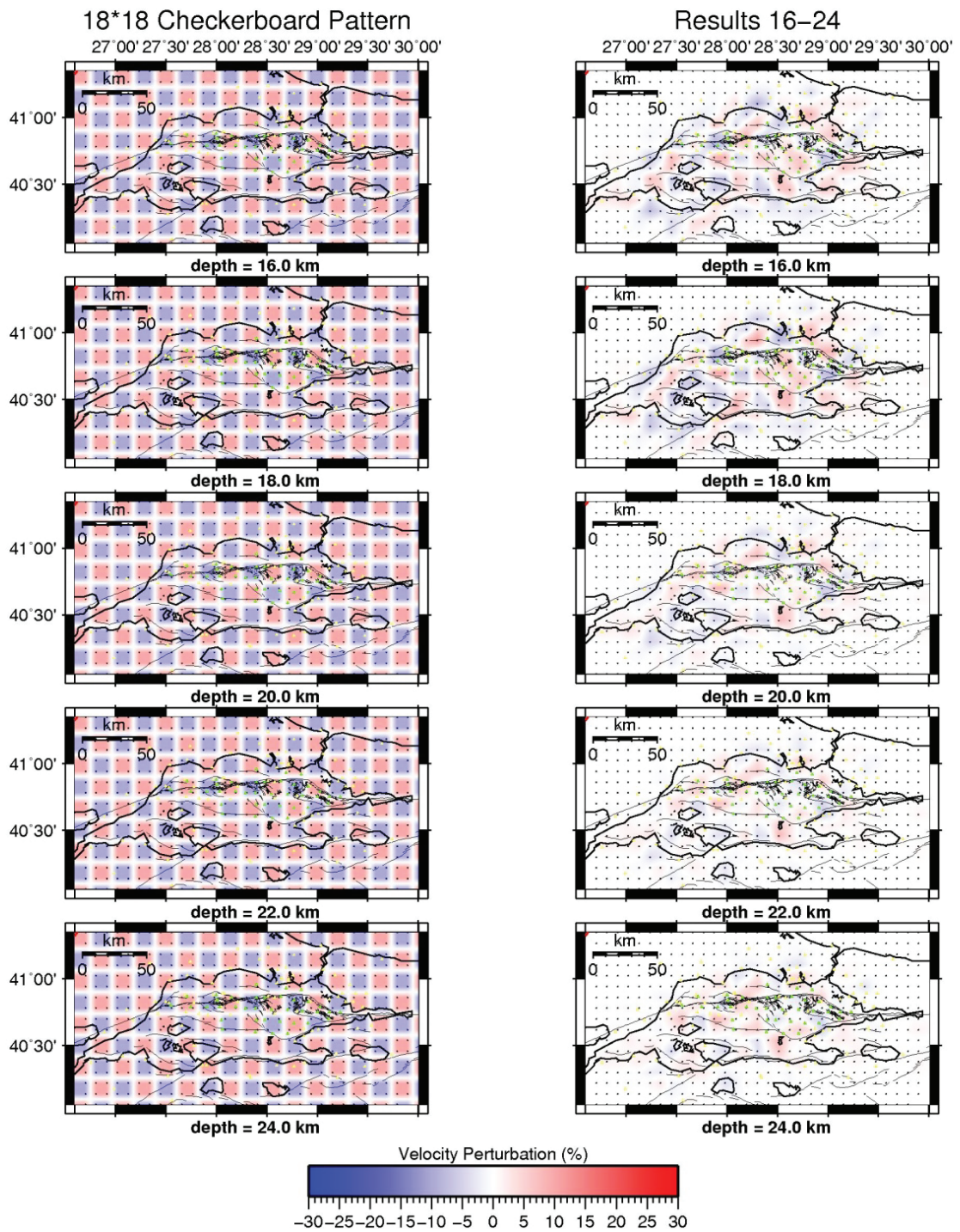
Figure 5. 24. Checkerboard test result of the İstanbul Zone Model (between 16 km and 24 km).

The checkerboard pattern was designed to include the effect of low velocity zones. The results (Figures 5.23 and 5.24) point the lack of ray coverage around the Marmara Sea (Land areas). It is not possible to see satisfying ray coverage after 10th km.

The final 3D model shows unrealistic velocities although it was chosen among 6 models to represent the medium best. After this inversion we decided that a pure 1D starting model would not answer to our expectations and we created 3 other 3D initial starting models by combining Istanbul Zone, Central Zone, and 1D minimum model. The details about combined models and their results will be presented in the next part.

5.8.1 Combining 1D Models

According to the 3D inversions of 6 1D models, the second best model is Central Basin model. It represents the basins best but still not proper enough to represent the land area. So, to test, we first created a model which has İstanbul Zone model at all depths but has Central Basin model under the basins until 6 km. The second combined model has the same velocities as in the Central Basin model until 6 km and the rest has the Istanbul Zone model. The aim to create these models here is to understand which part of the 1D model prevents a good inversion on the problematic areas. The first combined model includes low velocities only under the basin. The second combined model has low velocities until 6 km where we expect to see the end of the basin infill (Becel, 2006). After seeing that what makes the resulting model unrealistic at basin rims is that these zones have transitional velocities we decided to add intermediate velocities to these areas which is also suggested by Bayrakçı, (2009).
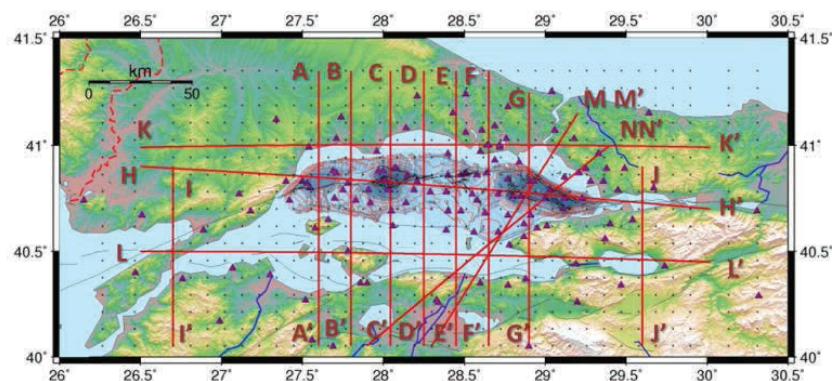
Figure 5. 25. Location of the cross sections
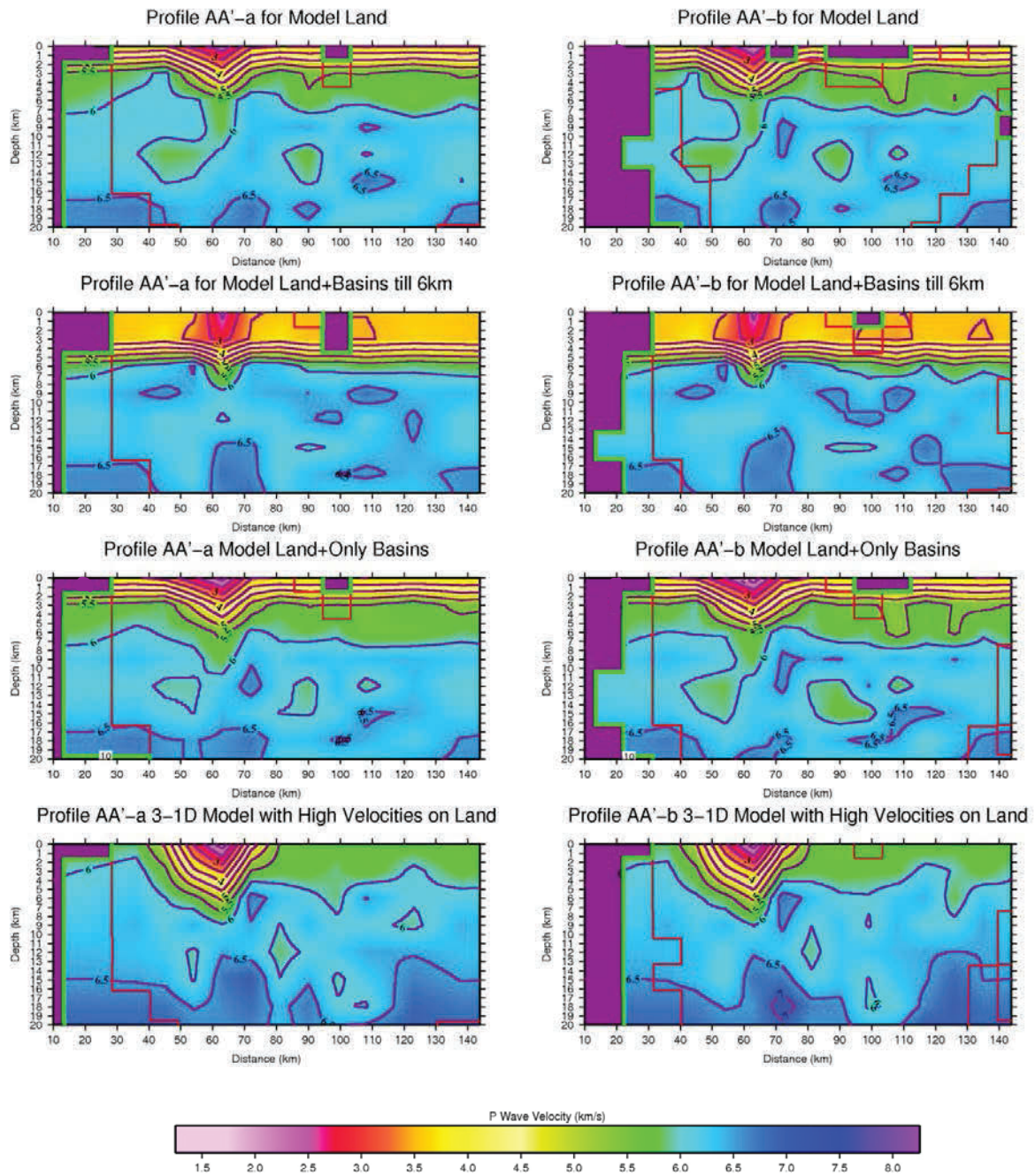
Figure 5. 7. The absolute P wave map of the cross section AA'.
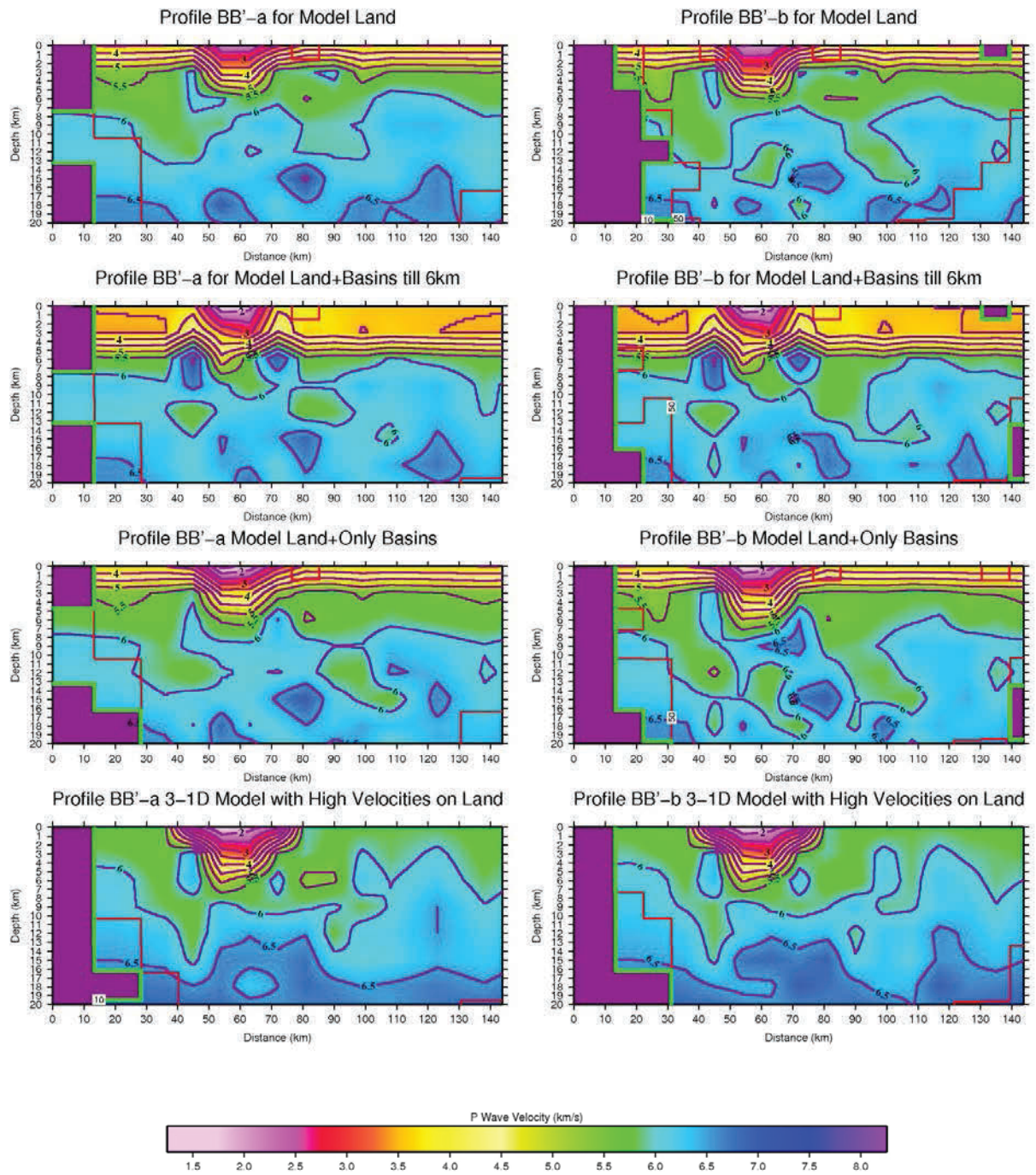
Figure 5. 8. The absolute P wave map of the cross section BB'.
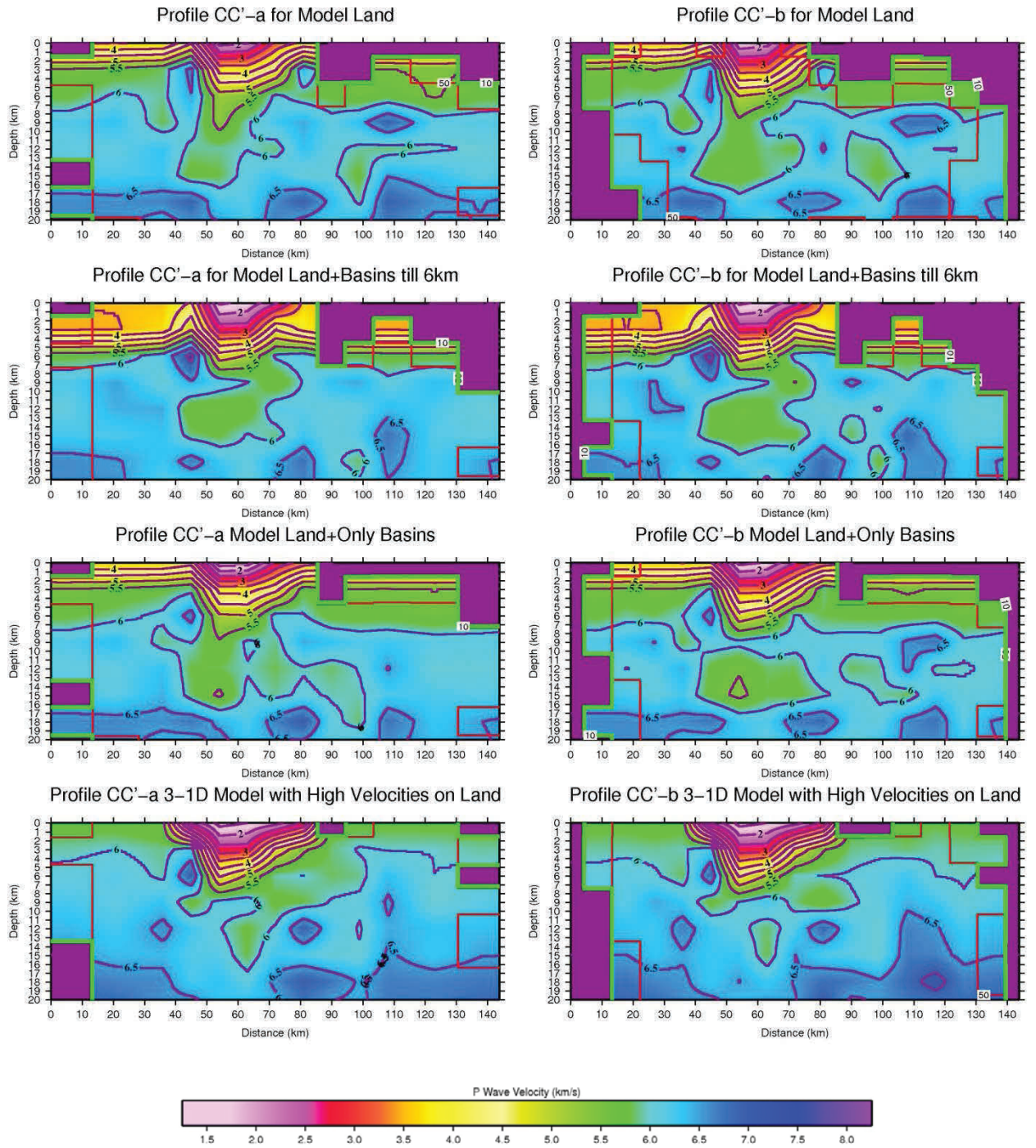
Figure 5. 9. The absolute P wave map of the cross section CC'.
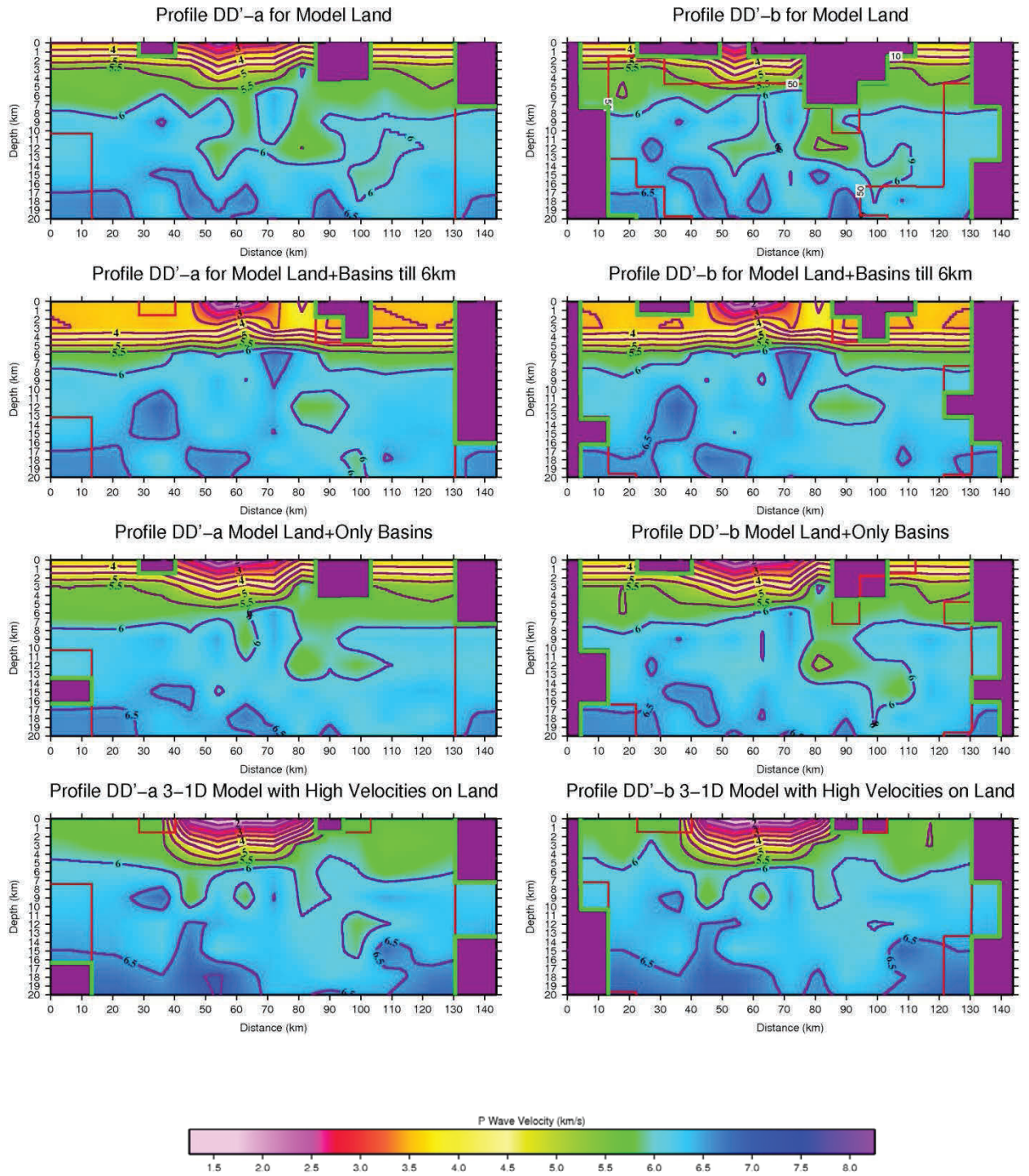
Figure 5. 10. The absolute P wave map of the cross section DD'.
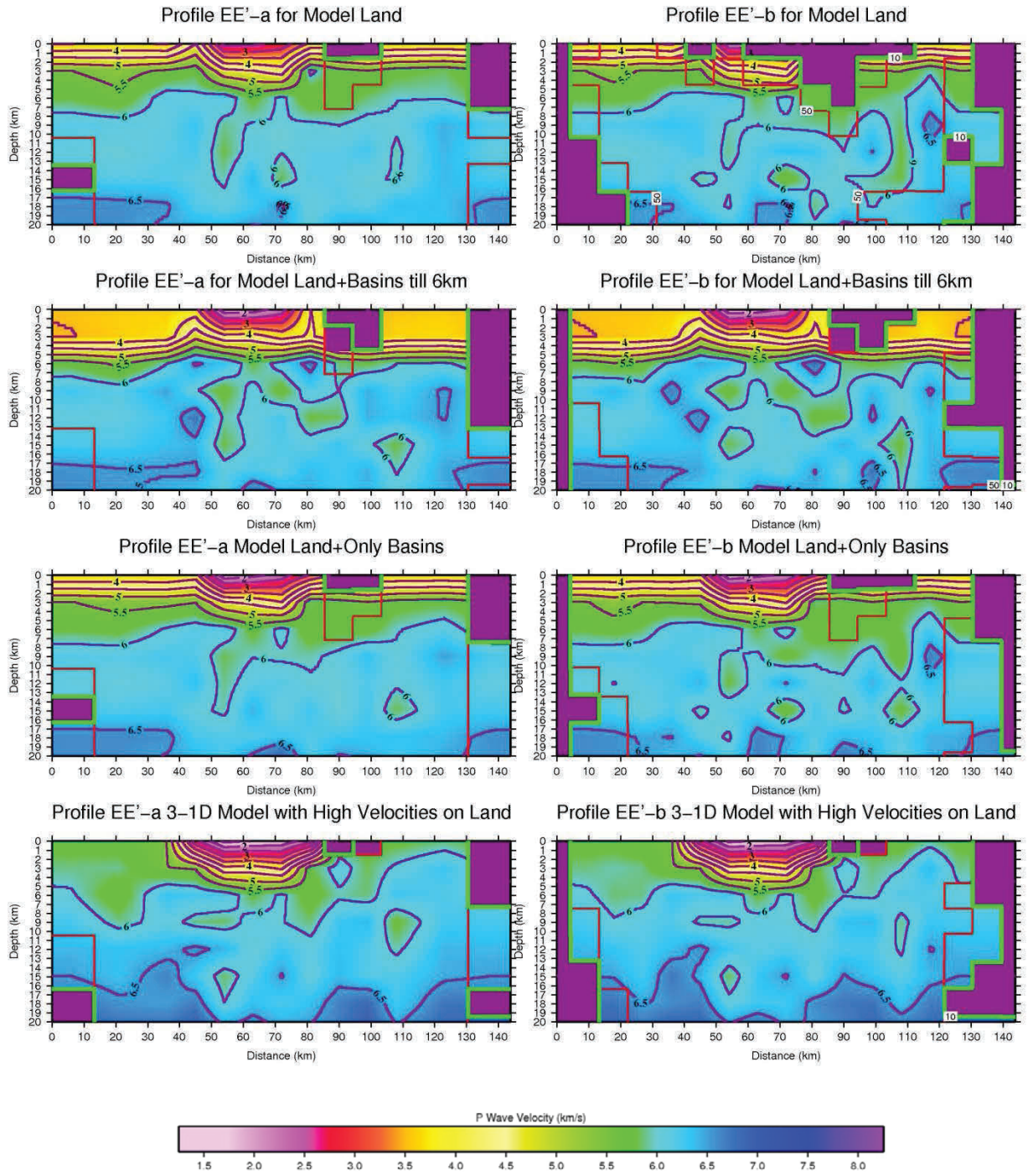
Figure 5. 30. The absolute P wave map of the cross section EE'.
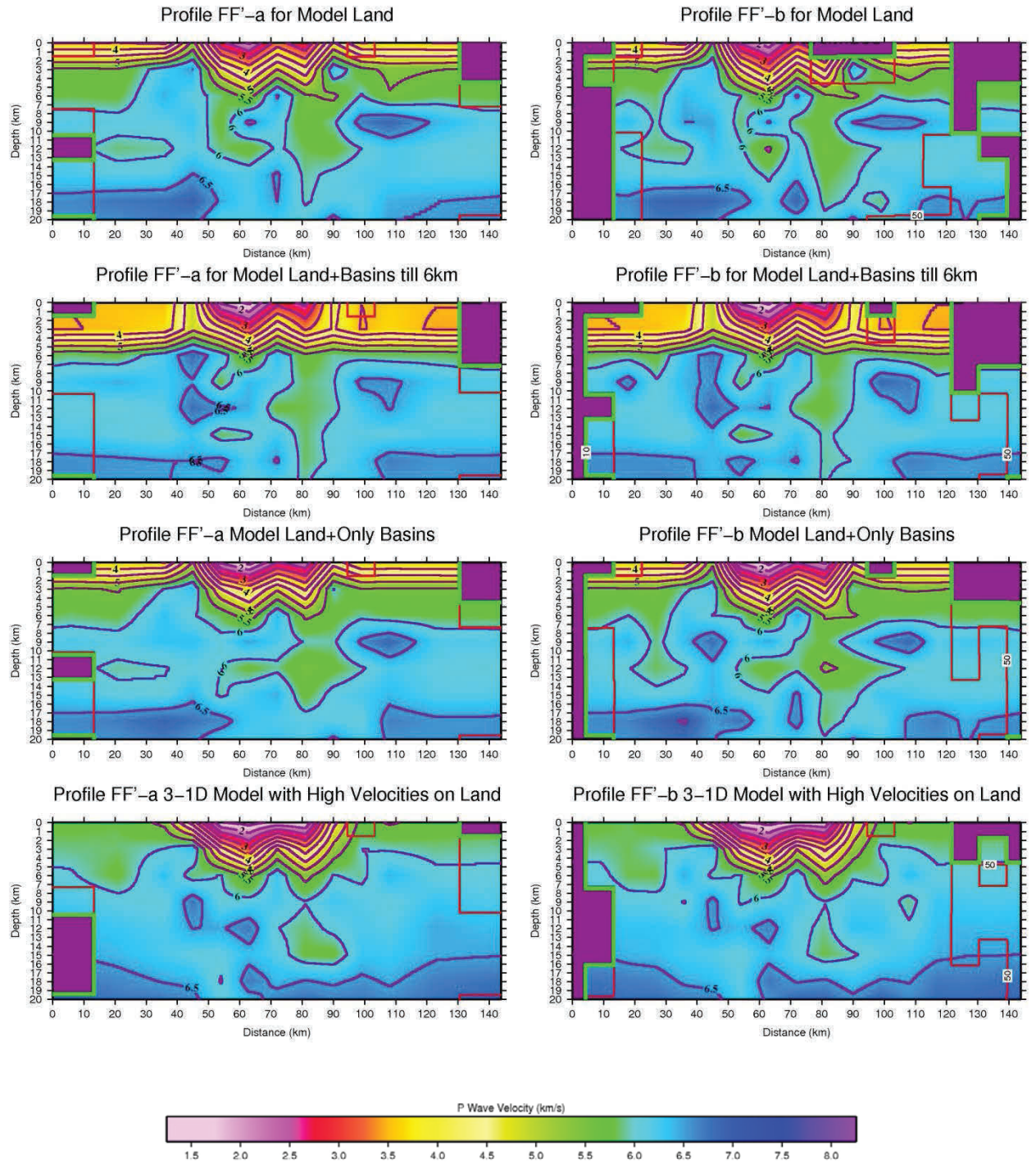
Figure 5. 31. The absolute P wave map of the cross section FF'.
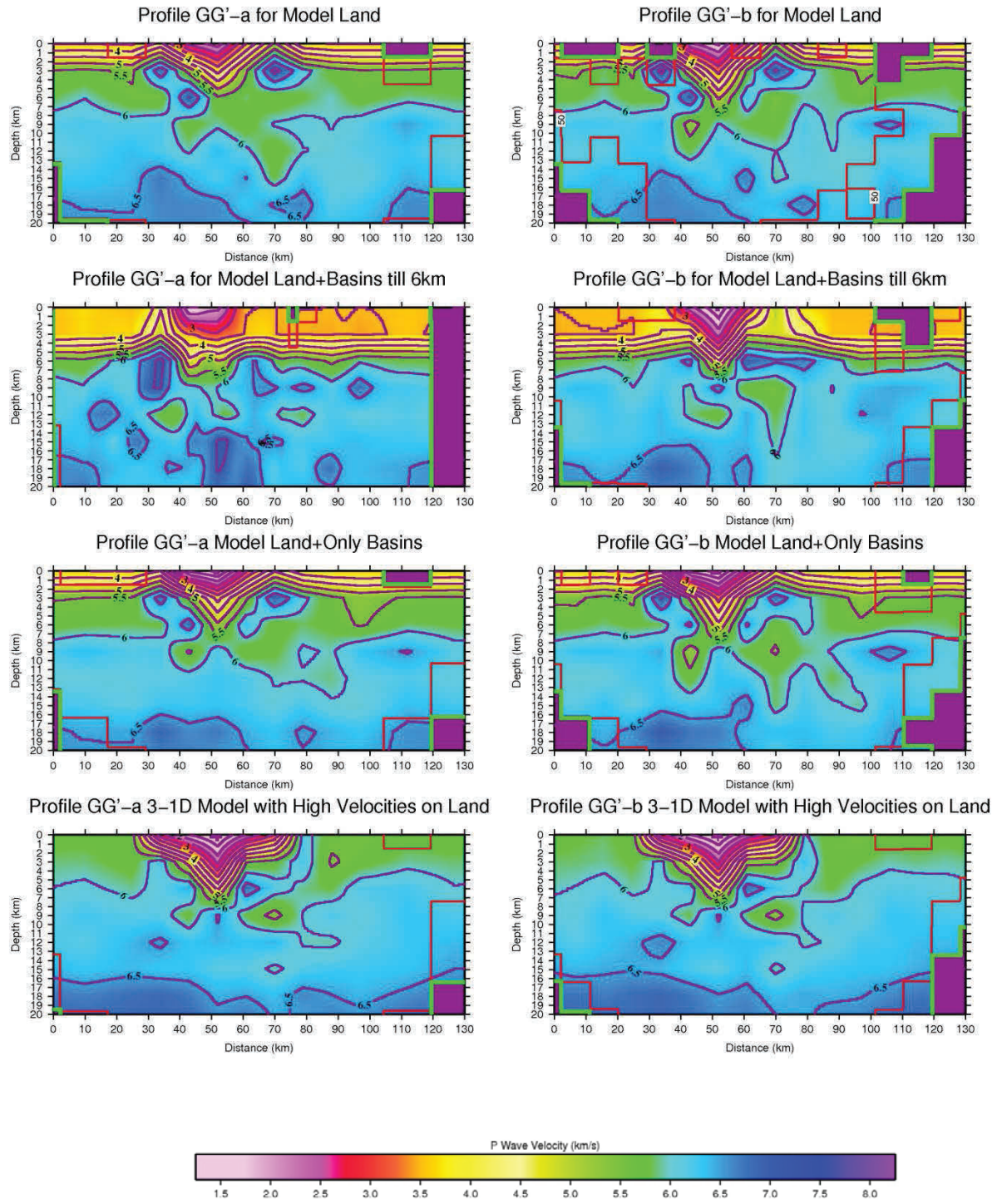
Figure 5. 11. The absolute P wave map of the cross section GG'.
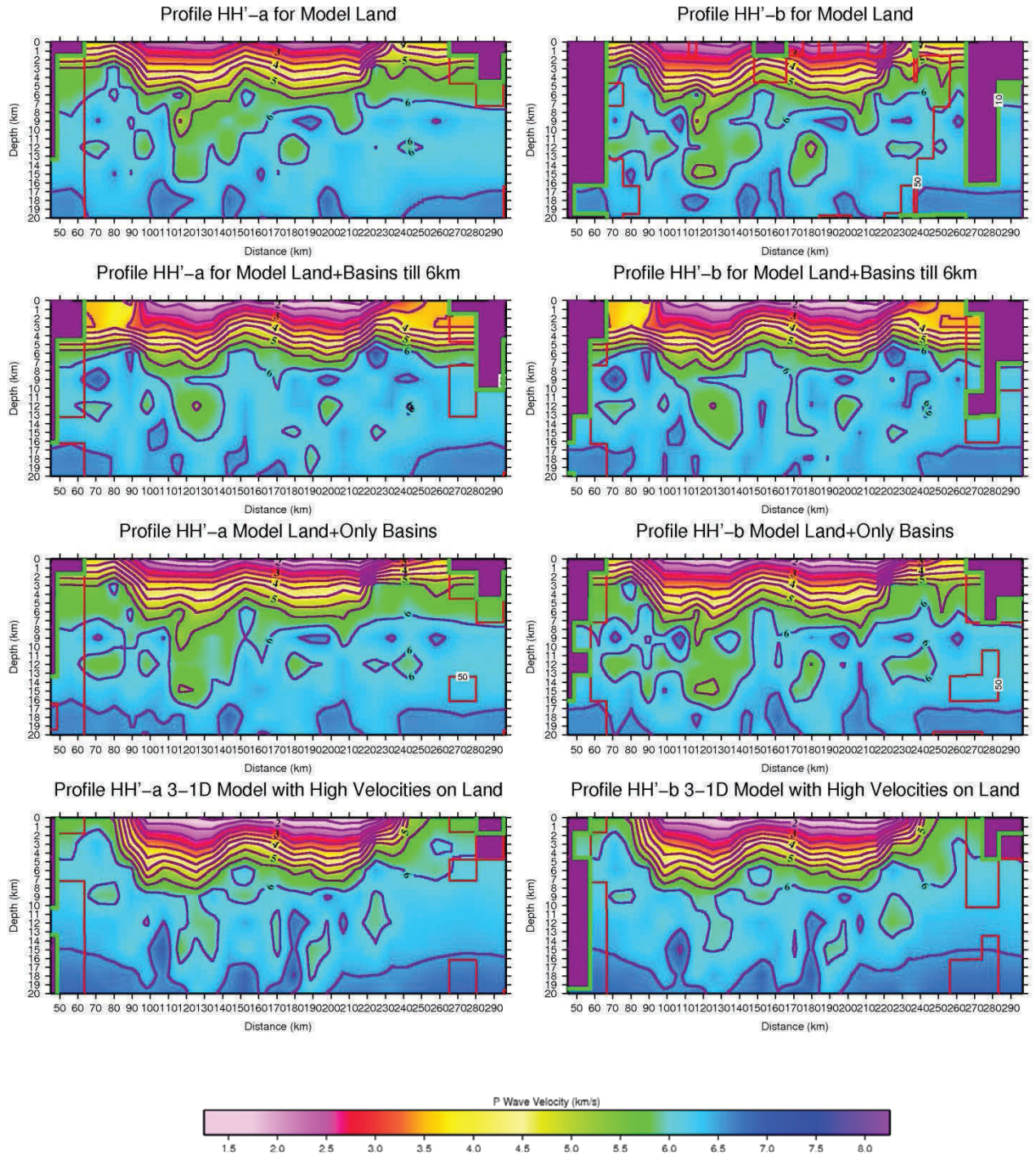
Figure 5. 12. The absolute P wave map of the cross section HH'.

Figures 5.26 to 5.33 shows the cross sections given on Figure 5.25. The red contours indicate the DWS 50, the purple masked areas indicate the zones with a hit-count less then 10. The left hand side of the figures are the results of random grid which was designed to compensate the areas with less ray coverage on land.

Figures 5.26 to 5.33 (a) (For Model Land) are the inversion results of the model extracted from the station KURN, representing the Istanbul Zone with a random grid. Figures 5.26 to 5.33 (b) (For Model Land) are the inversion results of the same model with a systematic grid. We prefer to consider the systematic grid since the random grid did not retrieve the basins structure in the sea. The second inversion result (Model land + Basins until 6 km) is the first combined model which includes only the low velocities under of Central Basin model until 6 km. The third inversion result (Model land + Only basins) is the combination of only the low velocities under the basins and the land model.

We have an idea of the basins depths and shapes from the previous studies (Becel, 2006, Bayrakçı, 2009, Faridfathi, 2011, Sorlien, *et al.,* 2011) . The inversions for all the cross sections do not completely overlap with the known depths. Figure 5.34 shows two previous different studies made in the area. According to the sea information we should expect to see high velocities on the basin rims. Since there is no previous information of land velocities we prefer to test the reliability of the land areas with quality estimators.

The problem with the combined models is that they do represent the basins and the land to some extend but they do not represent the transaction between the basins and land. So finally, we created a model which both includes the low velocity basins, the transmission zone between land and sea and the land. The inner model is the 1D minimum model that we observed with low velocities under the basins. The middle model is transition model with average velocities which supposed to represent the basin rims. The outer model is a high velocity model that is chosen to represent the land (Updated İstanbul Zone Model). See Figure 5.35.

The result of this model satisfies nearly all we expected to see (Figure 5.36). The iso-velocity contour of 4.5 km/s represents the pre-kinematic basement whereas the 5.7 km/s represents the crystalline basement (both in black). The red contours are the same (4.5 and 5.7 km/s) countours found by WARR study and exported on the tomographic result.
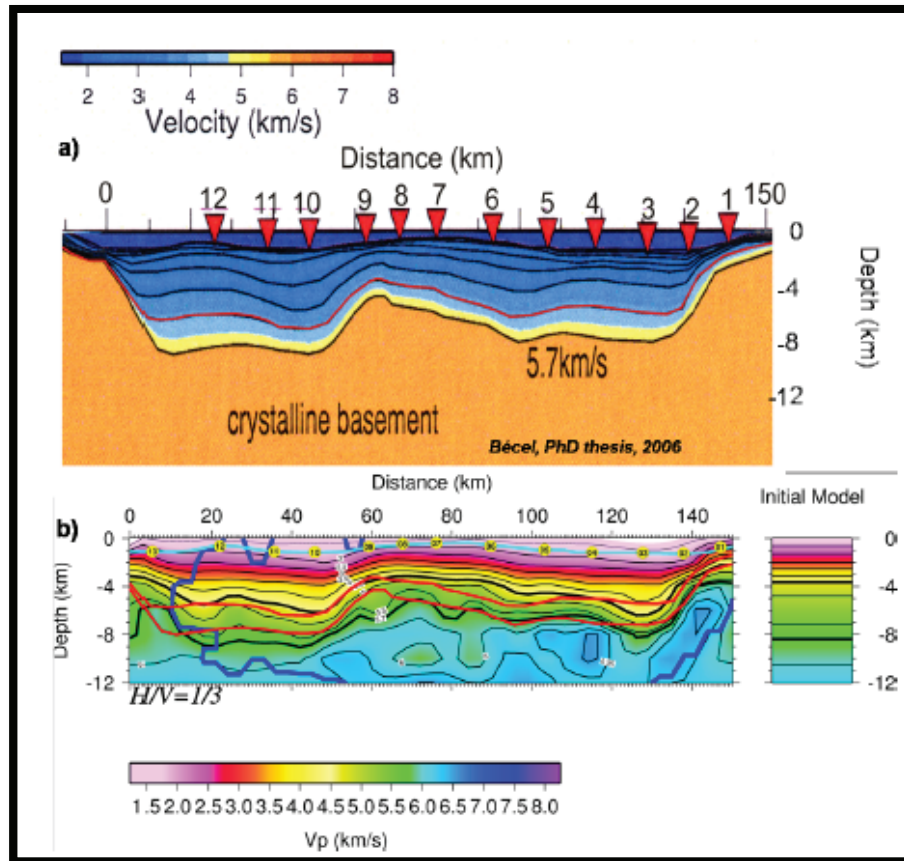
Figure 5. 13. a) TheWARR modeling result of the E-W profile (Profile 1) which cut across the middle part of the North Marmara Trough on whole (Bécel, 2006; *Bécel et al.*, 2009). b) The tomographic result along the same profile (Bayrakçı, 2009).
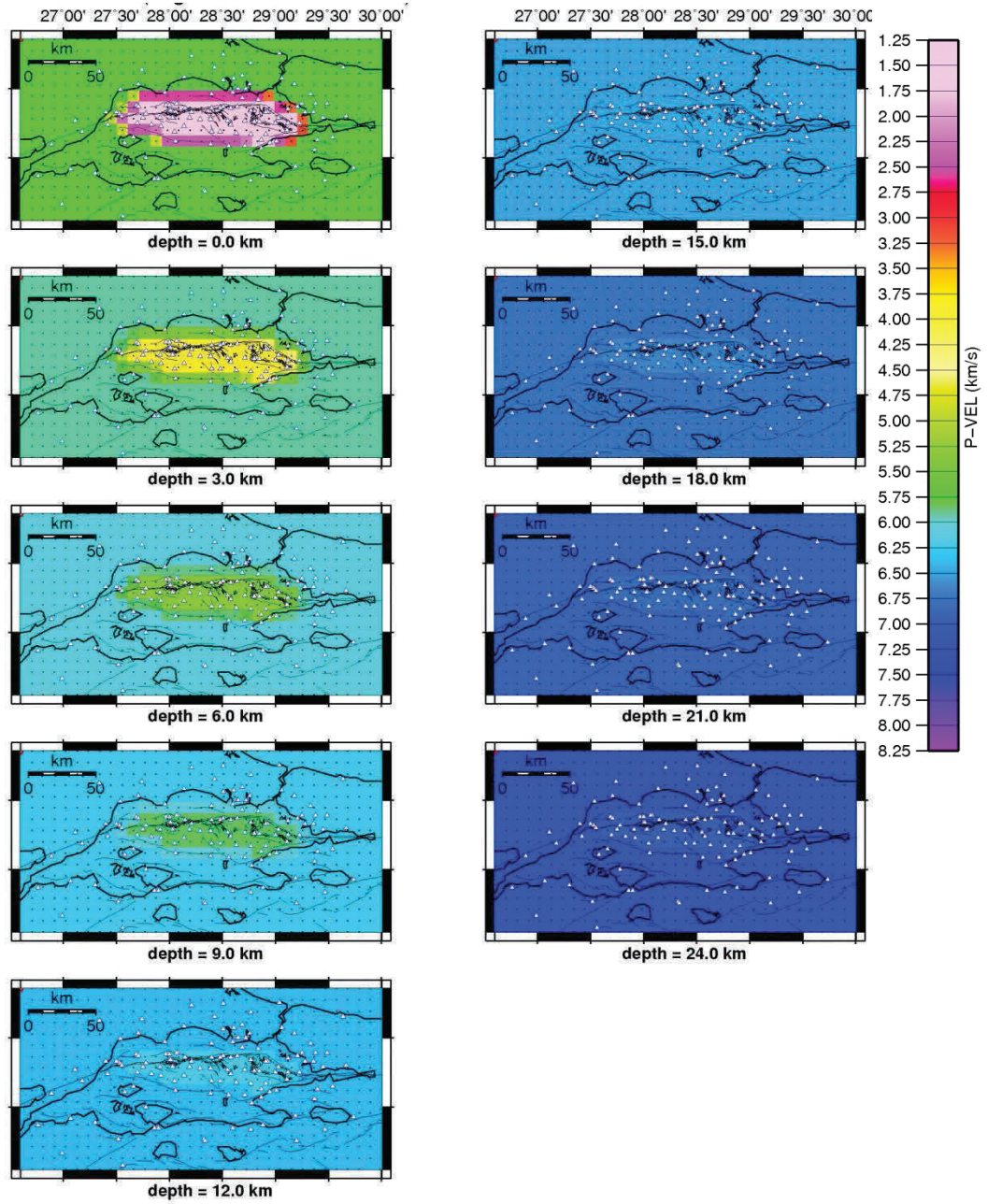
Figure 5. 14. The 3rd combined starting model.
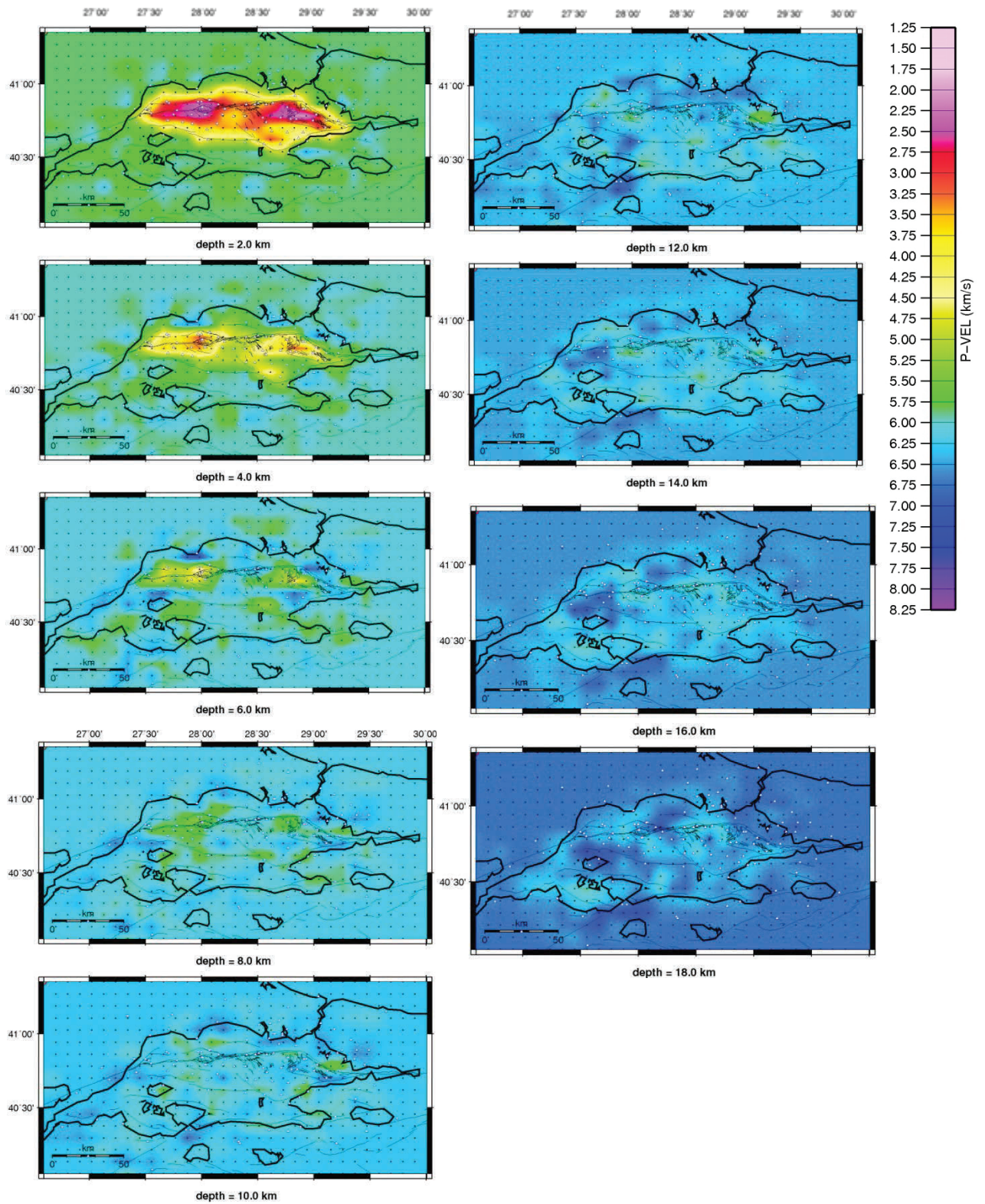
Figure 5. 15 The 3D inversion result of 3rd combined model with the small data set.

Although the result of the 3rd combined model seems satisfying this is valid only for the sea part of the model. This led us to use a denser data both to recover the areas with low resolution especially the land and to develop a deeper model which would represent both the land and sea. Since the resolution is not high enough to determine quality estimators like RDE, SP, hit-count, we preferred to make further tests after the inversion which is made with the large data set.

5.8.2 Inversion with a Starting Model Representing the Whole Region With the Large Area Data Set

We explained why a pure 1D model is not proper for a 3D inversion in the Marmara Region. The inversion result of 3rd combined model, which we determined to be the best model to represent the sea and the land, does not satisfy the land area. So as to reach a model of land as good as the sea, we added data from far distances both including TUBITAK and KOERI catalogue between the same dates October, 2009 and December, 2012) (Figure 5.37). To improve the resolution and go deeper all the earthquakes occurred around the Çanakkale Peninsula, some occurred in the Trace region, some earthquakes occurred in southern Marmara Region and some earthquakes from east of Marmara region added to the first data set. By making this we made all the stations receive earthquakes from a large variety of azimuths.

The resolution of the inversion is improved especially at the south of the Marmara Sea. However, most of the resolution lack was in the northwestern and northeastern Marmara. These areas are recovered to some degree.

In the previous inversions we observe a very low velocity perturbation on land. It is not possible to understand the reason for this whether the model was proper enough not to change or the resolution was too low. The previous checkerboard pattern was not perfectly retrieved but it was not also too bad to ignore land areas. After the inversion with the large data set we observed the difference between small data set and the large date set. This led us to the idea that making only a classical checkerboard does not give a clear reference of the resolution. For the sake of completeness, we made additional tests to define the trustable zones of the inversion result.
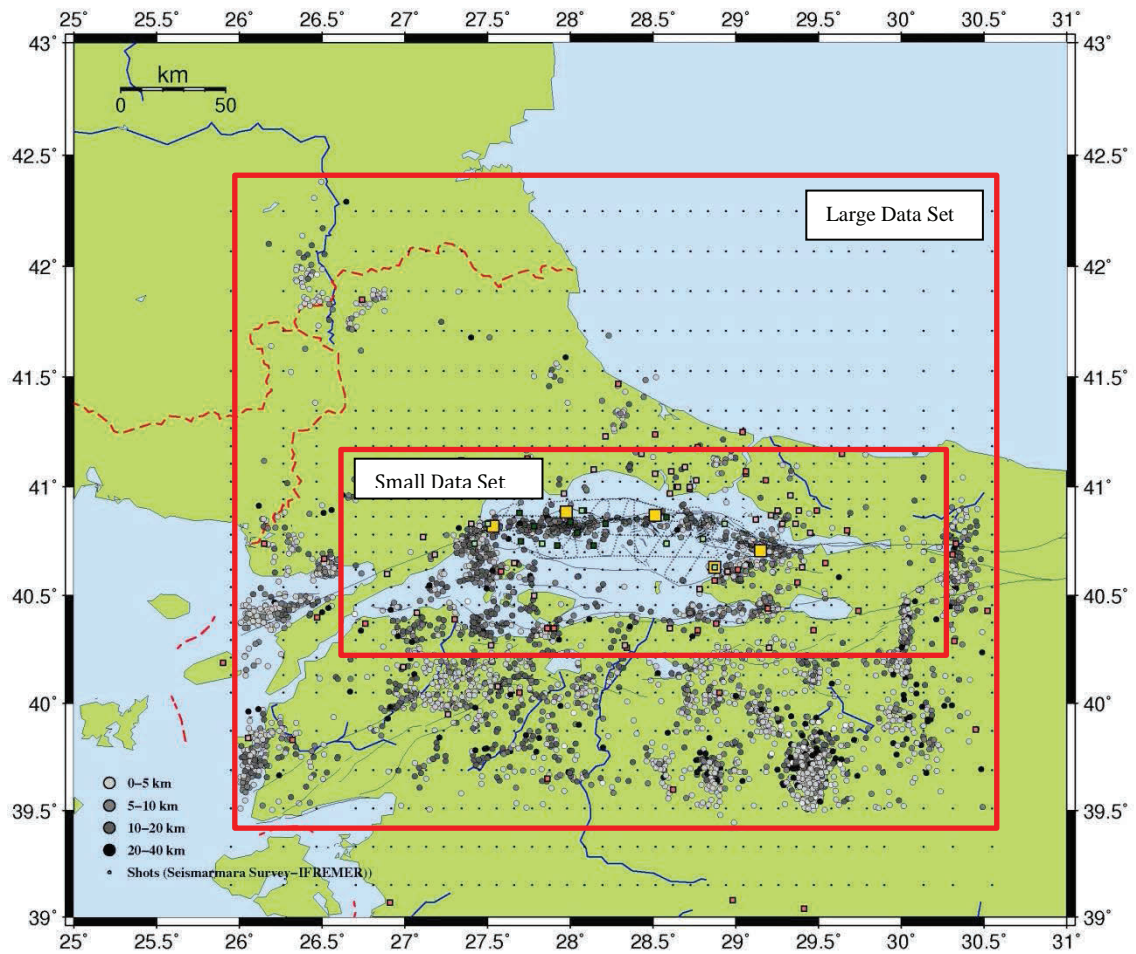
Figure 5. 16. The distribution of the large and small data set

The damping of the new data set (Figure 5.38) was observed as 100 with the classic method. Other parameters were kept the same.
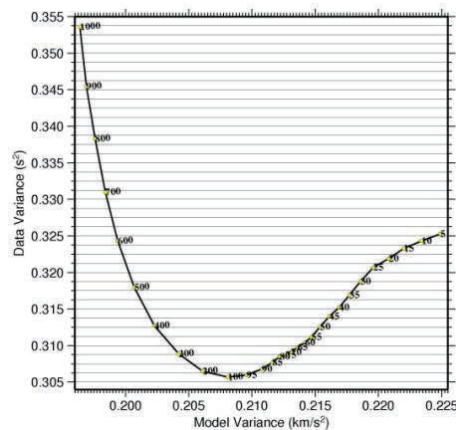
Figure 5. 17. The damping curve of the
large data set
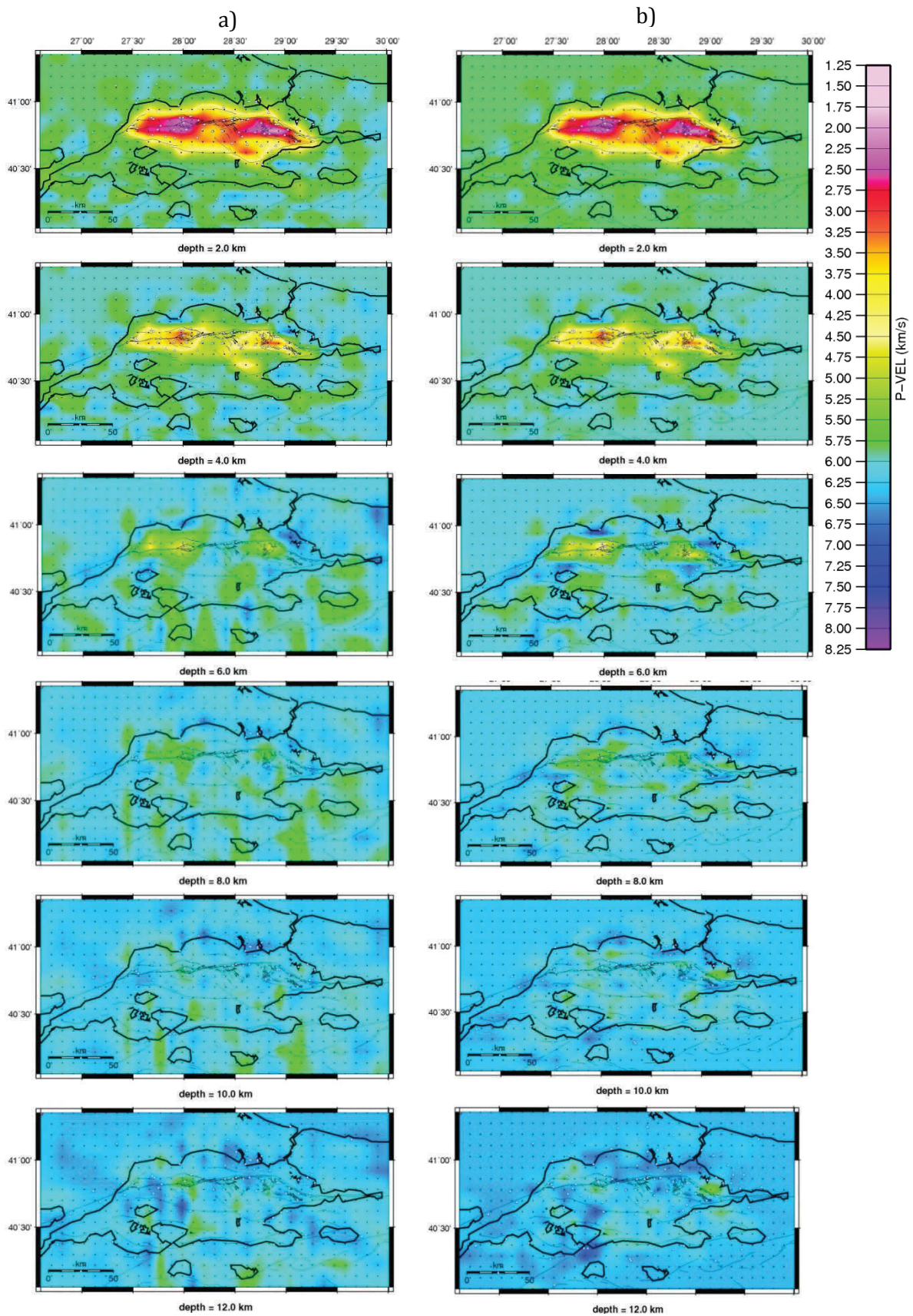
Figure 5. 18. Inversion result of 3rd combined model (2-12 km) with the large data set. a) Large area data set b) Small area data set.
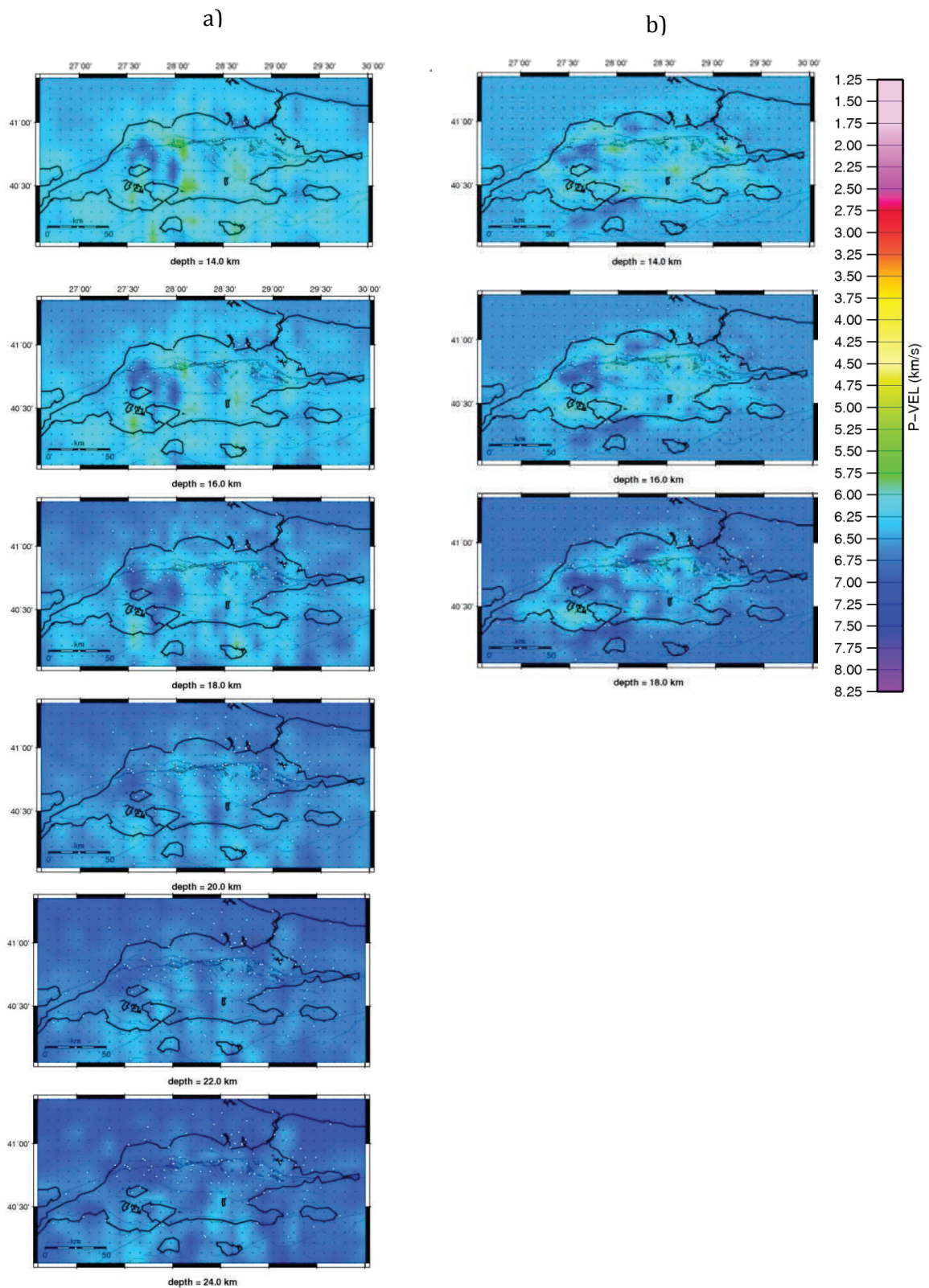
Figure 5. 40. Inversion result of 3rd combined model (14-24 km) with the large data set
a) Large area data set b) Small area data set.

Since the resolution of the inversion with the small data set is acceptable until 18 km, we prefferred to compare the results of two inversions with respect to the maximum realible resolution depth.

The model has changes with respect to the previous inversion result with the small data set both in the sea and especially on the land.
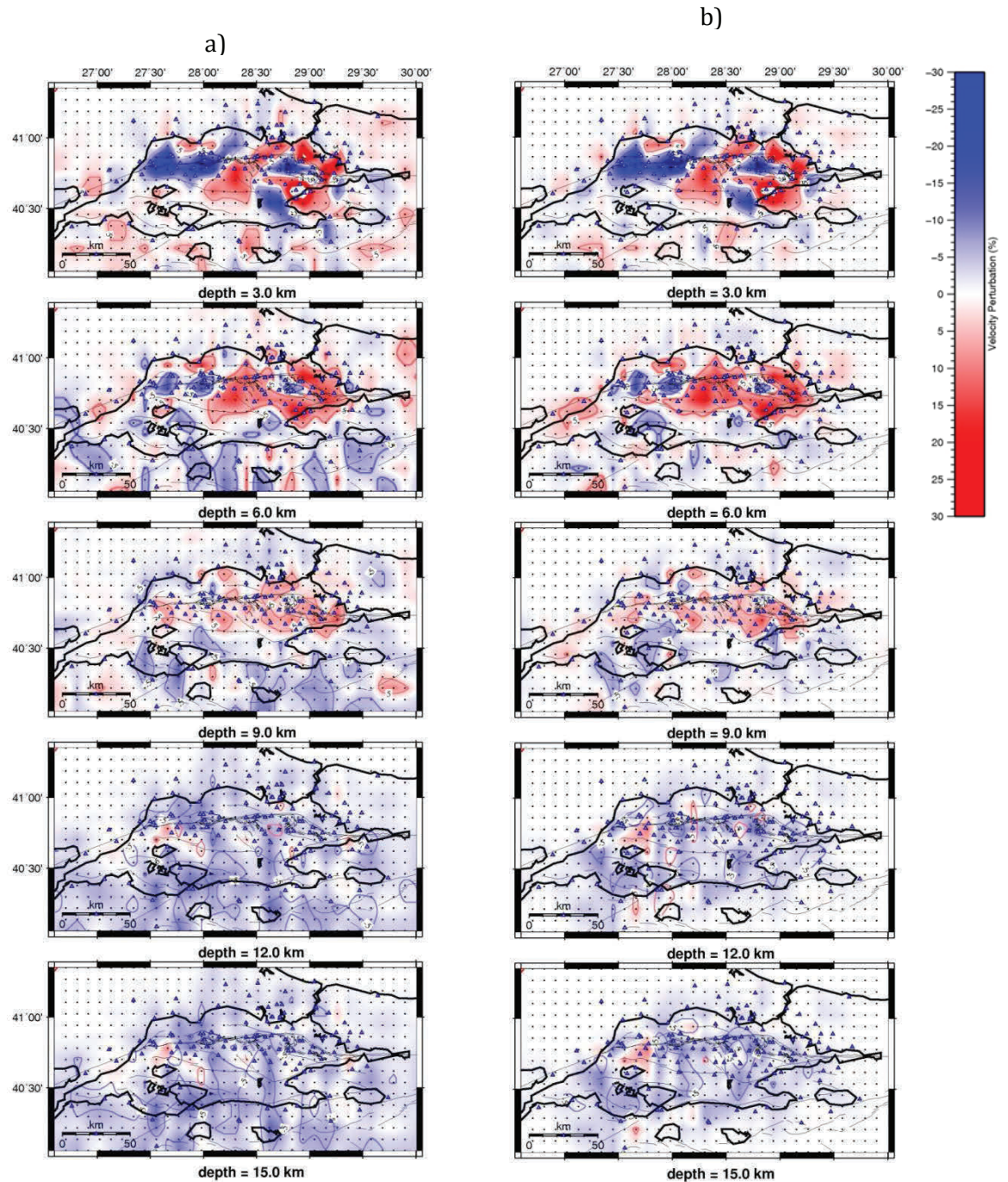
Figure 5. 41. Comparison of velocity change % of the inversions with the large data set (a) and the small data set (b) 3-15 km.
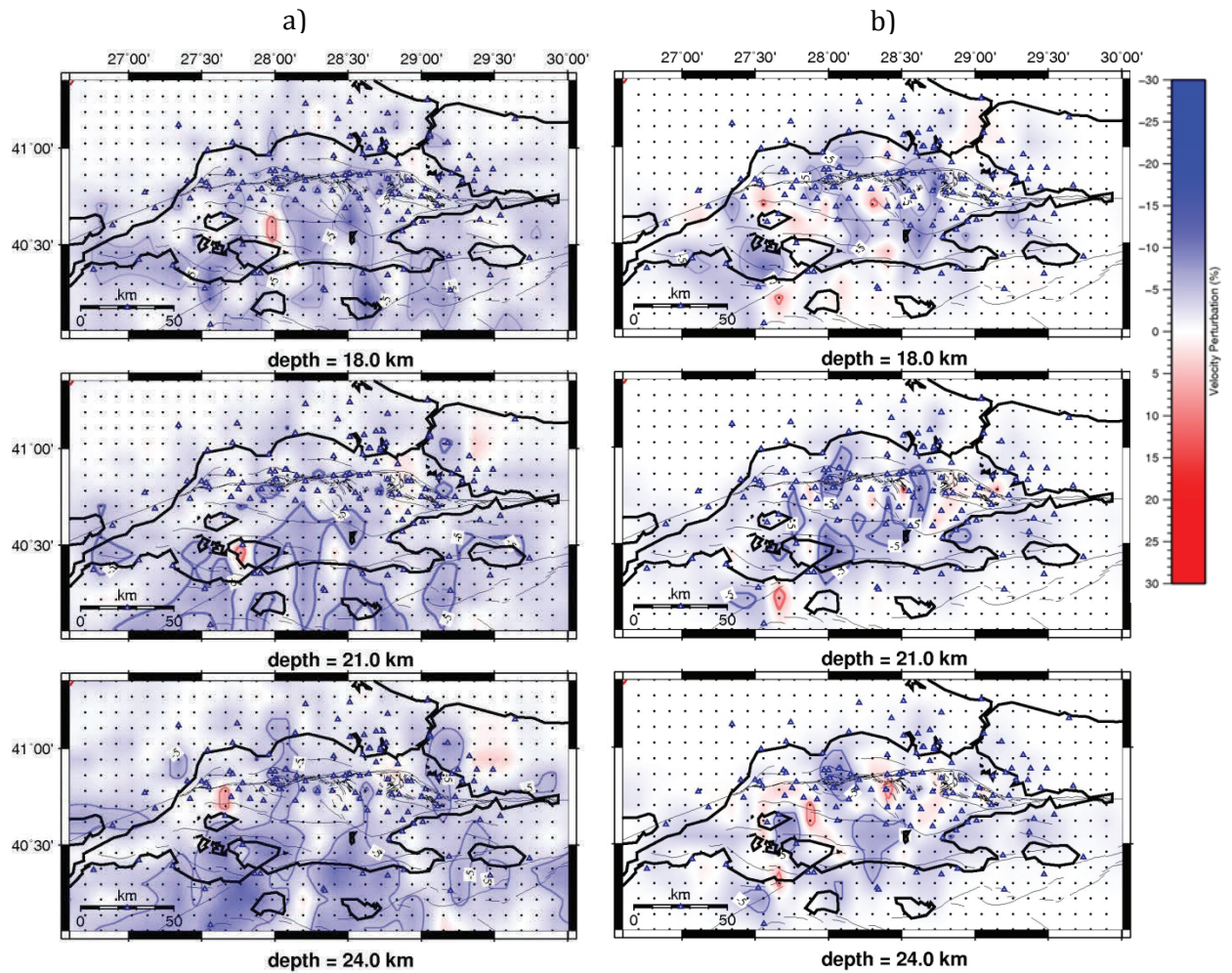
Figure 5. 19. Comparison of velocity change % of the inversions with the large data set (a) and the small data set (b) between 18 and 24 km.

The Hit Count maps show the ray distribution around the area (Figures 5.43). The resolution is expected to be quite good until 12 km in the sea and good in the land. After the depth of 12 km the resolution is fair.

The data variance is reduced from 0.45 s^2 to 0.06 s^2 after the inversion. The average rms of the earthquakes is 0.17 s after the inversion. The weighted RMS was 0.62 at the beginning, after the inversion it reduced to 0.25. The total number of the received earthquke arrivials at the stations is 47034, shot arrivals are 14162.

We see a high velocity zone between 12 km and 18 km right under the north of the Kapıdağ Island. This high velocity zone can be explained by the expansion of the Ganos High. The velocity change under the sea starts to provide a uniformity with the land velocities after 8 km.

5.9 Testing the Reliability of the Model

To define the trustable zones of the resulting inversion we need to estimate where the quality of the model is good and fair. The first test we applied is the Checkerboard Test with a realistic random perturbation. The second one is the Restoring Resolution Test which we use a test model which has exactly the same velocity perturbations as in the resulting model. The third and the final test we applied is the Characteristic Test which is designed to understand signs of the anomalies and make more correct quality estimation of the inversion result.

In order to make a good and realistic estimate of the trustable zones of a 3D inversion, we should consider all the tools for resolution. These tools are DWS, Hit count, RDE, SF in the case of tomographic inversions. Figures 5.43, 5.44, 5.45 and 5.46 shows the distribution of Hit count, DWS, RDE and SF of the resulting model, respectively. These tools works for different aspects of resolution estimation. Although we have the synthetic test to understand where the resolution is well, these test are effective when the quality estimators are known which helps us to define the boundries of the trustable zones. The DWS does not account for the direction of the ray paths. It is sensitive to the ray segment lenghts which samples the influence volume of a node. However, we still need to observe other resolutions tools to make a complete assesment. The RDE can be used as an indicative instrument to see the amount of independence of one model parameter. The spread function specifies how much the model parameter is resolved with the contribution of the information from the vicinity of the model parameter thus the independence of a node to the negbouthood nodes (Haslinger *et al.,* 1999).

In our results we see a coherence between the resolution tools. Each of them show a very good ray sampling along the North branch of the NAF especially around the basins. The reason for that is the very dense shot profiles which allows us to observe small wave length structure of Marmara Sea. In a general sense a large amount of the nodes has a fair resolution covering all the stations expecially in the south. However, still some stations far from the center of the study area located at the nortwest are outside the well resolved area even after the inversion with the large data set including earthquakes recorded from far nortwest stations.
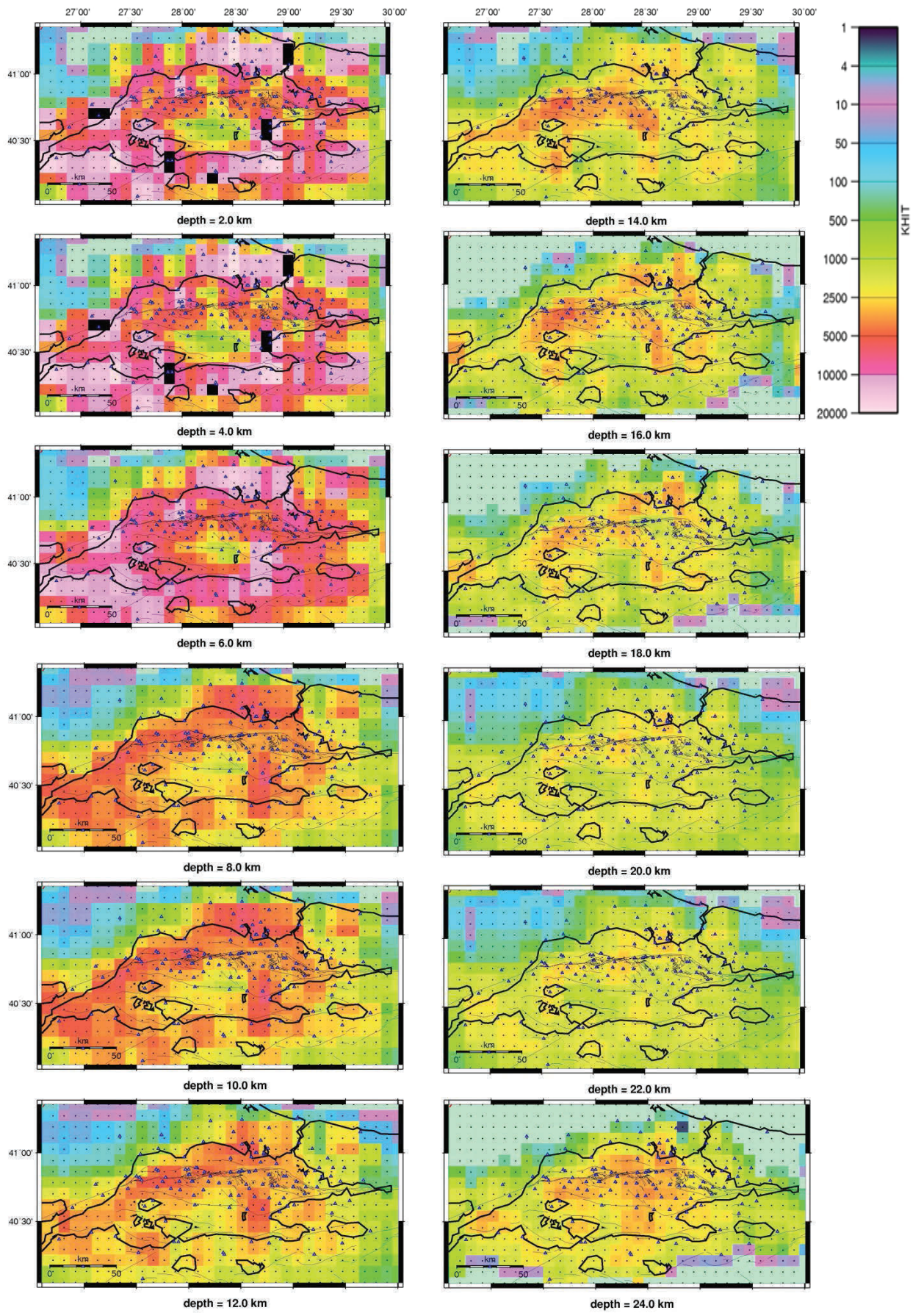
Figure 5. 20. Hit count distribution of the resulting model.
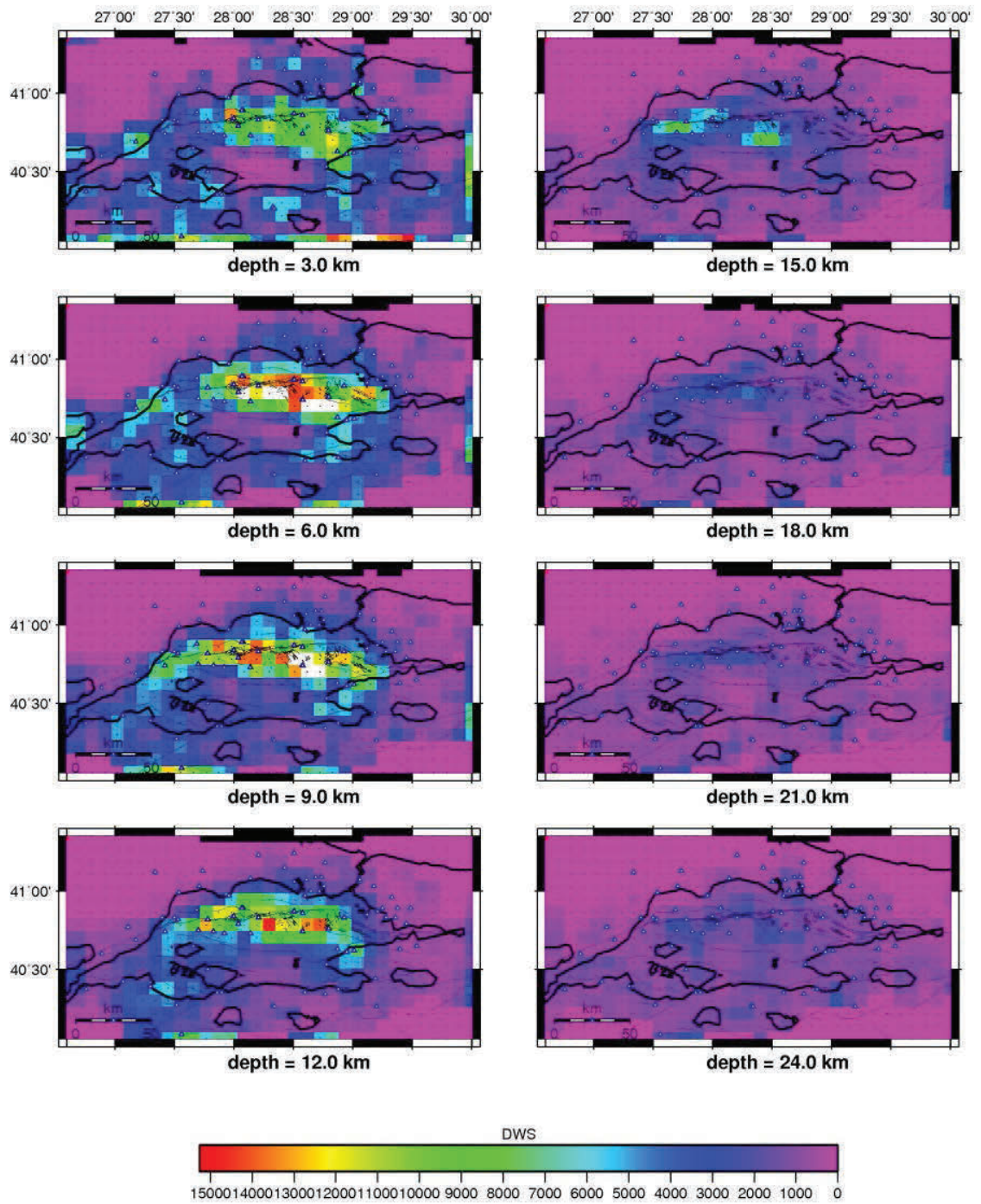
Figure 5. 21. DWS distribution of the resulting model.
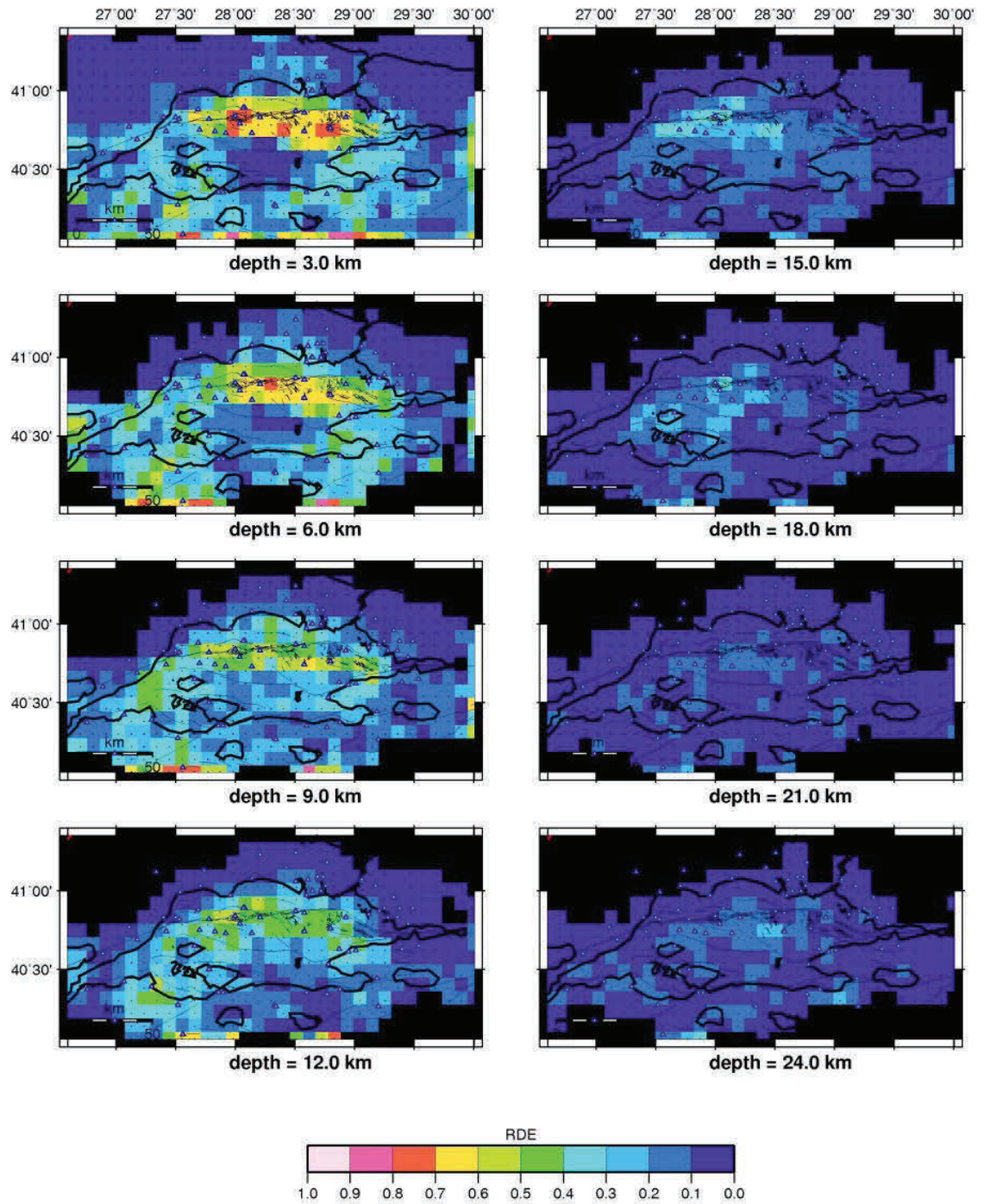
Figure 5. 22. RDE distribution of the resulting model.
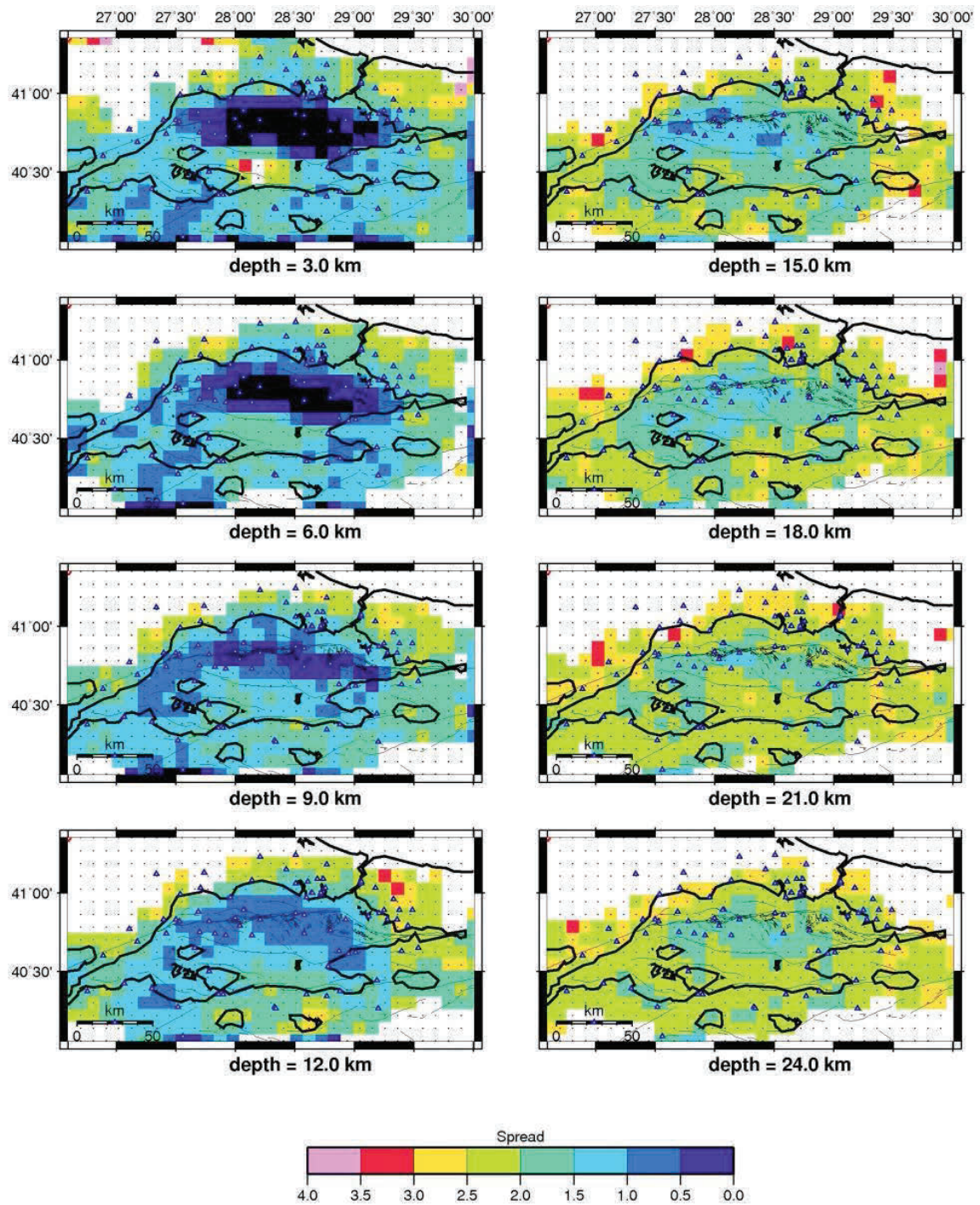
Figure 5. 23. SF distribution of the resulting model.

5.9.1   A Classical Approach, Checkerboard Test

The checkerboard test is an application which shows the image distortion in the medium (Spakman, 1993; Zhao *et al.,* 1992; Benz *et al.,* 1996; Zelt & Barton, 1998; Zelt *et al.*, 2001; Tong *et al.*,2003).

The perturbation percentage has a critical affect on the results of the test. If injected anomalies are different from the real ones the results would not be sufficient to understand the real coverage (Lévèque *et al.,* 1993).

In order to see how much the study medium covered by the data, realistic high and low velocities have been injected into the 3rd combined model. This time being different from the previous checkerboard tests, we inserted high perturbations only to the nodes along the basins. By making this we aim not to disturb too much the land areas. In the resulting model we observed velocity perturbations nearly −30% in the sea where the land areas showed maximum ±10%. The related nodes perturbed as ±30% and ±10% at 3km and as ±20% and ±10% at 6km. We preferred to decrease the perturbation at 6 km because the resulting model had less than ±30% perturbation. The land areas showed similar variations nearly at all depths so the perturbation has been kept fixed as ±10%. By looking at the real structures both in the sea and the land the checkerboard pattern designed as an 18*18 grid. After adding a Gaussian noise to the results of the synthetic travel times, we made an inversion with the same control parameters as in the real one (damping=95, velocity perturbation=0.25, 6 iterations).

Figures 5.47 and Figure 5.48 show the checkerboard pattern applied to the data and the synthetic inversion results. We see a very good coverage in the sea at all depths until 24km. The coverage is coarse in the northwest and northeast corners of the study area. Southern Marmara shows a good coverage.
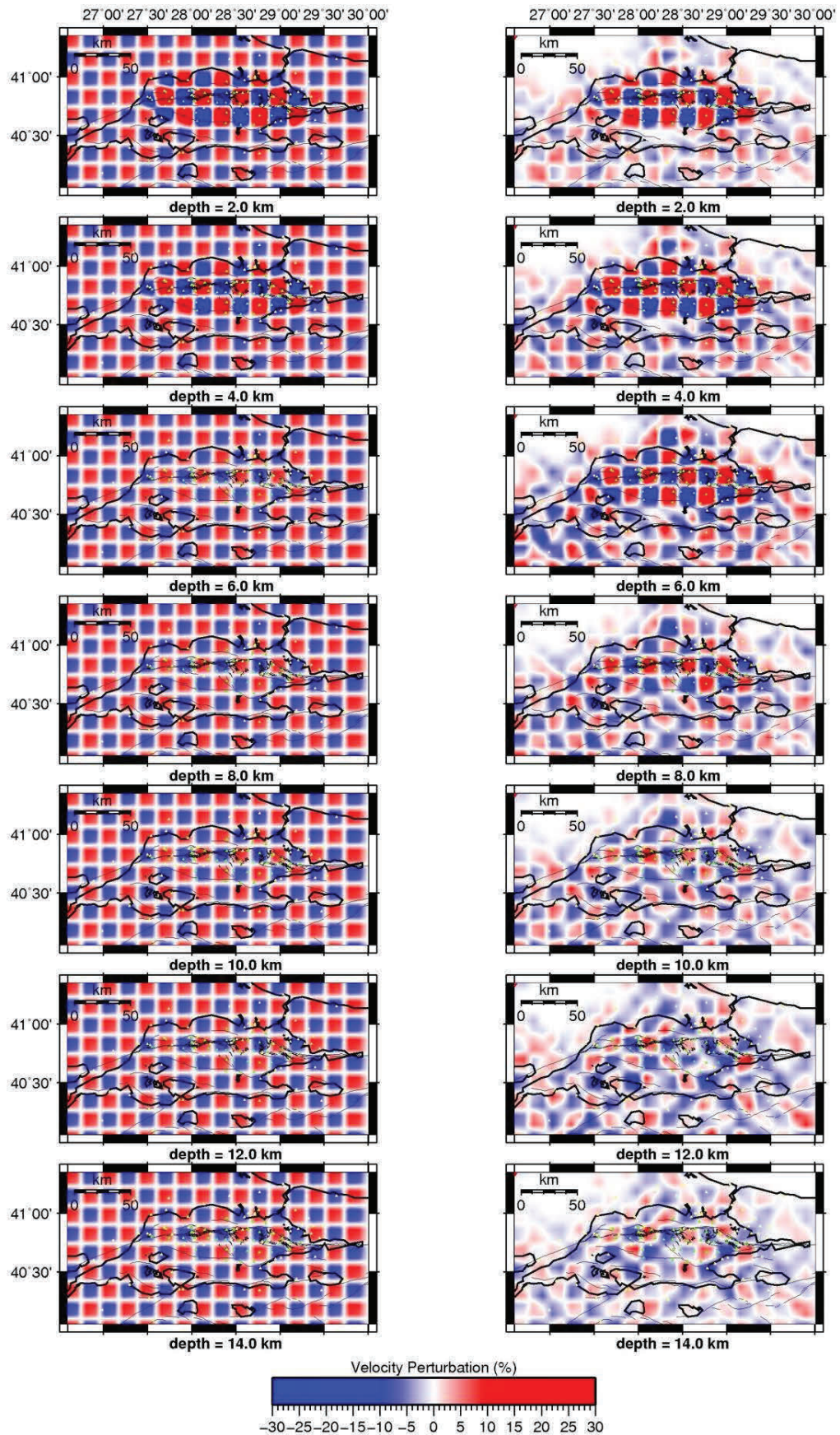
Figure 5. 24. Checkerboard test results of the resulting model between 2-14 km.
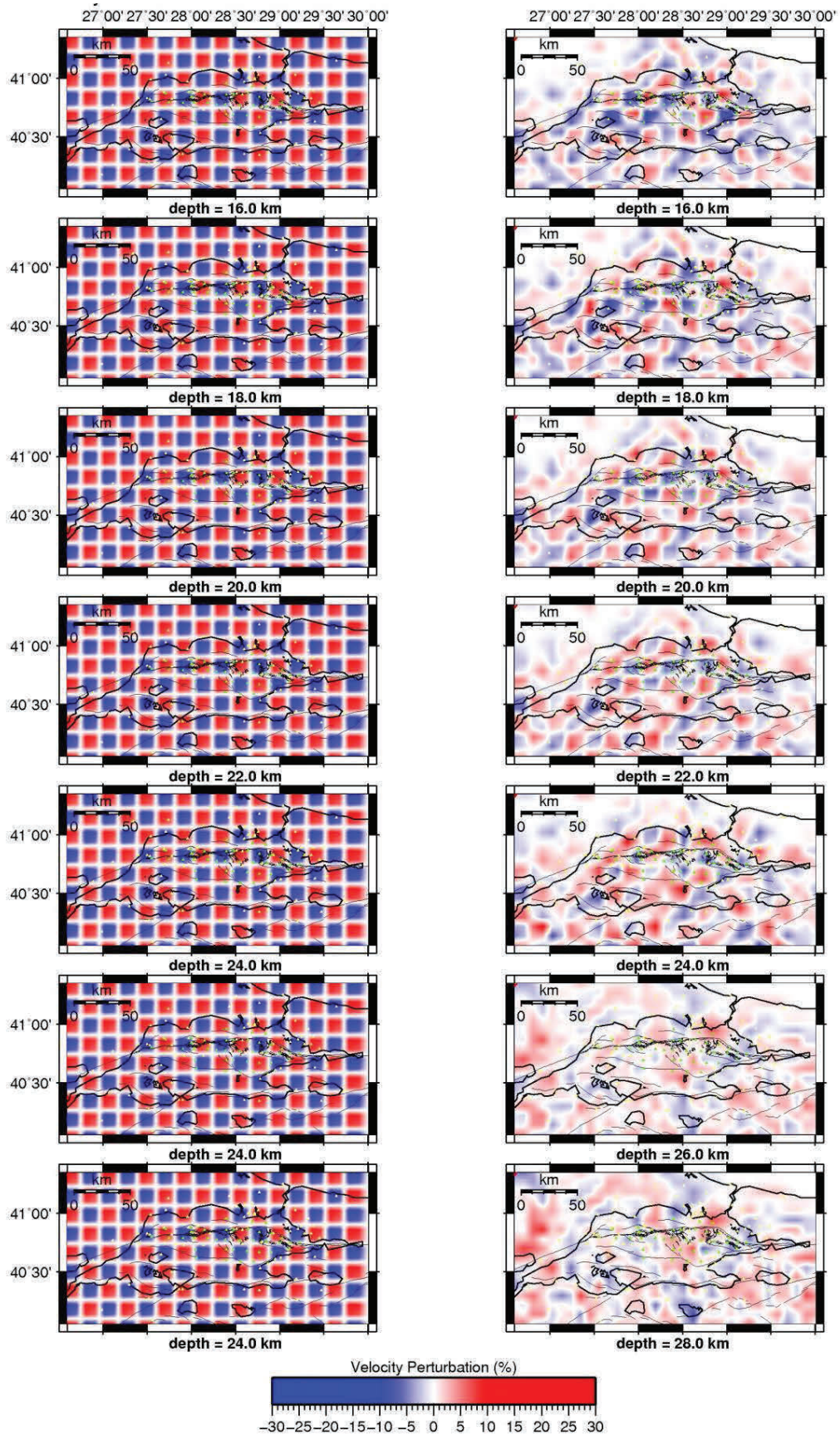
Figure 5. 25. Checkerboard test results of the resulting model between 16-28 km.

5.9.2 Restoring Resolution Test (RRT)

The checkerboard test gives an idea how much the data covers the study area but it does not give an idea about the resolving capacity of the shapes of the actual structure of the inversion. It shows how much the inversion grid is powerful to resolve the medium relating to the study area geometry (Zhao *et al.,* 1992, Husen *et al.,* 2000, Laigle *et al.,* 2000).

The synthetic travel times are computed thorough the resulting model so the less resolved nodes may show same kind of result which is a disadvantage of the RRT. Thus, making a good guess of where the trustable areas are located may be hard to be identified and it only works for a specific wave-length structure.

For the synthetic inversion we used the resulting 3D model to compute the synthetic travel times. A Gaussian noise is added to these synthetic travel times. The resulting travel times were inverted with the same control parameters used for the inversion of the 3rd combined model.

Figure 5.49 and Figure 5.50 show the results of the test results. Until 6 km depth, the resolving capacity of the data is very good. However, after 6 km depth the boundary of the well retrieved area starts to shrink. The northern part of the study area has less retrieved compared to the southern Marmara. Unfortunately, we could not add data from north of the northern stations. This leakage of data from a specific azimuth to the north stations can be contributed to the less retrieved areas on the north. The center of the study medium is well retrieved because of the dense small wave-length shot data.

At 6 km we see a leakage under the İznik Lake which can be related to the leaking data from southeast. From 18 km to 24 km only at the south and center of the study medium has been able to be retrieved. Between 12 km and 18 km only a little change can be observed on the north.
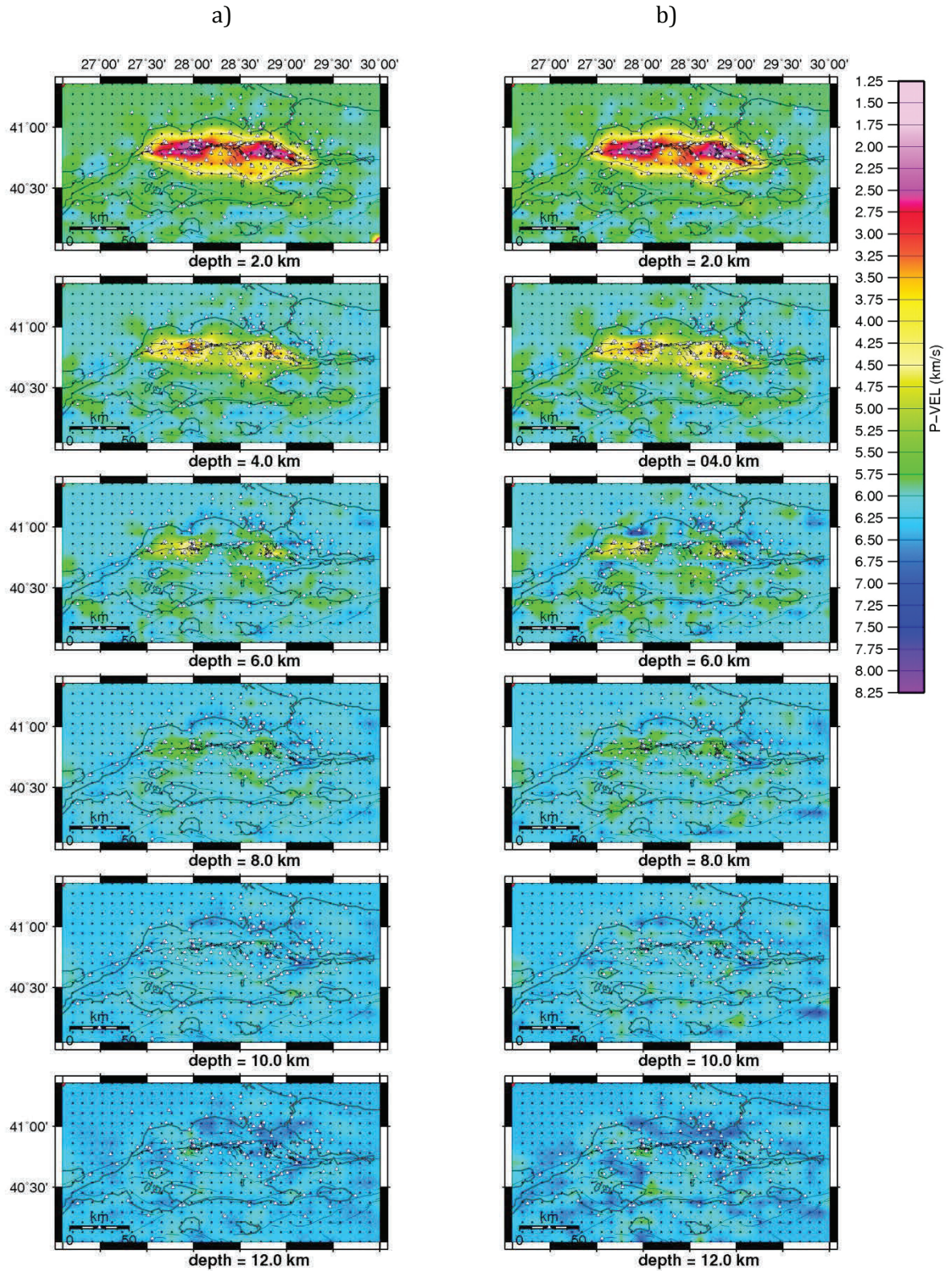
Figure 5. 26 RRT results between 2-12 km. a) Result of RRT. b) Real inversion result

a)   b)
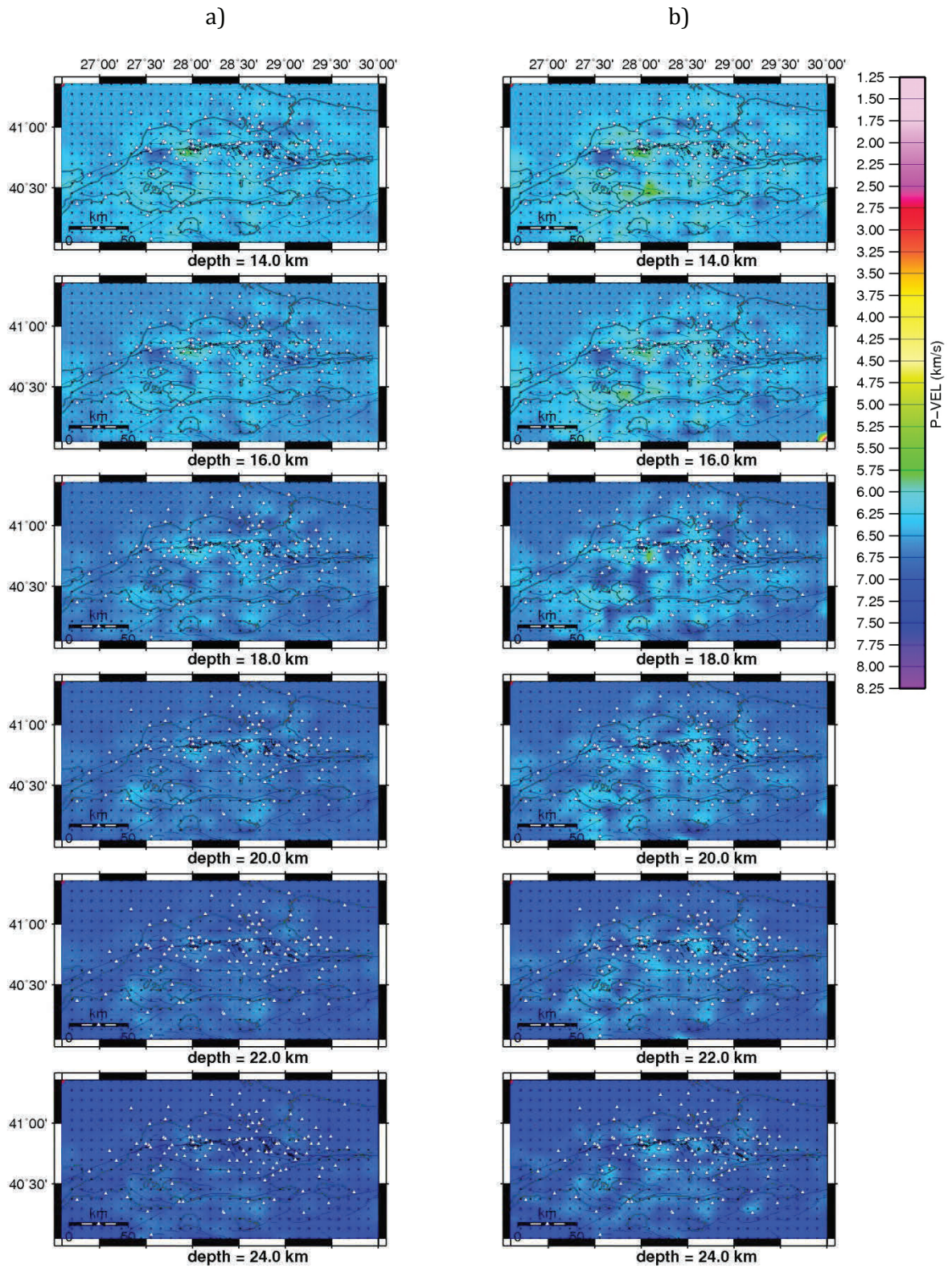
Figure 5. 50. RRT results between 14-24 km . a) Result of RRT. b) Real inversion result

5.9.3 Characteristic Test

Until now we presented two synthetic tests. The first one is he checkerboard test to define the data coverage and the second one is the RRT to define the structural resolving capacity of the data. These tests are not proper to identify the quality estimators because of the reasons stated under the related topics. We designed a characteristic test as described in Haslinger et al., (1999); Husen et al., (2000). A characteristic model is composed of anomalies and size as in the resulting model but with different shapes and signs. So the test is able to define the structural resolving capacity of the data set with respect to the inversion grid. As a result, the test gives an idea whether the signs and the shapes are realistic or not within the boundaries defined by the quality estimators.

Here in the Marmara Sea we already have a priori idea of how the velocity changes horizontally and vertically. So we do not need to test the signs of the anomalies.

Figure 5.51 shows the characteristic model we created. In this model we injected nearly the same size of anomalies both in the sea and on the land. For the center of the study we know that the velocities decrease and make a strong contrast to the surrounding area. −20% perturbed model is inserted into the center of the study medium at 3 km. It is reduced to −15% at 6 km. The land is perturbed again like in the checkerboard test ±10%. Not like the sea area we do not have a clear idea of the signs of the perturbation for the land. Therefore, we preferred to change the sign of the perturbation at some depths.

Figure 5.52 shows the result of the characteristic test. The center of the volume is retrieved well until 15 km. However, the northwest and the northeast corners did not show same quality which is probably related to the leaking data from these directions.

We know that the ray sampling is good at south but here in the characteristic test results, the model is not retrieved as much as in the synthetic model. This might be the reason of the size of the injected anomalies but still the well retrieved areas give information of the quality estimators to some extent.
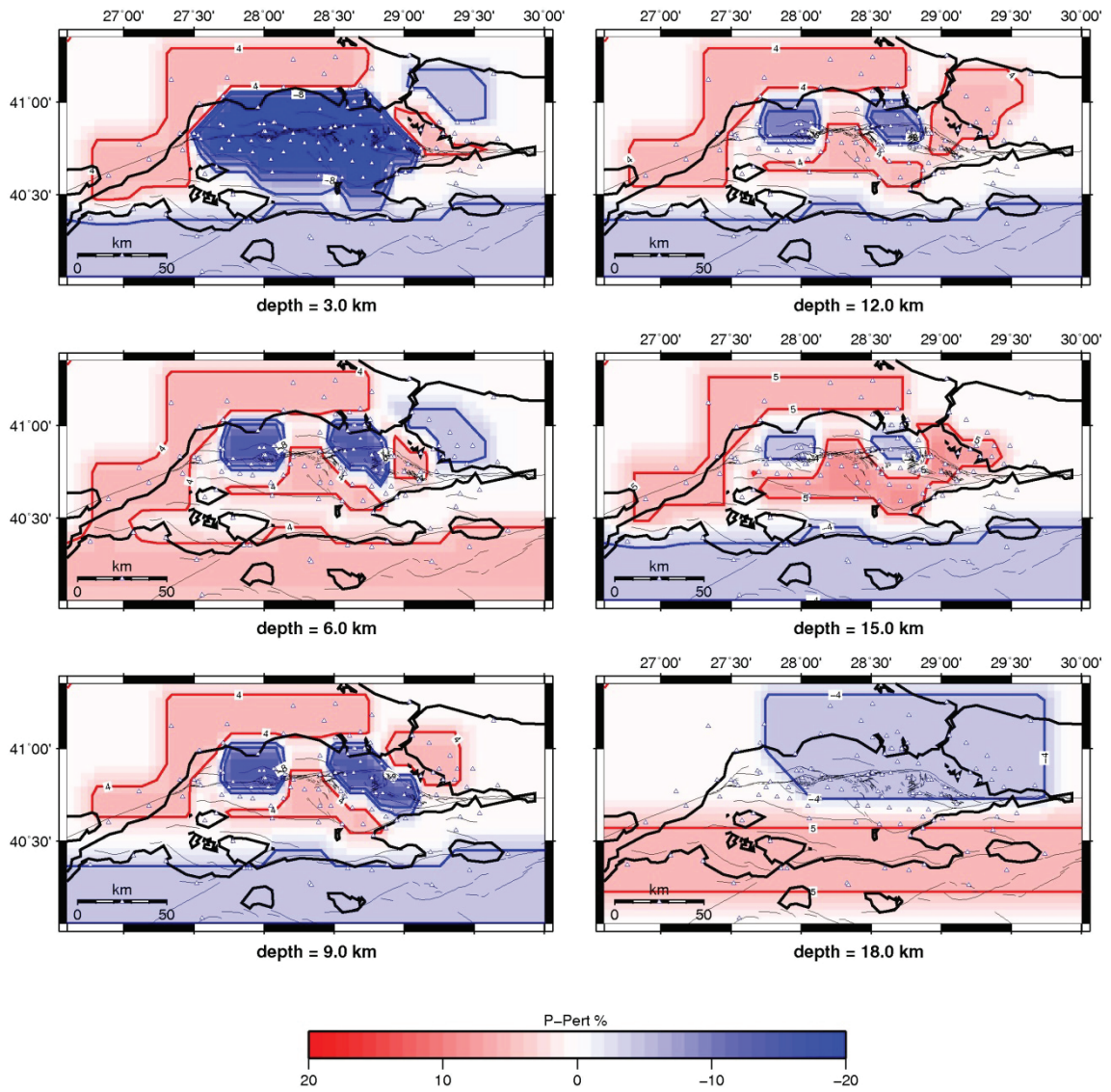
Figure 5. 51. Injected characteristic model

5.10   IDENTIFICATION OF THE QUALITY ESTIMATORS

Thanks to the characteristic test that we are able to estimate the quality tools such as RDE and SF. If we plot the RDE and SF contours of the synthetic inversion on the synthetic results, we can decide which contour limits the well retrieved areas and plot these contours on the real inversion results we would make a guess of the real RDE and SF contours to define the good and fair resolution.

Figure 5.52 shows the synthetic RDE contours on the resulting synthetic inversion. The 0.2 and 0.1 contours indicate the areas with well and fair resolution. Figure 5.53 shows the synthetic fair SF 1.51 contour on the synthetic inversion results. We plot these contours on the real RDE and SF distribution maps to identify the real RDE and SF contours. Figure 5.54 and 5.55 show related maps. After the guess of the RDE and SF we plot these on the inversion results and also on the cross sections from the inversions to define the trustable zones.

The RDE contour of the trustable zone is defined as 0.2. The spread function contour of the trustable zones defined as 1.15 according to the characteristic test results.

The contours on Figure 5.56 exclude north part of the inversion result on land but include southern part at deeper parts. This again shows the insufficient earthquake information from north direction.
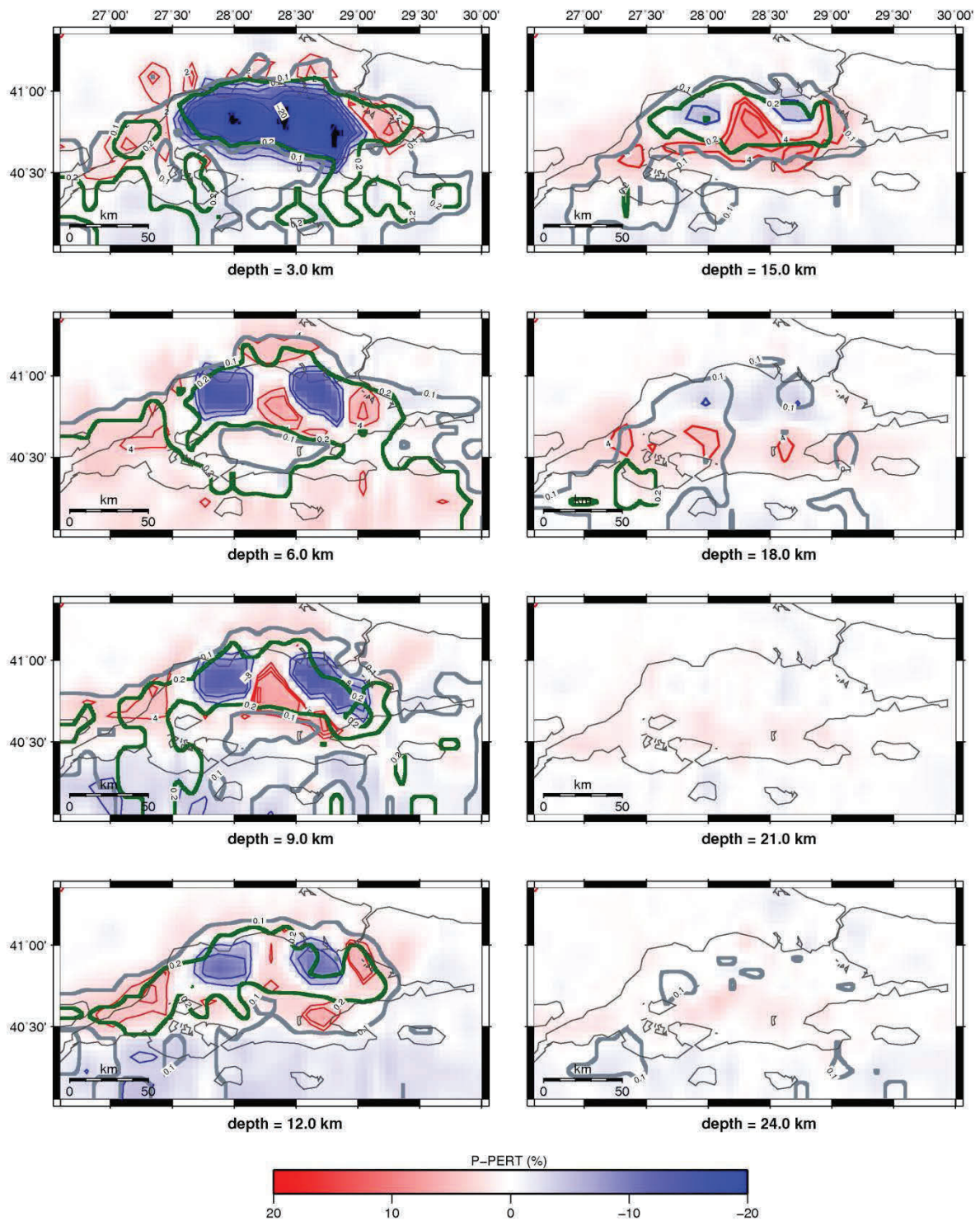
Figure 5. 5227. Characteristic test results and the synthetic RDE contours
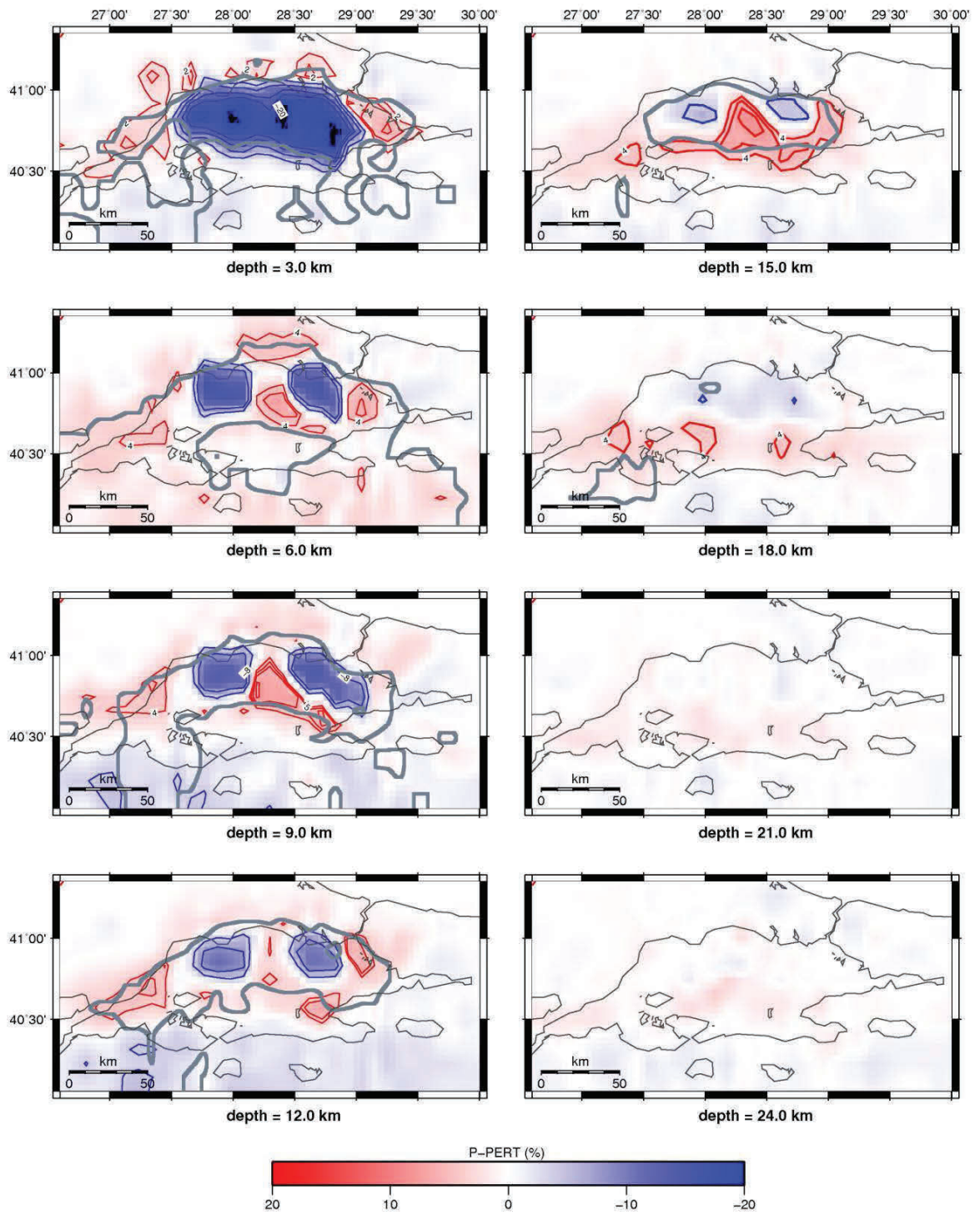
Figure 5. 28. Characteristic test results and the synthetic SF contours
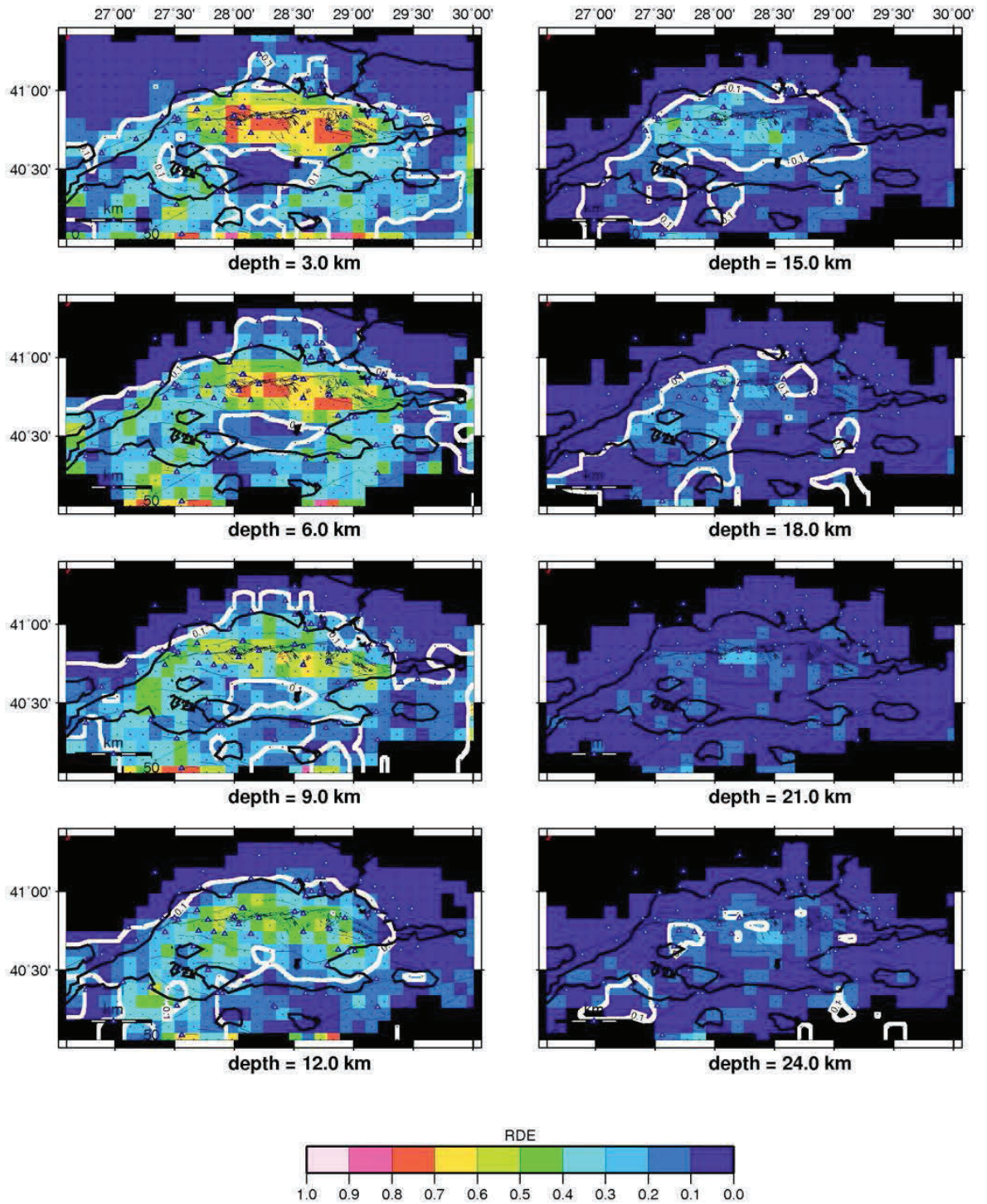
Figure 5. 29. RDE distribution of the resulting model and the synthetic RDE contour
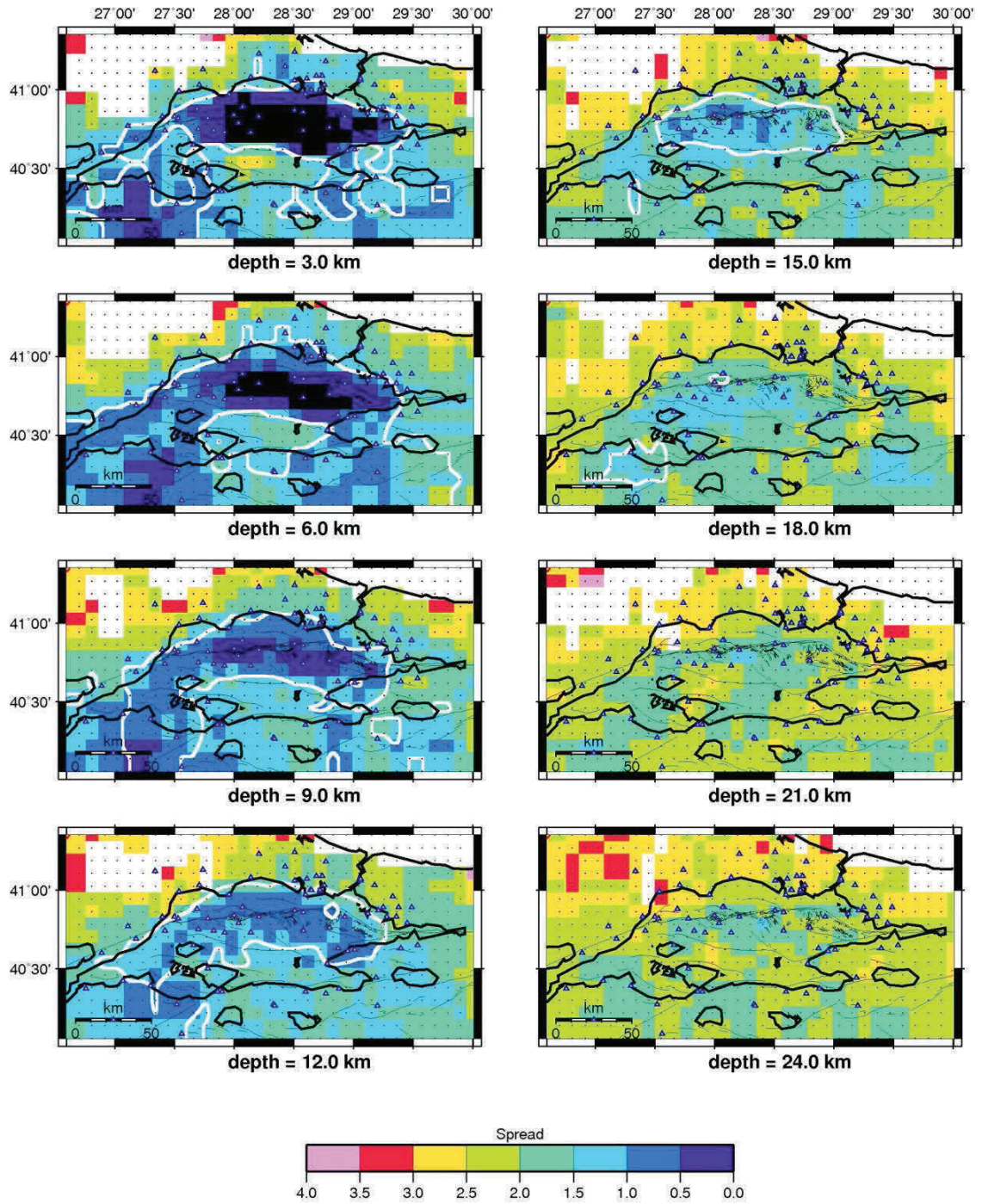
Figure 5. 30. SF distribution of the resulting model and the synthetic SF contour
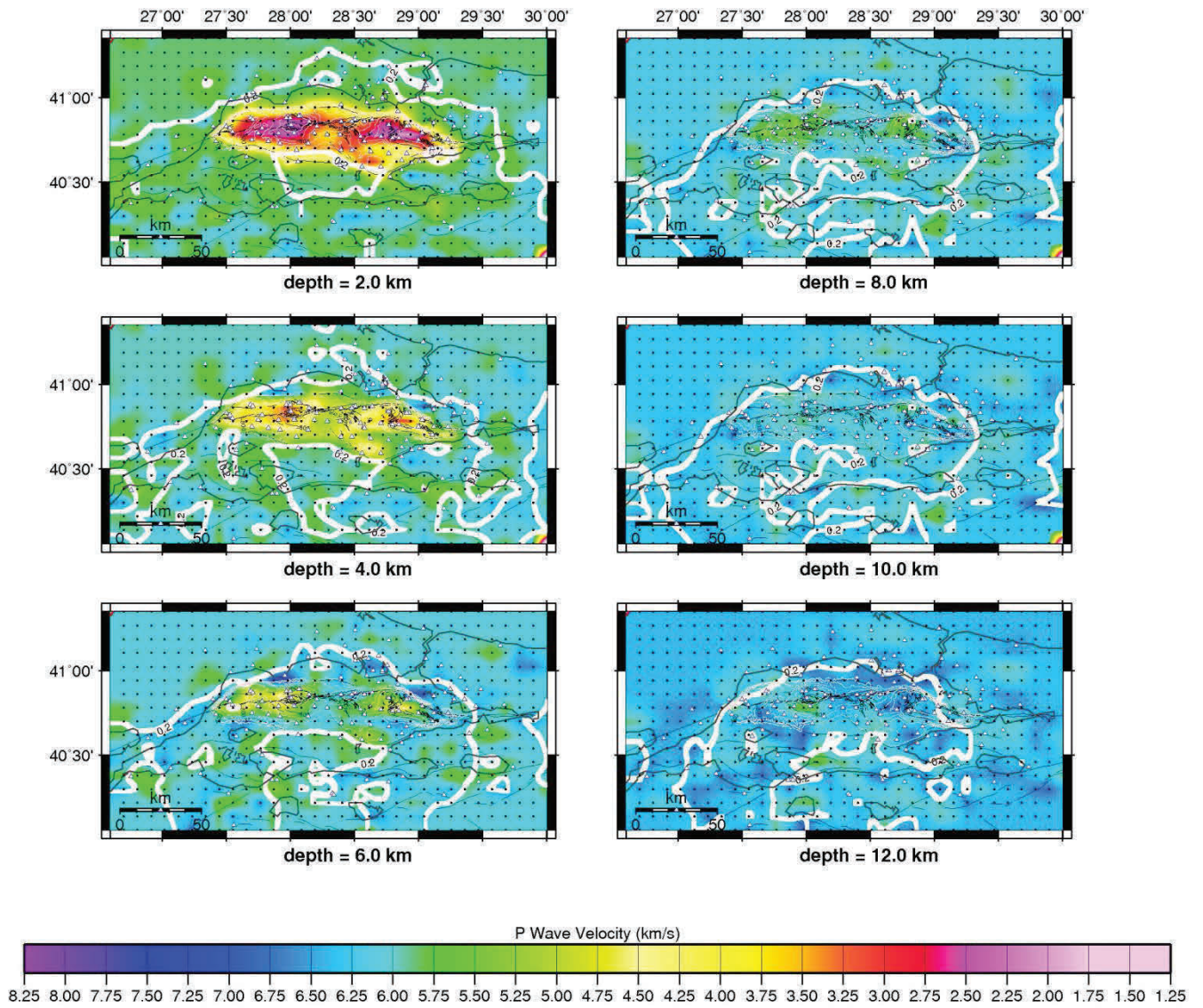
Figure 5. 31. Resulting model and the real 0.2 RDE contour 2-12 km
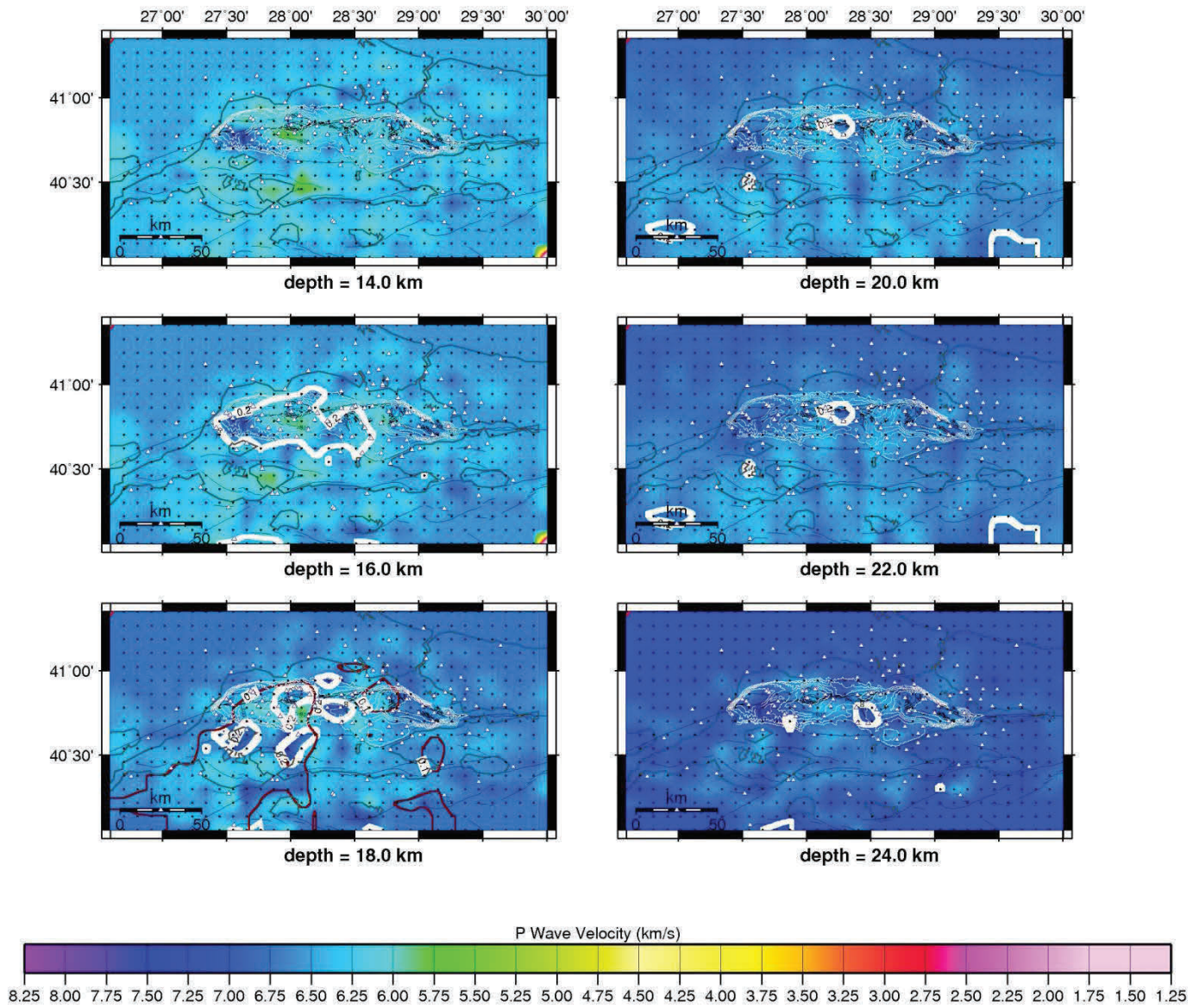
Figure 5. 57. Resulting model and real RDE 0.2 contour 14-24 km
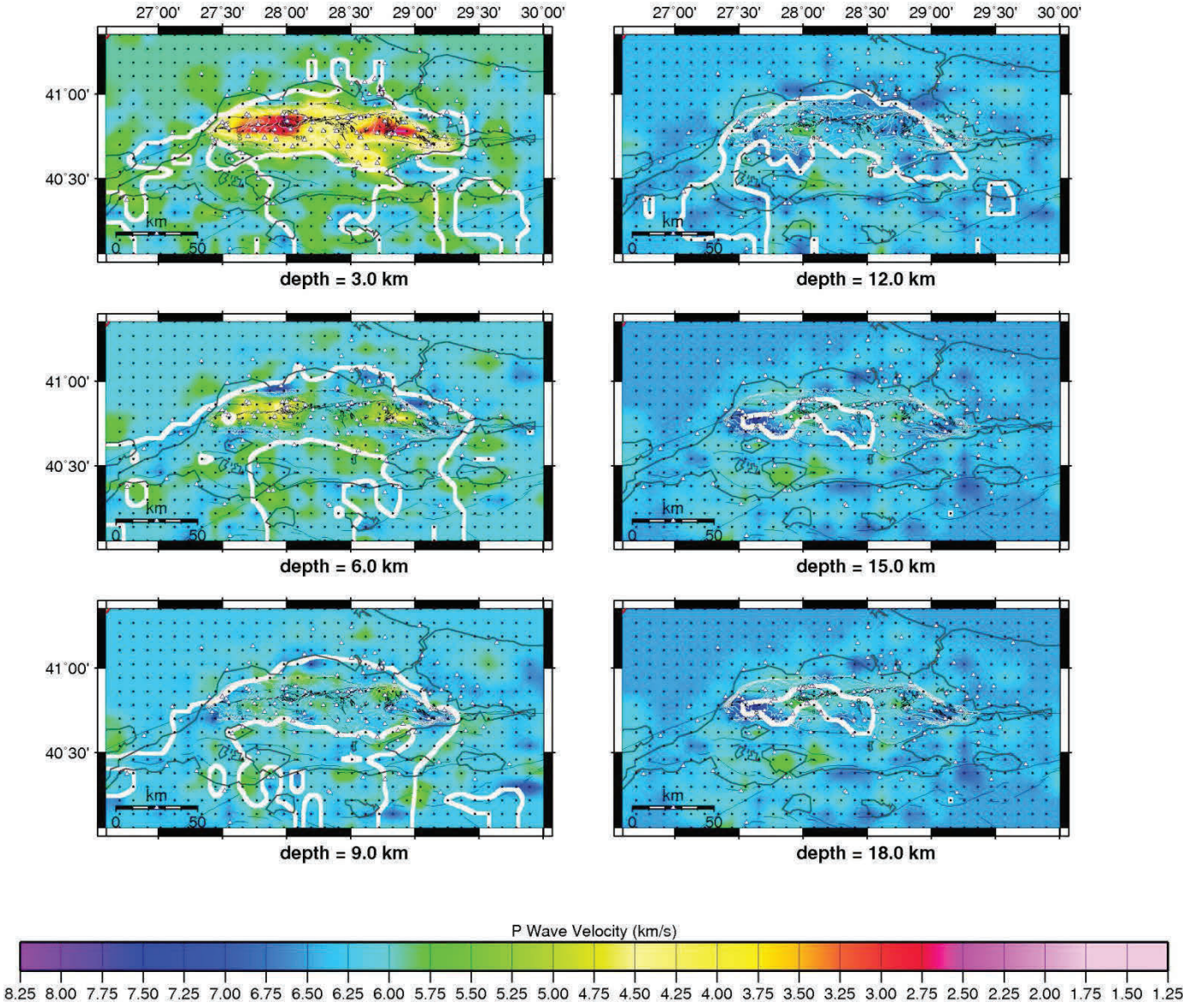
Figure 5. 32 Resulting model and real SF 1.15 contour 3-15 km

5.11 Relocation with the 3D P Wave Velocity Model

The study region has been compressing under a shear stress and twisting towards the southwest which make here a natural museum of geologic change of Turkey (Yılmaz, Y., Morphplogy of Turkey, Lecture notes, İTÜ, 2013). Because of the complexity of the Marmara Region with its sub-basins and an active complex fault branch creating large earthquakes, it is very important to make true locations to understand the seismicity of the region. The main aim of this study is to make better locations with a realistic 3D model. In this section we want to show the differences between a priori and a posteriori locations before and after the 3D inversion.

First, we will make a relocation of an earthquake occurred in Tekirdağ Basin 25th of July 2011, at 14 km. Secondly we will make a relocation of several earthquakes occurred in Marmara Region greater than a magnitude 3.
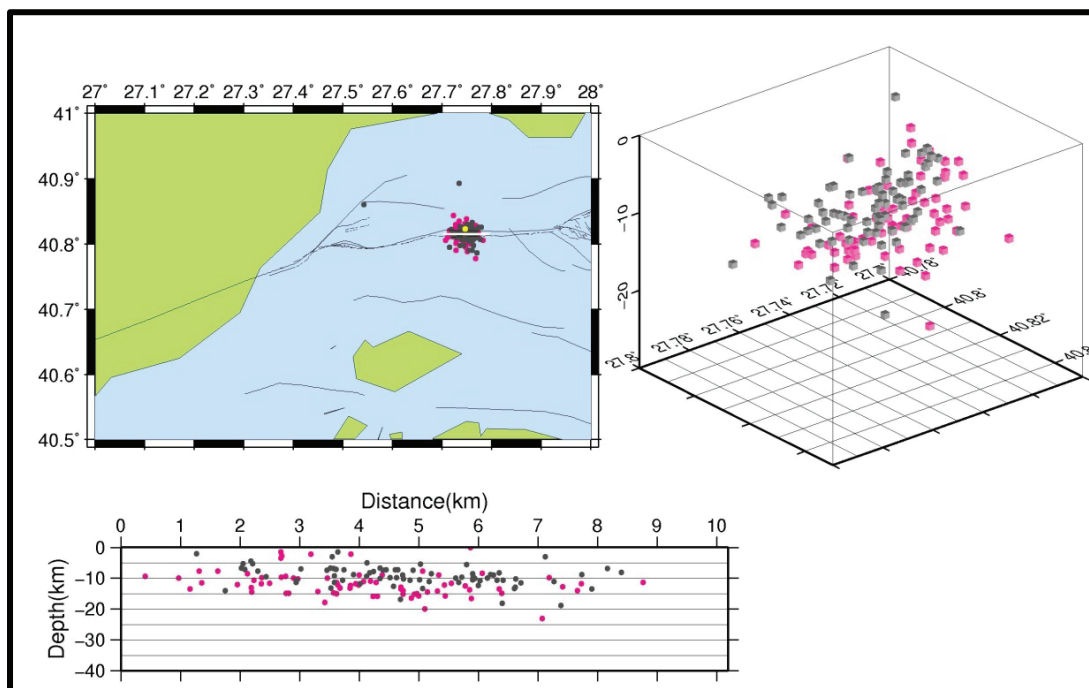
Figure 5. 33. The relocation of a large earthqake occured on 25th July 2011, Tekirdağ Basin

The gray dots show a posteriori locations. The pink dots show the priori locations.

The 3D location has a remarkable effect on the depths of the earthquakes. The aftershocks gathered and lifted. The locations recovered which is the result of a realistic 3D model.
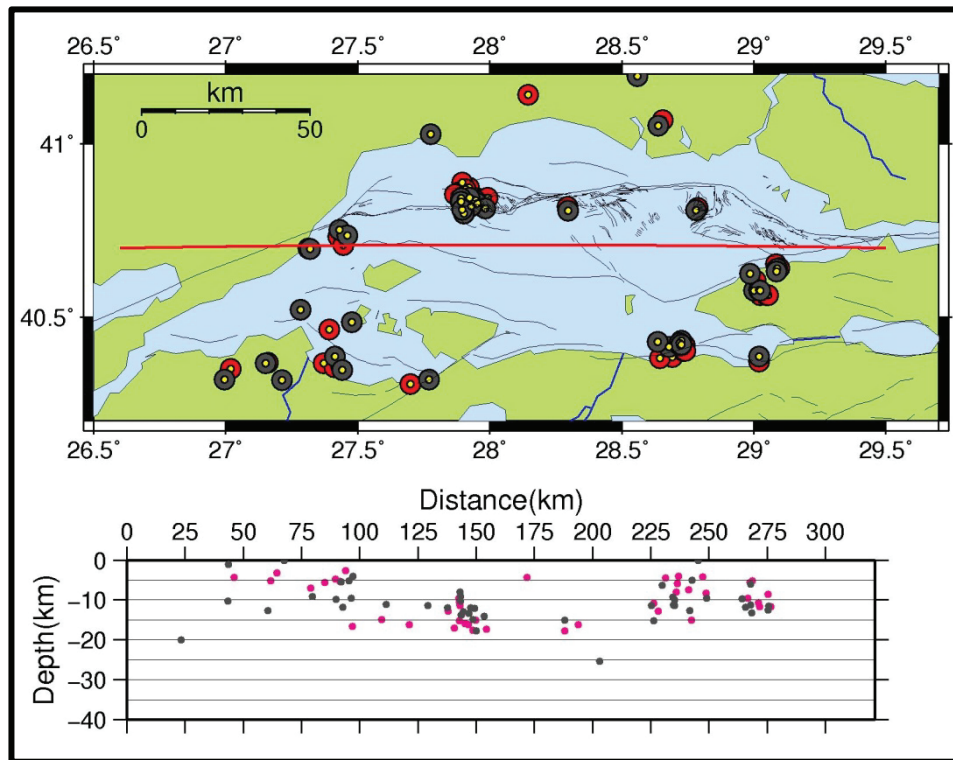
Figure 5. 60. The relocations of earthquakes larger than magnitude 3 in the Marmara Region

After making a relocation of the earthquakes at least magnitude 3, we observed that there is not only the depth of the events changed but also the locations changed too. On Figure 5.60, where gray dots are the latest locations and the pink ones the posteriori locations, the earthquakes lifted in the sea where the 3D model includes low sediment velocity not like the 1D minimum model. There is also a change around the Gemlik Bay because the initial model has been inverted in south more remarkably due to the dense earthquake data.

6. DISCUSSION AND CONCLUSSION

After defining the threshold values for quality estimators, we plotted the vertical and horizontal cross sections cutting across the faults, basins and the land. The checkerboard test lets us to decide until which depth the data coverage is acceptable and the resolution is fair. The RDE and SF limits of the well resolved areas defined as 0.2 and 1.15, respectively. The cross sections maps are masked according to the limit of the RDE with a transparent layer and hit count < 10 with darker transparent layer.

The P wave velocity variation along the profile AA' (Cutting across the Tekirdağ Basin) masked mostly on north with transparent color due to the low RDE values here (Figure 6.1). The red contour indicates the crystalline basement with 5.8 km/s. The deepest point of the basin in this cross section is 8 km. The black contour represents the boundary of the pre-kinematic basement with 4.5 km/s which is composed of Mesozoic carbonate. There is a velocity contrast between the basin rims and the basin infill due to the low velocity sedimentary infill surrounded by the carbonates of the outer layer. The white RDE contour covers both the pre-kinematic and the crystalline basement. The 6.3 km/s indicates the Conrad discontinuity and it is lifted towards the south of the Tekirdağ Basin. There is no significant velocity change and contrast under the land and the P wave velocity is between 6 km/s and 6.3 km/s.

In a recent study of Korkusuz (2012), Tekirdağ Basin region showed NW-SE trended transtentional state with almost purely normal fault mechanisms with some right lateral strike-slip and a few oblique components which is also similar to the results of the previous studies such as Armijo *et. al.* (2005), Sato *et al.* (2004) and Pınar (2003) but also reveals new sights. In our result the main fault seems to generate earthquakes at the north of the Tekirdağ Basin between 5 km and 17 km. The fault zone here is surrounded by the faster velocities of lower crust at least between 12 km and 17 km which can be accepted as an indicator of a vertical fault.

The results of Bayrakçı (2009), profile 2 which crosses the Tekirdağ Basin in NW-SE direction coincides to our results to some extent. In Figure 5.59 both our results and the shot tomography results show high velocity zones at the south of the basin. However, in

our results the crystalline basement continues to south unlike the result of the shot tomography. The RDE and SF values are reliable at the south of the basin in our results so we can interpret that the extension of the crystalline basement continues to south basin until about 4 km. The thickness of the crystalline basement increases at the north of the basin in both our study and shot tomography. There is another continuation of the crystalline basement at the north of the basin but it appears until about 2 km under the land.

On the cross section figures, black boxes indicate the faults. White contours inticate the RDE = 0.2. Dark transparent areas are Hit count < 10. Pink dots are earthquakes. Black contour indicates the pre-kinematic basement as 4.5 km/s. Red contour shows the crystalline crust boundary as 5.8 km/s. On the figures of previous studies (Bécel, 2006; Bayrakçı, 2009) the iso-velocity contours of 4.5 km/s and 5.7 km/s representing the pre-kinematic and crystalline basements are in green and blue respectively. The RDE is represented in black and SF in white.
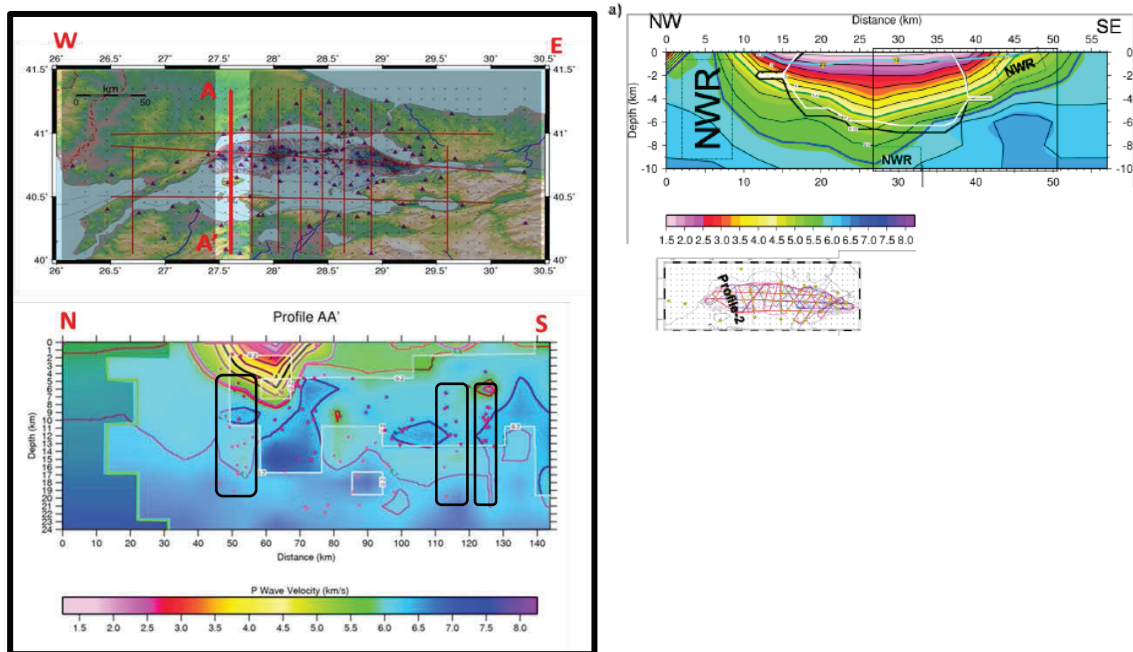
Figure 6. 1. Left hand side is the vertical cross section along profile AA'. a) NW-SE profile crossing the Tekirdağ Basin by shot tomography study of Bayrakçı, (2009).

Profile BB' cuts across the area located between Tekirdağ Basin and the Central Basin, closer to the eastern Tekirdağ Basin. The depth of the pre-kinematic basement shows similarity with respect to the Tekirdağ Basin. However, the width of the sediment layers here is a little bit larger than the Tekirdağ Basin and the shape of the basement dips north. The thickness of the Crystalline Basement is thicker than under the Tekirdağ basin. There is a low velocity zone indicating the crystalline basement with 5.8 km/s under the land and it has an extension under the west of the Kapıdağ Peninsula until about 10 km (Figure 6.2). The contour of Conrad discontinuity is lifted toward the sediments. The northern edge of the sediments has a northern dip cut by the active fault here. The fault crossing the basin at north is active between 5 km and 17 km like in the Tekirdağ Basin. The fast velocities around the fault appear between 12 km and 17 km but only at its south. The black box shows the locations of earthquakes indicating the faults. The box under the basin points to the northern main branch of the NAF cutting the basin. Another box dipping to north from the Kapıdağ Peninsula indicates the fault located at the north of the Kapıdağ Peninsula (See yellow arrow on the position map of the cross sections)
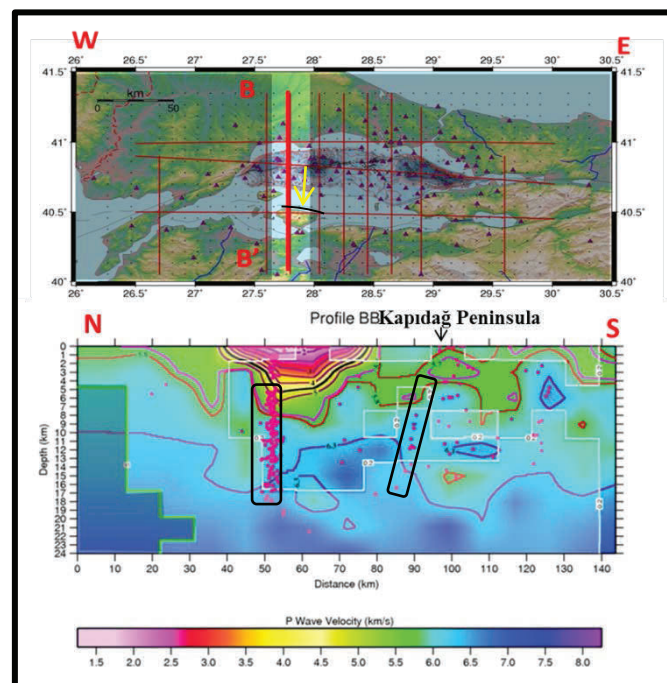
Figure 6. 2. The Velocity variation along BB' profile.

Profile CC' cuts across the Central Basin in the sea. The sedimentary basin infill reaches 6 km depth, dipping to north and the crystalline basement reaches 9 km where the basin ends. The crystalline basement reveals until 4 km at the north of the Central Basin. At the south of the basin the crystalline basement lifts up to 2 km. The northern and the southern areas of the Central Basin show asymmetry both for the land areas and the sea. Here, in this profile Conrad discontinuity is excluded by the RDE contour. Thus, the depth variation of the Conrad discontinuity is not interpreted in this profile. There is a high velocity zone like a wall at the north of the basin and main fault is settled right in front of this high velocity wall. The dip of the basin and the high velocity wall appear with almost same degree. The WARR study of Becel (2006), shows a flat basement in the basin. However, both the shot tomography study (Figure 6.3-a) and our results show a clear northern dip which is seems like to be stopped by a high velocity zone lifted up almost 10 km. So, we interpret this fault as a vertical fault bounded by a high velocity wall from north between 8 km and 18 km indicated by the black box. The crystalline basement seems to continue both under the north and south of the profile until maximum 2 km. The Kumburgaz Basin is detected by the MCS method with a northward fanning of sedimentary layers down to 3.5 km depth and a negative flower structure at the position of the strike-slip fault mapped at the sea bottom.
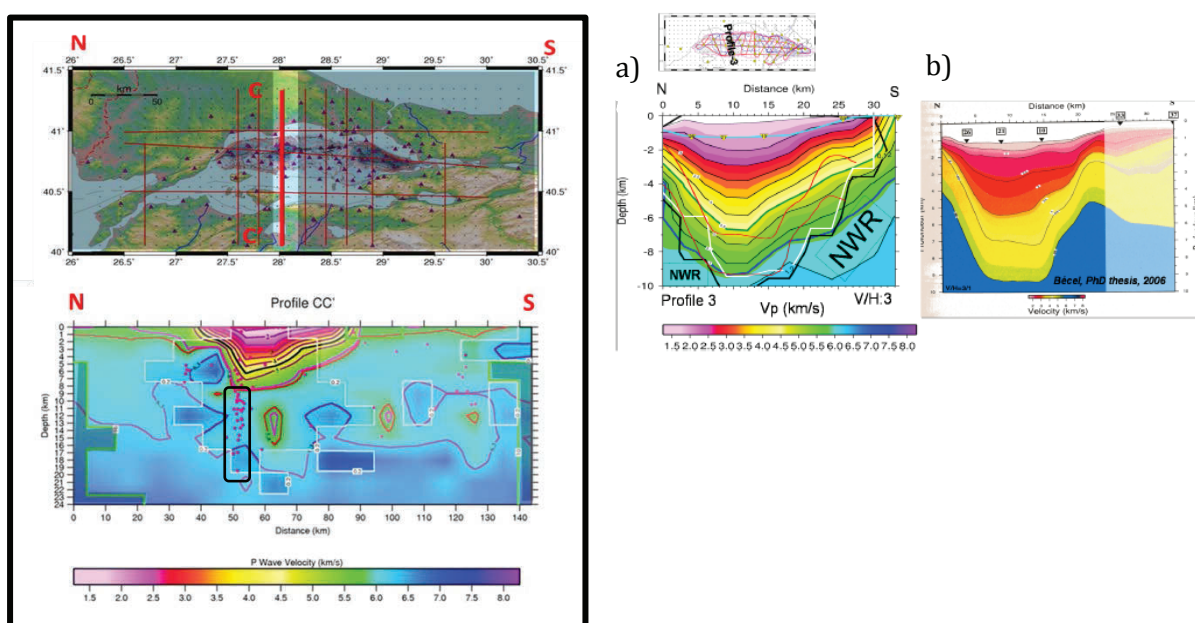
Figure 6. 3. Left hand side: The Velocity variation along CC' profile. a) Cenrtal basin cross section from the shot tomography. b) The depth section of profile 3 obtained by joint MCS and WARR modelling. NWR : not well resolved (Bayrakçı, 2009).

Profiles DD' and EE' cut across the Central High along two different lines. Profile DD' represents the eastern end of the Central Basin and Central High, while Profile EE' represents the western start of the Kumburgaz Basin and Central High.
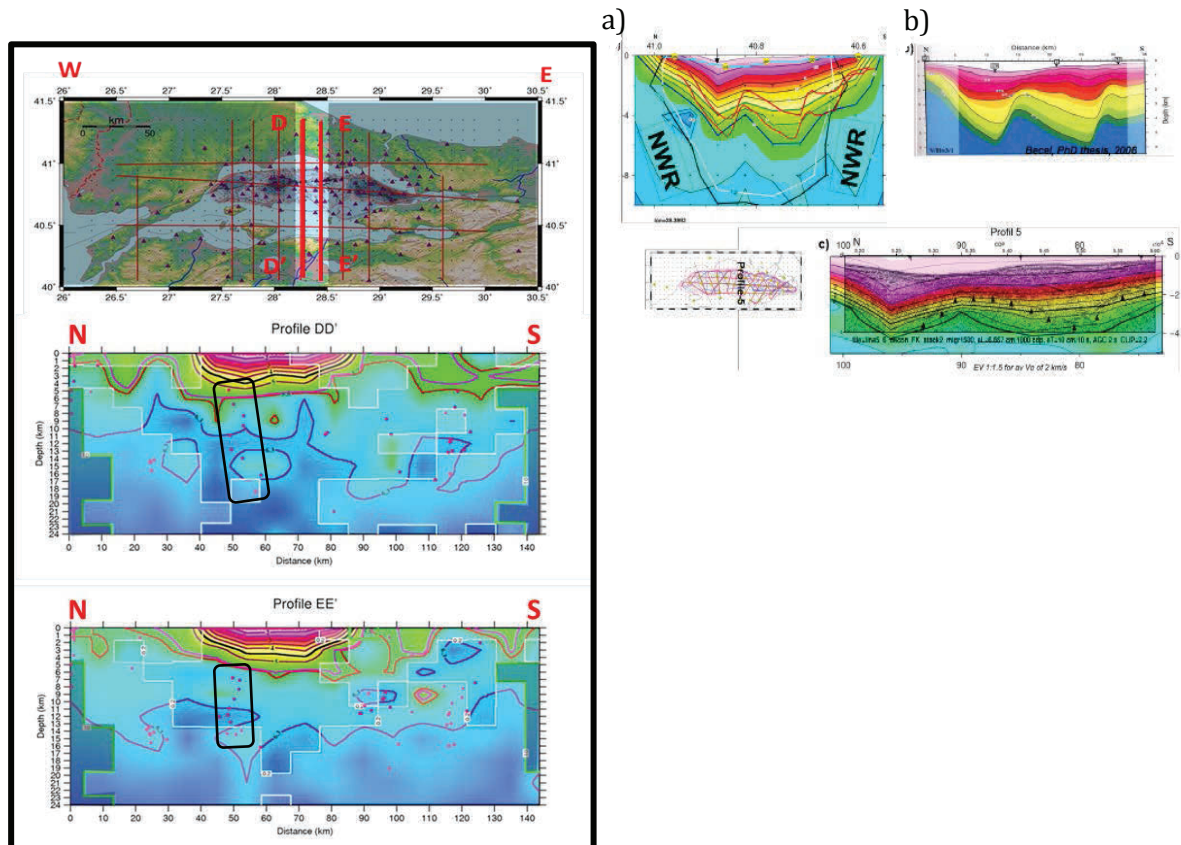
Figure 6.4. Left hand side: The vertical cross sections along Central High. The right hand side: The vertical cross section along the N-S profile-5 which cuts across the Central High as well as the western part of Kumburgaz Basin (Bayrakçı, 2009; Becel, 2006)

On Profile DD' the crystalline basement depth changes both under land and under the sea. We can say that the depth of the crystalline basement is thicker at the north of the sediment deposits. On profile EE' the crystalline basement seem to be quite thinned while reaching the land then appears until 4 km but this part of the model is out of the RDE contour. The earthquakes occurred at both profiles point out the location of the fault between 5 km and 20 km dipping to south (See black box on Figure 6.4).

The shot tomography profiles coincides the Profile EE'. The depths of pre-kinematic and crystalline basement are 4 km and 6 km, respectively on both local earthquake tomography and the shot tomography.

When move a little towards east to the western edge of the Çınarcık Basin, the depth contrast due to the rising up crystalline basement clearly seen between the western edge of Çınarcık Basin and the İmralı Basin. The crystalline basement rises up to 3 km from 8 km between two basins at the north of the İmralı Basin (Figure 6.5). On this profile the crystalline basement continues towards the north under land until maximum 3 km. The black box on Figure 6.5 shows the activity under the western edge of the İmralı Basin between 5 km and 15 km which is located within the upper crust.
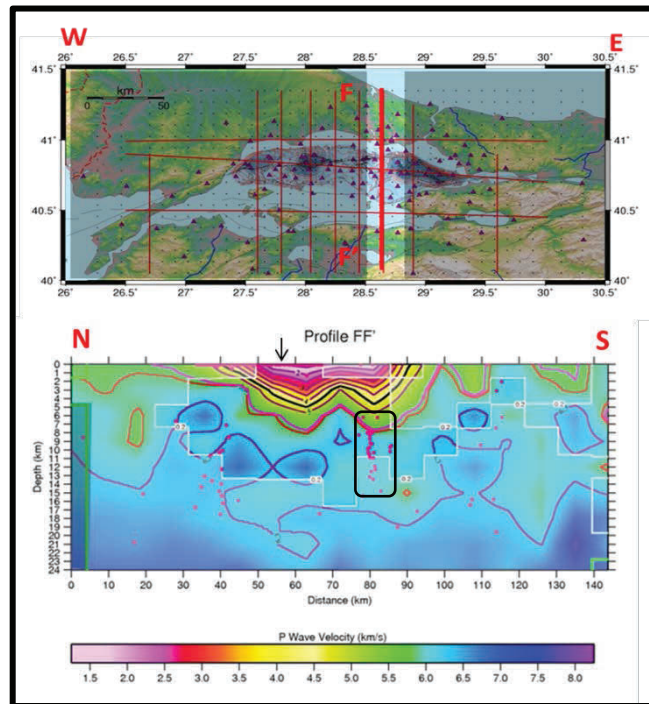
Figure 6.5. The vertical cross section along the profile cutting western edge of Çınarcık Basin and the İmralı Basin.

The Profiles GG', MM' and NN' cross Çınarcık Basin and İmralı basin along different lines. Profile GG' and MM' reveal almost symmetrical basin structure. There is no flat basement under the basin on these profiles. However, profile NN' appears like the shape of the Central Basin. The dip of the crystalline basement is to north by making a smooth angle creating a slightly flat basement. The depth of the crystalline basement under

the Çınarcık Basin reaches 8 km at both shot tomography and profiles MM' and NN'. However, the depth of the same basement reaches almost 10 km under the İmralı Basin while it is about 7 km in the shot tomography results. Although our results here are excluded by the RDE contour the similarity of the depth and shape of the İmralı Basin in the shot tomography profile and our study, we accept that these solutions are reliable. The crystalline basement continues towards south and north under the land until maximum 5 km. We see that the basin is surrounded by high velocity zones which might be an indicator of the normal faulting here. On Figure 6.6, the black boxes dip south under the İmralı Basin. The black boxes under the Çınarcık Basin are positioned vertically pointing out normal faulting which is also suggested by Bayrakçı (2009), Korkusuz (2012).
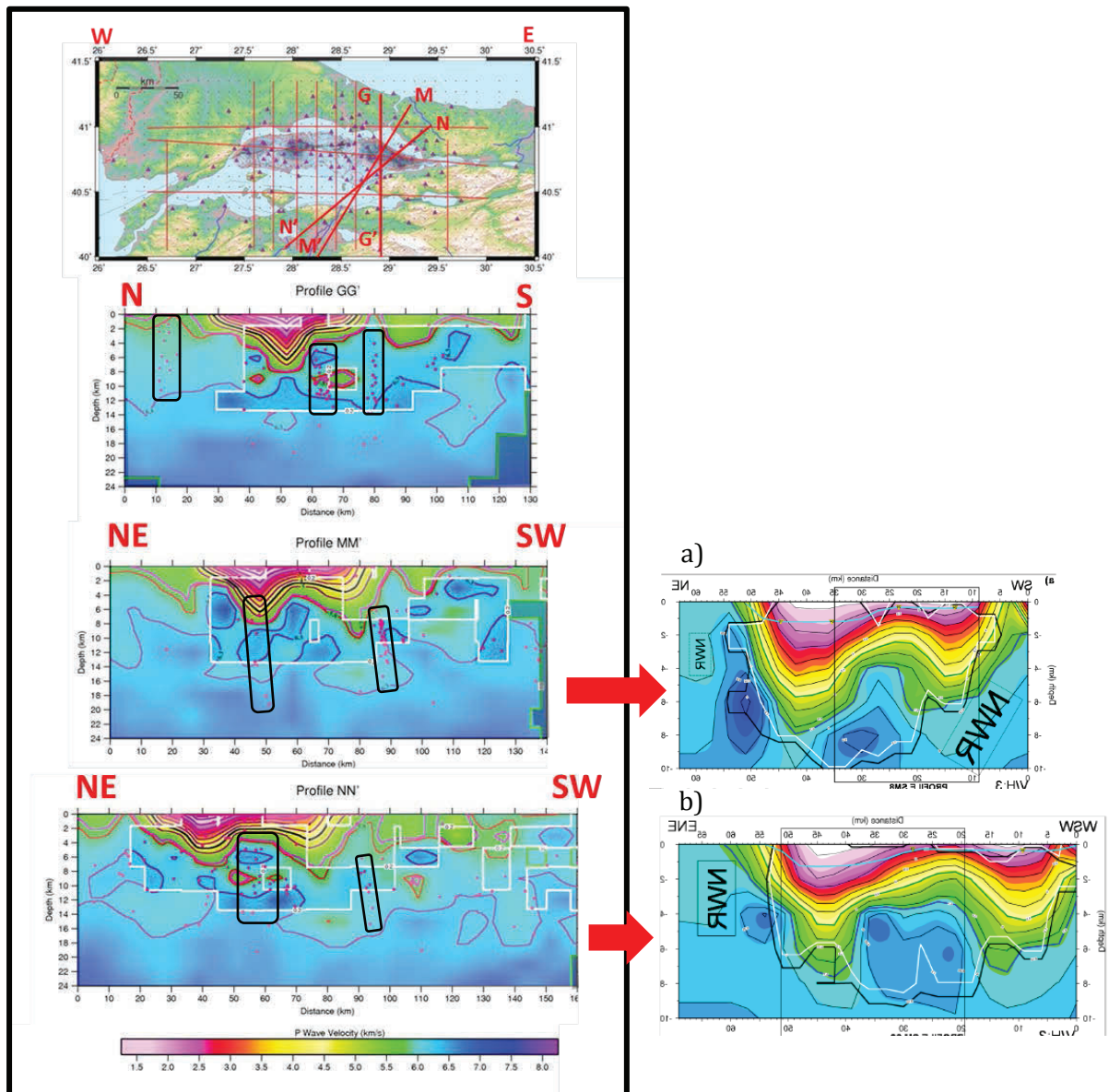
Figure 6.6. Left hand side: Cross sections from Çınarcık BasinRight hand side: a) The tomographic result along the SW-NE profile 8 which cuts across the eastern part of the Imralı Basin, the central part of the Çınarcık Basin and its north-eastern rim from the shot tomography (Bayrakçı, 2009).. b) The tomographic result along the profile-36 from shot tomography (Bayrakçı, 2009).

Kaya *et al.* (2013), revealed the 2D resistivity variation along two profiles crossing the Çınarcık Basin in NE-SW direction. On Figure 5.65 we showed the consistency between the vertical P wave variation along same profiles and the resistivity variation along the Profile P1 and Profile P2 from the MT study applied using sea bottom receivers (Kaya *et al.,* 2013). On Figure 6.7, R1 and R2 are resistive and C1, C2 and C3 are conductive zones. White dots are microseismic activity from 2007 to 2010 (Bulut, GFZ). Red arrows indicate the branches of NAF. The relatively low velocity zone under the İmralı Basin seems to match the conductor zone on the resistivity map until ~18 km on Profile P1. As they suggested that the seismogenic zones appear at the boundary of conductive and resistive zones, our locations with the 3D velocity model for both profiles match the boundaries of the conductive areas.
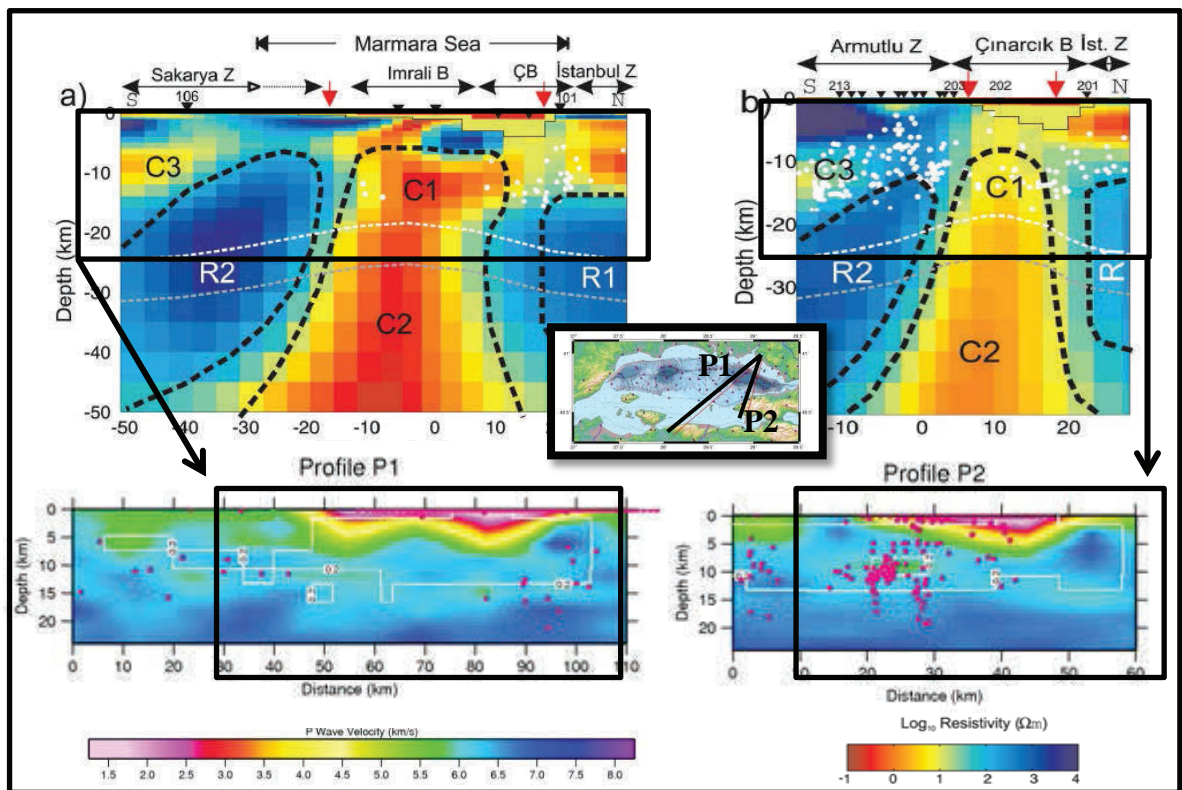
Figure 6.7. The vertical resistivity variation along Profile P1 and P2 (Kaya *et al.,* 2013) and P wave velocity variation along Profile P1 and P2 from local earthquake tomography.

Profiles II' and JJ' are observed in order to show the difference between the northern Marmara Region and the southern Marmara Region. Northern Profile II' appears with low velocities crystalline crust until about 11 km which is quite thick. It thins towards southern Marmara Region. Unlike to the profile II', Profile JJ' is reveals a thinner crystalline basement but it also thins towards the south. From these results we can interpret that the crystalline crust thins towards south but still thicker at west and thinner at east.
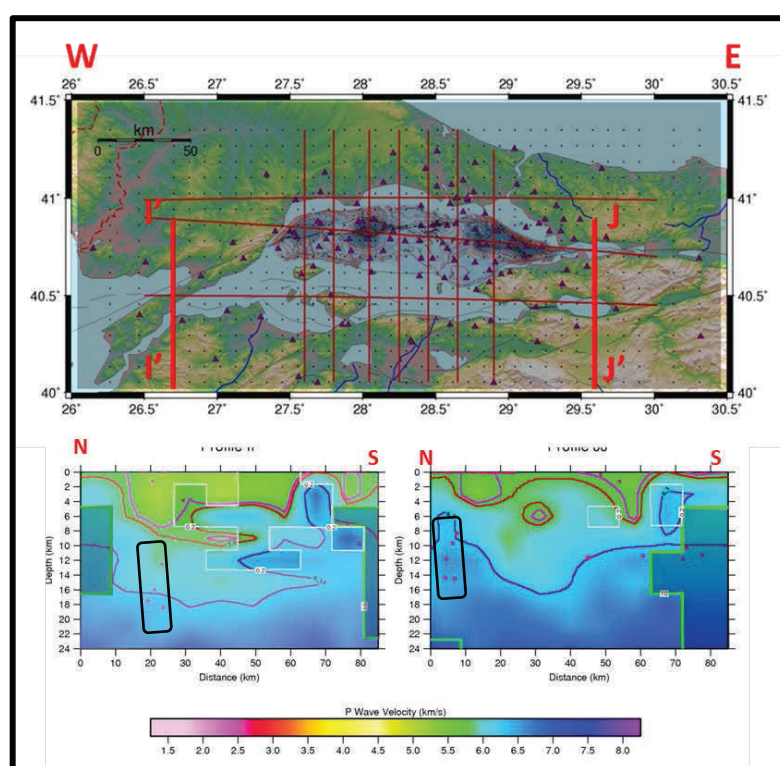
Figure 6. 8. Vertical profiles along Ganos High and
Armutlu High.

Profile KK', HH' and LL' are the horizontal cross sections along northern land, basin are and the southern land, respectively. The insufficient ray coverage at north causes the model to be discarded at almost all of the profile. However, we are able to guess the average crystalline basement and Conrad depth as 6 km and 14 km respectively (Figure 6.8- Profile KK'). Profile HH' shows the velocity variation along all the low velocity area. We can say that the average crystalline basement depth under the basin area is about 9 km with a thickness of 2-2.5 km. It also seems to be thinned towards west under the land area

as 1-1.5 km. We also can say that the shape Conrad discontinuity under the sedimentary deposits shows consistency with the shape of the basin area and changes between 10 and 20 km for the whole profile. Profile LL' shows a good ray sampling because of the dense earthquake information here. The Conrad discontinuity here appears deeper than the northern profiles at averagely 18 km. The cross section from the shot tomography, Profile 1, shows almost the same vertical velocity change and the results coincide with each other.

The black boxes of Profile HH' on the Figure 6.9 indicates that a fault under the sea is hold by a high velocity zone at least from one side. This proposal would be viewed if a denser data and grid used.
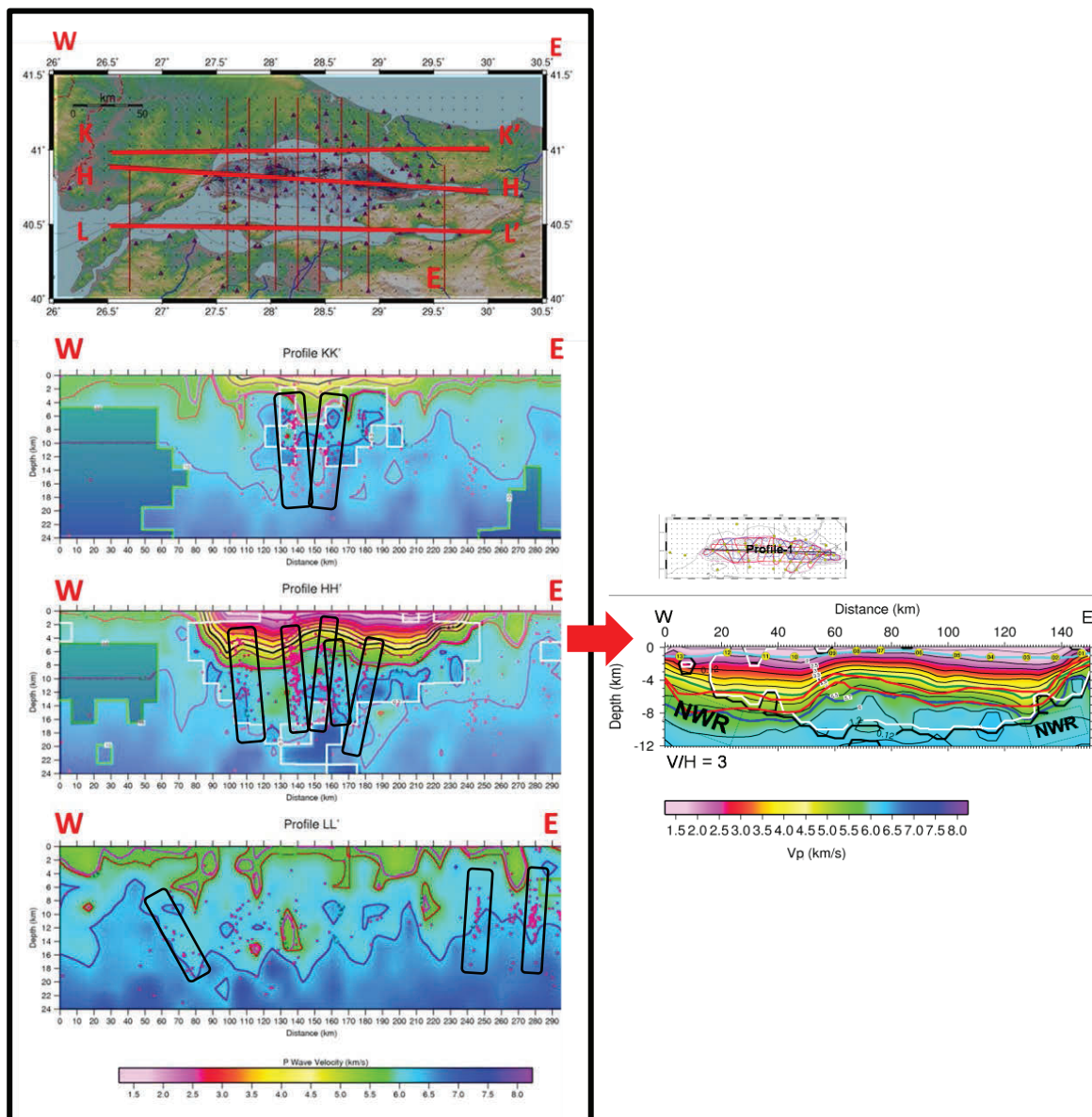
Figure 6. 9. Left hand side: Profiles KK', HH' and MM' corossing land on North sea from the basins and land from the South. Right hand side: The vertical section of tomographic result along E-W shot profile, Profile 1 from shot tomography.
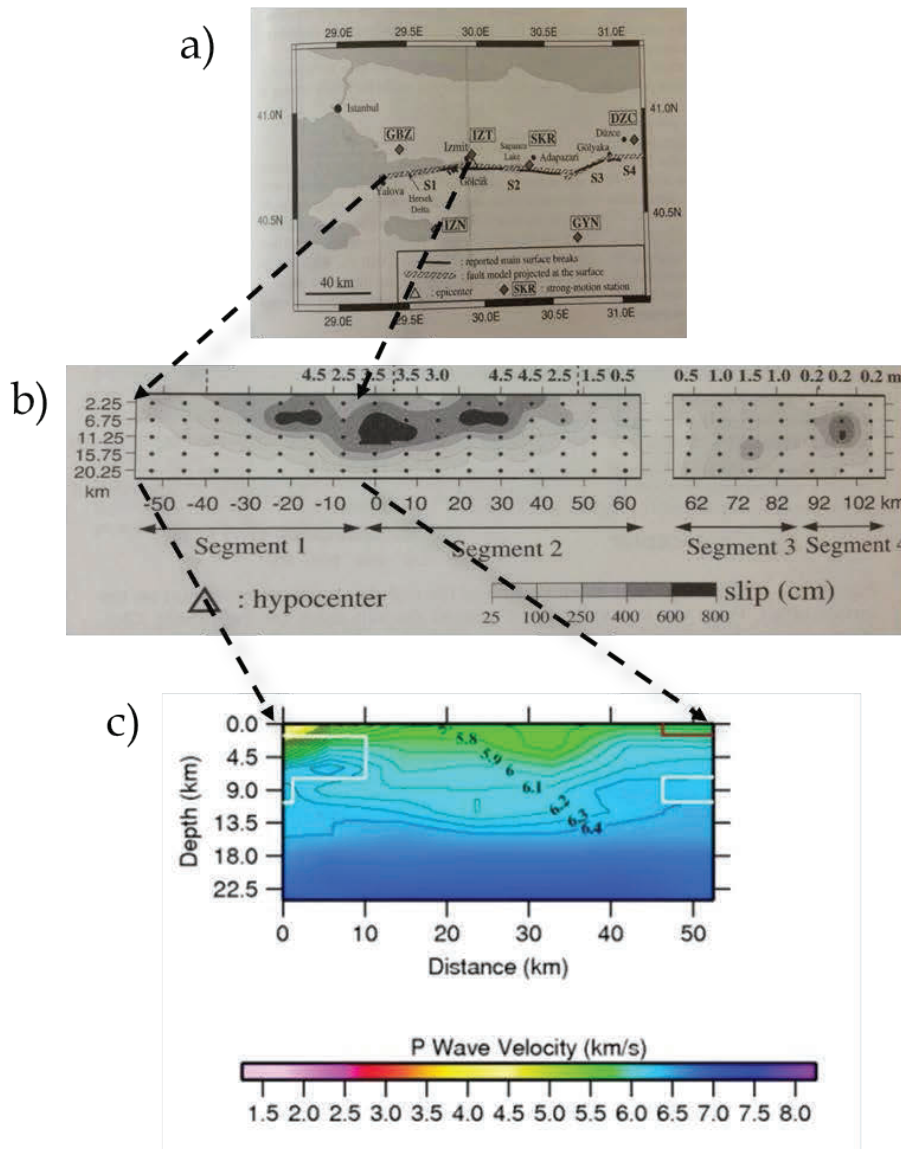
Figure 6. 2. Slip rate and P wave velocity comparision along the segment 1 stated in Delois, (2002).

We have investigated relation of the slip rate with the seismic tomography results. This was possible only in the Eastern Marmara Region. The fault position map of the North Anatolian Fault in Eastern Marmara Region is shown in Figure 6.10a (Delois, 2002). Figure 6.10-b shows the slip distribution along four segments of the fault after 17 August 1999 earthquake. It can be assumed for the Segment 1 that the slip values increases where $V_P > 6$ km/s after 4.5 km. Thus, it can be suggested that the slip rate gained higher values under the crystalline basement. Unfortunately, our data coverage is not enough to compare the slip distribution along other faults segments with the P wave velocity distribution.

In the present study we showed the 3D velocity variation in Marmara Region. Thanks to the previous studies (Becel, 2006, Becel, 2009, Bayrakçı, 2009), we are able to compare the results with MSC (multi-channel seismic), WARR (wide angle reflection, refraction) and shot tomography studies applied in Marmara Sea. However, these studies do not include velocity information from the land stations. So, we discuss the inversion results of the land areas with respect to the synthetic test results. The shot tomography study applied in Marmara Sea only gives information of upper crust until 12 km but the WARR and MSC studies revealed both the whole crust and the Moho. In our study we could not interpret the results of the inversion after 24 km because of the low resolution.

The velocities of the pre-kinematic basement and the crystalline basement are defined as 4.5 km/s and 5.7 km/s, respectively (Bécel, 2006; Bécel *et al.,* 2009). The contours of the threshold values of the quality estimators (RDE, SF) were estimated through the inversion result of the 3rd combined model. They give a reliable idea of the well resolved zones. All the cross sections are consistent with the previous studies; thanks to the shot data from the multi-method survey Seismarmara (2001), we improve the ray coverage in the center of the study. The entire basin area is well resolved according to the RDE, SF and DWS values. Only the northern land area is not well resolved compared to the rest of the study region.

In the previous shot tomography study, the velocity structure at the western edge of the Tekirdağ Basin could not be understood because of the low resolution there. In the result of the 3rd combined model, the RDE, SF, DWS and hit count have better values than the previous study. Thus, we can make interpretation on the results around Tekirdağ Basin due to the DWS >1000, which we rely on until 21 km.

The sediments deposits in the sea appear with very low velocities as 3-3.5 km/s with almost the same depths between 5 and 6 km. The velocity contrast between the land and sea becomes negligible after 10 km. The crust after 10 km has the average velocity between 6 km/s and 6.3 km/s until Conrad discontinuity. Although we had an idea of the upper limit of the lower crust from the inversion results, we do not observe a clear depth variation of the Conrad. We can still say that under every basin the Conrad contour is lifted towards the basin which is also suggested by Bécel (2009).

Apart from comparision of results with other seismological studies we also compared our results with geomagnetic study done in the Marmara Region. The aeromagnetic study of Ateş (2003), showed that anomalies of the Marmara region suggests that the Curie isotherm level lies 6–8 km shallower than on the continent. Also the base of sedimentary layer is at the same depth as the Curie depth under the sea. So, we can assume that the low velocity deposits of the sub-basins of Marmara Sea are the reason for the positive aeromagnetic anomalies suggested by Ateş (2003).

We do not observe a similarity between Western High and Central High. The pre-kinematic basement under the Western high is located at 5.5 km while it is located at 4 km under the Central Basin. Bayrakçı (2009), suggested that this structure of the Western high is most likely resulted from that it is a relief formed by the sediments rather than being formed by a basement which rises up.

The İmralı and Çınarcık Basins are separated from each other with contrast high velocity zone. The thickness of the sedimentary infill of the İmrali basin is close to the Çınarcık basin and they are separated from each other by the crystalline basement which makes a rise up to 2-3 km. From 12 km to 18 km we observe a high velocity zone compare to its vicinity located north of the Kapıdağ Peninsula in NW-SE direction which can be raleted to the rise of the lower crust here. However, we do not observe high velocity zones as significant as under the Tekirdağ Basin which might result from the insufficient ray coverage here.

The lower crust velocity information showed similarities under Central Basin and the Çınarcık Basin. These are surrounded by high velocity zones which can be accepted as an indicator of the normal faulting.

Between 8 km and 12 km the northern edge of the Europian side of the Marmara Region appears with 6-6.5 km/s. The vertical profiles II' and JJ' reveals that the crystalline basement is thicker at the western Marmara Region and thinner at the eastern Marmara Region.

It is also observed that the lower crust seem to make prolongations towards the sub-basins of Marmara Sea between 10-18 km which might be resulted from the strong shear deformation in the region.

REFERENCES

Altıner, D., A. Koçyiğit, A.Farinacci, U. Nicosia, M.A. Conti, 1991, "Jurassic, Lower Cretaceous stratigraphy and paleo geographic evolution of the southern part of north western Anatolia", *Geologica Romana,* 28, pp. 13-80.

Altunel, E., A.A. Barka, H.S. Akyuz, 2000, "Slip distribution along the 1912 Murefte-Sarkoz earthquake, North Anatolian Fault, Western Turkey". In: Barka, A.A., O. Kozac, S. H. Akyuz, E. Altunel (Eds.), "1999 Izmit-Duzce Earthquakes: Preliminary Results", *Istanbul Technical University Publ.,* pp. 341-349.

Ambraseys, N.N., J. A. Jackson, 1998, "Faulting associated with historical and recent earthquakes in the Eastern Mediterranean region", *Geophysical Journal International,* 133, pp. 340-406.

Armijo, R., N. Pondard, B. Meyer, B. Mercier de Lépinay, G. Uçarkus, the MARMARASCARPS cruise party, 2005, "Submarine fault scarps in the sea of marmara pull-apart (north anatolian fault): Implications for seismic hazard in İstanbul", *Geochemistary Geophysics Geosystems*, 6 ,Q06009, DOI:10.1029/2004GC000896.

Ates, A., P. Kearey, 1993, "Structure of the Blackdown Pericline, Mendip Hills from gravity and seismic data", *Journal of Geological. Society (London),* 150, 729–736.

Aydın, Y., 1974, Etude pétrographique et géochimique de la parte centrale du Massif d'Istranca (Turquie), PhD Thesis, Université de Nancy, pp. 131.

Barış, Ş., J. Nakajima, A. Hasegawa, Y. Honkura, A. Ito, and B. Üçer, 2005, "Three-dimensional structure of Vp, Vs and Vp/Vs in the upper crust of the Marmara region, NW Turkey", *Earth Planets Space*, Vol. 57, pp. 1019-1038.

Bayrakçıi G., 2009, Hétérogénéité 3D de la croûte supérieure sous la Mer de Marmara: tomographie sur une grille de sismomètres fond de mer et de profils de tirs, Ph. D. Thesis, Institut de Physique du Globe de Paris Université Denis Diderot.

Bécel, A., 2006, Structure Sismique de la faille Nord Anatolienne en Mer de Marmara, Ph.D. Thesis, Institut de Physique du Globe de Paris.

Bécel, A., M. Laigle, B. de Voogd, A. Hirn, T. Taymaz, A. Galvé, H. Shimamura, Y. Murai, J. Lépine, M. Sapin, & S. Özalaybey, 2009, "Moho, crustal architecture and deep deformation under the North marmara trough, from the seismarmara leg1 offshore-onshore reflection-refraction survey". *Tectonophysics,* Vol. 467, pp. 1–21.

Bécel, A., M. Laigle, B. Voogd, A. Hirn, T. Taymaz, S. Yolsal-Cevikbilen, H. Shimamura, 2010. "North Marmara Trough architecture of basin infi ll, basement and faults, from PSDM refl ection and OBS refraction seismics", *Tectonophysics*, Vol. 490, pp. 1–14, DOI:10.1016/j.tecto.2010.04.004.

Benz, H. M., B. Chouet, P. B. Dawson, J. c. Lahr, R. A. Page, J. A. Hole, 1996, "Three-dimensional P and S wave structure of redoubt volcano, Alaska", *Journal of Geophysical Research,* Vol. 101, pp. 8111–8128.

Crosson, R. S., 1976, "Crustal structure modelling of earthquake data : 1.simultaneous least squares estimation of hypocenter and velocity parameters", *Journal of Geophysical Research*. Veol. 81, pp. 3036–46.

Dean, W.T., F. Martin, O. Monod, O. Demir, R. B. Rickards, P. Bultynck, N. Bozdogan, 1997, "Lower Paleozoic stratigraphy, Karadere–Zirze area, Central Pontides. In: Göncüoglu, M.C., Derman, A.S. (Eds.), Early Palaeozoic Evolution in NW Gondwana", *Turkish Association of Petroleum Geologists,* Vol. 3, pp. 32–38 (special publications).

Delois, B., D. Giardini, P. Lundgren and J. Salichon, 2002, "Joint Inversion of InSAR, GPS, Teleseismic, and Stron-Motion Data for Spatial and Temporal Distribution of Earthquake Slip: Application to the 1999 İzmit Mainshock", Bulletin of the Seismological Society of America, Vol. 92, No. 1, pp. 278-299.

Denli, A., 2008, 3-D Velocity structure of eastern Marmara Region from local earthquake tomography, M.Sc. Thesis, KOERI., B.U.

Dolu, E., E. Gökaşan, E. Meriç, M. Ergin, T. Görüm, H. Tur, B. Ecevitoğlu, N. Avşar, M. Görmüş, F. Batuk, B. Tok, O. Çetin, 2007, "Quaternary evolution of the Gulf of Izmit (NW Turkey): a sedimentary basin under control of the North Anatolian Fault Zone", *Geo-Marinne Letters,* 27/6, pp. 355–381.

Eberhart-Phillips, D., 1990, "Three dimensional p and s velocity structure in the coalinga region", *California. Journal of Geophysical Research*, Vol. 95, pp. 15,343–15,363.

Faridfathi, F. Y., M. Ergin, 2011, "Holocene sedimentation in the tectonically active Tekirdag Basin, western Marmara Sea, Turkey", *Quaternary International,* Vol. 261, pp. 75-90

Gazioğlu, C., Z.Y. Yücel, E. Doğan, 2005, "Morphological features of major submarine landslides of Marmara Sea using multibeam data", *Journal of Coastal Research*, Vol. 21 (4), 664–673.

Gökaşan, E., B. Alpar, C. Gazioğlu, Y. Z. Yücel, B. Tok, E. Doğan, C. Güneysu, 2001, "Active tectonics of the İzmit Gulf (NE Marmara Sea): from high resolution seismic and multi-beam bathymetry data", *Marine. Geology*, Vol. 175 (1-4), pp. 271–294.

Gökaşan, E., T. Ustaömer, C. Gazioğlu, Y. Z. Yücel, K. Ozturk, H. Tur, B. Ecevitoglu, B. Tok, 2003, "Morpho-tectonic evolution of the Marmara Sea inferred from multi-beam bathymetric and seismic data", *Geo Marine Letters*, Vol. 23 (1), pp. 19–33.

Görür, N., A. Okay, 1996, "A fore-arc origin for the thrace basin, NW Turkey", *Geol Rundsch,* Vol. 85, pp. 662–668.

Görür, N., M. N. Çağatay, M. Sakınç, M. Sümengen, K. Şentürk, C. Yaltrak, A. Tchapalyga, 1997, "Origin of the Sea of Marmara as deducted from the Neogene to

Quaternary paleogeographic evolution of its frame", *International Geology Review*, Vol. 39, pp. 342–352.

Gürbüz, C., M. Aktar, M., H. Eyidoğan, A. Cisternas, H. Haessler, A. Barka, M. Ergin, N. Türkelli, O. Polat, B. Üçer, S. Kuleli, Ş. Barış, B. Kaypak, T. Bekler, E. Zor, F. Biçmen, A. Yörük, 2000, "The seismotectonics of the Marmara region (Turkey): results from a microseismic experiment", *Tectonophysics*, Vol. 316, pp. 1-17.

Haslinger, F., E. Kissling, J. Angsore, D. Hatzfeld, E. Papadimitru, K. Karakostas, V. Makropoulos, Y. Peter, 1999, "3D crustal structure from local earthquake tomography around the gulf of arta (ionian region, NW greece)", *Tectonophysics*, Vol. 304, pp. 201–218.

Haslinger, F., E. Kissling, 2001, "Investigating the effects of 3-d ray tracing methods in local earthquake tomography", *Physics of the Earth and Planetary Interiors*, Vol. 123, pp. 103–114.

Husen, S., E. Kissling, E. Flueh, 2000, "Local earthquake tomography of shallow subduction in North chile: A combined onshore and offshore study", *Journal of Geophysical Research*, Vol. 155, pp. 11–32.

İmren, C., X. Le Pichon, C. Rangin, C., E. Demirbag, B. Ecevitoğlu, N. Görür, 2001, "The North Anatolian Fault within the Sea of Marmara: a new evaluation based on multichannel seismic and multi-beam data", *Earth Planetary Science Letters*, Vol. 186, pp. 143–158.

Kalafat, D., 1995, Anadolu'nun Tektonik Yapıların Deprem Mekanizmalar Açısından İrdelenmesi, Ph.D. Thesis, Institute of Marine Sciences and Management, Istanbul University.

Karabulut, H., M-P. Bouin, M. Bouchon, M. Dietrich, C. Cornou, M. Aktar, 2002, "The seismicity in the Eastern Marmara Sea after the 17 August 1999 İzmit Earthquake", *Bullutin of Seismological Society of America*, Vol. 92, pp. 387-393.

Karabulut, H., S. Özalaybey, T. Taymaz, M. Aktar, O. Selvi, A. Kocaoğlu, 2003, "A tomographic image of the shallow crustal structure in the Eastern Marmara", *Geophysical Research Letters*, Vol. 30, pp. 10-1–10-4.

Karabulut H., J. Schmittbuhl, S. Özalaybey, O. Lengliné, A. Kömeç-Mutlu, V .Durand, M. Bouchon, G. Daniel, M. P. Bouin, 2011, "Evolution of the seismicity in the eastern Marmara Sea a decade before and after the 17 August 1999 Izmit earthquake", *Tectonophysics*, Vol. 510, pp. 17–27

Kaşlılar-Özcan, A. Boztepe-Güney, B. Ecevitoğlu, 2002, "Estimates of attenuation structure in the Çınarcık Basin of the Marmara Sea, northwest Turkey", *Physics of the Earth and Planetary Interiors,* Vol. 130, pp. 1–16

Kaya T., T. Kasaya, B. Tank, Y. Ogawa, M. Tunçer, N. Oshiman, Y. Honkura, and M. Matsushima, 2013, "Electrical characterization of the North Anatolian Fault Zone underneath the Marmara Sea, Turkey by ocean bottom magnetotellurics", *Geophysical Journal International*, DOI: 10.1093/gji/ggt025

Kissling, E. 1988, "Geotomography with local earthquake data", *Reviews of Geophysics*, Vol. 26, pp. 659–698.

Kissling, E., W. L. Ellsworth, D. Eberhart-Phillips, U. Kradolfer, 1994, "Initial reference models in local earthquake tomography", *Journal of Geophysical Research*, Vol. 99, pp. 19.635-19.646.

Korkusuz, Y., 2012, The Present Day Stress States in the Marmara Region, M.Sc. Thesis, KOERI, B.U.

Laigle, M., A. Hirn, M. Sachpazi, N. Roussos, 2000, "North aegean crustal deformation: a new active fault imaged to 10 km depth by marine reflection seismics", *Geology* Vol. 28, pp. 71–74.

Laigle, M., A. Bécel, B. de Voogd, A. Hirn, T. Taymaz, S. Ozalaybey, M. of SEISMARMARA Leg1 Team, 2008, "A first deep seismic survey in the sea of marmara : Deep basins and whole trust architecture and evolution", *Earth Planet. Science Letters*, Vol. 270, pp. 168–179.

Le Pichon, X., A.M.C. Şengör, E. Demirbağ, C. Rangin, C. İmren, R. Armijo, N. Görür, N. Çağatay, B. Mercier de Lepinay, B. Meyer, R. Saatçılar, B .Tok, 2001, "The active Main Marmara Fault", *Physics of the Earth and Planetary Interiors*, Vol. 192, pp. 595-616.

Lévèque, J. J., L. Rivera, G.Wittlinger, 1993, "On the use of checker-board test to assess the resolution of tomographic inversion", *Geophysical Journal International*, Vol. 115, pp. 313–318.

McKenzie, D.P., 1972, "Active tectonics of Mediterranean region", *Geophys. J. R. Ast. Soc.,* Vol. 30, pp. 109-185.

Moore, W.J., E.H. McKee, Ö. Akinci, 1980, "Chemistry and chronology of plutonic rocks in the Pontid Mountains, northern Turkey", *European Copper Deposits*, Vol. 1, pp. 209–216.

Okay, A.I., O. Tüysüz, 1999, "Tethyan sutures of northern Turkey. In: Durand, B., Jolivet, L., Horváth, F., Séranne, M. (Eds.), The Mediterranean Basins: Tertiary Extension within the Alpine Orogen", *Geological Society, London*, pp. 475–515 (special publications).

Okay, A., 2008, *Geology of Turkey, Anschnitt*, Vol. 21, pp. 19–42.

Pinar, A., K. Kuge, Y. Honkura, 2003, "Moment Tensor Inversion of Recent Small to Moderate Sized Earthquakes: Implications for Seismic Hazard and Active Tectonics beneath the Sea of Marmara", *Geophysical Journal International*, pp. 133-145.

Piper, J.D.A., H. Gürsoy, O. Tatar, M. E. Beck, A. Rao, F. Koçbulut, B. L. Mesci, 2010, "Distributed neotectonic deformation in the Anatolides of Turkey: a paleomagnetic analysis", *Tectonophysics,* Vol. 488, pp. 30–49.

Pondard, N., 2002, "Escarpement sous-marins et sequences sismiques dans le pull-appart de Marmara" Stage effectue au laboratoire de tectonique, IPGP.

Rawlinson, N., S. Pozgaya, S. Fishwick, 2010, "Seismic tomography: A window into deep Earth", *Physics of the Earth and Planetary Interiors*, Vol. 178, pp. 101–135.

Sato, T., J. Kasahara, T. Taymaz, M. Ito, A. Kamimura, T. Hayakawa, O. Tan, 2004, "A fore-arc origin for the thrace basin, NW Turkey". *Geol Rundsch* Vol. 85, pp. 662–668.

Sorlien C., S. D. Akhun, L. Seeber, L., M. S. Steckler, M. S., D. J. Shillington, D. J., H. Kurt, H.,   G. Çifçi, G., D. Timur-Poyraz, D., S. Gürçay. S., D. Dondurur, C. İmren, E. Perinçek, S. Okay,   H. M. Küçük,   J. B. Diebold, 2012, "Uniform basin growth over the last 500 ka, North Anatolian Fault, Marmara Sea, Turkey", *Tectonophysics,* 518–521, 1–16.

Spakman, W., 1993, "Iterative strategies for non-linear travel time tomography using global earthquakedata. Seismic Tomography :Theory and practice", Edited by H.M. Iyer and K. Hishahara. Published by Chapman and Hall.

Tank S.B., Y. Honkura, Y. Ogawa, M. Matsushima, N. Oshiman, M. Kemal‑Tunçer, C. Celik, E. Tolak, M. Isikara, 2005, "Magnetotelluric imaging of the fault rupture area of the 1999 Izmit (Turkey) earthquake". *Physics of the Earth and Planetary Interiors*, Vol. 150, pp. 213‑225.

Taymaz, T., 1990, "Earthquake Source Parameters in the Eastern Mediterranean Region", Ph.D. Thesis, Cambridge University, Cambridge, pp. 244.

Taymaz, T., 1999, "Seismotectonics of the Marmara region: Source characteristics of 1999 Golcuk-Sapanca-Duzce earthquakes", Proc. ITU-IAHS, International Conference on the Kocaeli Earthquake 17 August 1999, Istanbul, pp. 55-78.

Taymaz, T., 2000, "Seismotectonics of the Marmara region: source characteristics of 1999-Sapanca-Duzce earthquakes". In: Barka, A.A., Kozacı, O., Akyuz, S.H., Altunel, E. (Eds), 1999 Izmit-Duzce Earthquakes: Preliminary Results. Istanbul Technical University Publications, Istanbul, pp.79-97.

Taymaz, T., J. Jackson, D. P. McKenzie, 1991, "Active tectonics of the North and Central Aegean Sea,. *Geophysical Journal International*, Vol. 106, pp. 433-490.

Taymaz, T., J. Kasahara, A. Hirn, T. Sato, 2001, "Investigations of microearthquake activitiy within the Sea of Marmara and surrounding regions by using ocean bottom seismometers (OBS) and land seismographs: Initial results. In: Taymaz, T. (Ed.), Symposia on Seismotectonics of the North-Western Anatolia-Aegean and Recent Turkish Earthquakes. Scientific Activities", Faculty of Mines, Istanbul Technical University, Istanbul, pp. 42-51.

Thurber, C., 1981, Earth Strucutre and Earthquake Locations in the Coyote Lake Area, Ph.D. Thesis, MIT, Cambridge.

Thurber, C., 1983, "Earthqake locations and three-dimensional crustal structure in the coyote lake area, central California". *Geophysical Journal International*, 88.

Thurber, C., 1993, "Local Earthquake tomography : velocitises and Vp/Vs - theory. Seismic Tomography :Theory and practice", Edited by H.M. Iyer and K. Hishahara. Published by Chapman and Hall.

Tong, C., P. Barton, R. White, M. Sinha, S. Singh, J. Pye, R. Hobbs , 2003, "Influence of enhanced melt supply on upper crustal structure at a mid-ocean ridge discontinuity : A threedimensional seismic tomograpic study of 9°n east pacific rise", *Journal of Geophysical Research*, 108(B10), 2464, DOI:10.1029/2002JB002163,2003.

Tüysüz, O., 1993, "Karadeniz'den Orta Anadolu'ya bir jeotravers: Kuzey neo-Tetis'in tektonik evrimi", *Türkiye Petrol Jeologlari Dernegi Bülteni*, 5, pp. 1–33.

Thurber, C., J. Um, 1987, "A fast algorithm for two-point seismic ray tracing", *Bulletin of Seismological Society America*, Vol. 77, pp. 972–986.

Virieux, J., 1991, "Fast and accurate ray tracing by hamiltonian perturbation", *Journal of Geophysical Research,* Vol. 96, pp. 579–594.

Virieux, J., V. Farra, 1991, "Ray tracing in 3D complex isotropic media : An analysis of the problem", *Geophysics*, 56.

Virieux, J., V. Farra, R. Madariaga, 1988, "Ray tracing for earthquake location in laterally heterogeneous media", *Journal of Geophysical Research,* Vol. 93, pp. 6585–6599.

Yaltirak, C., 2002, "Tectonic evolution of the Marmara sea and its surrounding", *Marine Geology*, Vol. 90, pp. 493–529.

Yaltırak, C., B. Alpar, 2002, "Kinematics and evolution of the northern branch of the North Anatolian Fault (Ganos fault) between the Sea of Marmara and the Gulf of Saros", *Marine Geology,* Vol.190, pp. 307–327.

Yilmaz, Y., S. Genc, E. Yigitbas, M. Bozcu, K. Yilmaz, 1995, "Geological evolution of the late mesozoic continental margin of northwestern Anatolia", *Tectonophysics*, Vol. 243, pp. 155–171.

Yılmaz, Y., E. Gökaşan, A. Y. Erbay, 2010, "Morphotectonic development of the Marmara Region", *Tectonophysics,* Vol. 488, pp. 51–70.

Zattin, M., W. Cavazza, A. I. Okay A, I. Federici, M. G. Fellin, A. Pignalosa, P. Reiners, 2010, "A precursor of the North Anatolian Fault in the Marmara Sea region", *Journal of Asian Earth Sciences,* Vol. 39, pp. 97–108

Zelt, B. & P. Barton, 1998, "Three-dimensional seismic refraction tomography : A comparison of two methods applied to data from the faeroe basin", *Journal of Geophysical Research,* 103.

Zelt, B., B. Taylor, A. Goodliffe, 2001, "3-d crustal velocity structure at the rift tip in the western woodlark basin", *Geophysical Research Letters*, 28.

Zhao, D., J.R.Kayal, 2000, "Impact of seismic tomography on earth sciences", *Current Science*, Vol. 79, pp. 1208-1214.

Zor, E., S. Özalaybey, C. Gürbüz, 2006, "The crustal structure of the eastern Marmara region, Turkey by teleseismic receiver functions", *Geophysical Journal International*, Vol. 167, pp. 213-222.

APPENDIX A. TABLES OF ITERATION NUMBER DECISIONS

Table A.1. 0.25 maximum allowed P wave perturbation 9*9 model-TRAKYA BASIN 1D MODEL

Iteration number	Data Variance (s^2)	% Change Between Iteration Steps	% Change in Total
0	0.431348		
1	0.294848	31.6450	31.6450
2	0.210537	28.5947	45.9044
3	0.173525	17.5798	55.4143
4	0.150997	12.9826	61.2026
5	0.133073	11.8704	65.8081
6	0.116352	12.5653	70.1044
7	0.107745	7.39738	72.3159
8	0.100759	6.48383	74.1109
9	0.096240	4.48496	75.272
10	0.093439	2.91043	75.9917
11	0.093312	0.135918	76.0243
12	0.091675	1.75433	76.4449
13	0.091176	0.544314	76.5731
14	0.090329	0.928973	76.7908
15	0.091194	-0.957611	76.5685
16	0.091098	0.10527	76.5932
17	0.090236	0.946234	76.8146
18	0.089258	1.08382	77.0659
19	0.088854	0.45262	77.1697
20	0.091036	-2.45571	76.6091

Table A.2. 0.25 maximum allowed P wave perturbation 9*9 model-ISTANBUL ZONE 1D MODEL

Iteration number	Data Variance (s^2)	% Change Between Iteration Steps	% Change in Total
0	0.525242		
1	0.344495	34.4121	34.4121
2	0.280299	18.6348	46.6343
3	0.232435	17.0761	55.7471
4	0.198200	14.7288	62.265
5	0.169966	14.2452	67.6404
6	0.143598	15.5137	72.6606
7	0.120607	16.0107	77.0378
8	0.109034	9.59563	79.2412
9	0.098973	9.2274	81.1567
10	0.096564	2.434	81.6153
11	0.093998	2.6573	82.1039
12	0.092744	1.33407	82.3426
13	0.091502	1.33917	82.5791
14	0.094093	-2.83163	82.0858
15	0.094003	0.09565	82.1029
16	0.095584	-1.68186	81.8019
17	0.096081	-0.519961	81.7073
18	0.095810	0.282054	81.7589
19	0.097210	-1.46123	81.4923
20	0.094458	2.83098	82.0163

Table A.3. 0.25 maximum allowed P wave perturbation 9*9 model-TEKİRDAĞ BASIN
1D MODEL

Iteration number	Data Variance (s^2)	% Change Between Iteration Steps	% Change in Total
0	0.441901		
1	0.294546	33.3457	33.3457
2	0.200257	32.0116	54.6828
3	0.172642	13.7898	60.932
4	0.153390	11.1514	65.2886
5	0.135157	11.8867	69.4146
6	0.121541	10.0742	72.4959
7	0.109284	10.0847	75.2696
8	0.101305	7.30116	77.0752
9	0.097518	3.73822	77.9322
10	0.094188	3.41475	78.6857
11	0.094014	0.184737	78.7251
12	0.096353	-2.48793	78.1958
13	0.095821	0.552136	78.3162
14	0.094570	1.30556	78.5993
15	0.093087	1.56815	78.9349
16	0.093245	-0.169734	78.8991
17	0.093745	-0.536222	78.786
18	0.093276	0.500293	78.8921
19	0.092963	0.335563	78.9629
20	0.093559	-0.641115	78.8281

Table A.4. 0.25 maximum allowed P wave perturbation 9*9 model-SAKARYA ZONE 1D MODEL

| Iteration number	Data Variance (s^2)	% Change Between Iteration Steps	% Change in Total
0	0.580511		
1	0.362432	37.5667	37.5667
2	0.274588	24.2374	52.6989
3	0.236037	14.0396	59.3398
4	0.207085	12.2659	64.3271
5	0.177306	14.3801	69.4569
6	0.150643	15.0378	74.0499
7	0.133727	11.2292	76.9639
8	0.114044	14.7188	80.3545
9	0.101441	11.051	82.5256
10	0.094261	7.07801	83.7624
11	0.091331	3.10839	84.2671
12	0.089724	1.75953	84.544
13	0.089358	0.407918	84.607
14	0.091435	-2.32436	84.2492
15	0.089939	1.63613	84.5069
16	0.090784	-0.939526	84.3614
17	0.092813	-2.23498	84.0118
18	0.094188	-1.48147	83.775
19	0.093877	0.330191	83.8286
20	0.093892	-0.0159784	83.826

Table A.5. 0.25 maximum allowed P wave perturbation 9*9 model-ÇINARCIK BASIN 1D
MODEL

Iteration number	Data Variance (s^2)	% Change Between Iteration Steps	% Change in Total
0	0.528827		
1	0.504214	4.654	4.654
2	0.397003	21.263	24.9276
3	0.343232	13.5442	35.0956
4	0.280340	18.3235	46.9883
5	0.238892	14.7849	54.8261
6	0.207703	13.0557	60.7238
7	0.177515	14.5342	66.4323
8	0.152281	14.2151	71.204
9	0.136012	10.6835	74.2804
10	0.129779	4.58268	75.4591
11	0.120571	7.09514	77.2003
12	0.113813	5.605	78.4782
13	0.116421	-2.29148	77.985
14	0.117898	-1.26867	77.7058
15	0.110697	6.10782	79.0674
16	0.113546	-2.57369	78.5287
17	0.115887	-2.06172	78.086
18	0.113575	1.99505	78.5232
19	0.112865	0.625138	78.6575
20	0.112993	-0.11341	78.6333

Table A.6. 0.25 maximum allowed P wave perturbation 9*9 model-CENTRAL BASIN 1D
MODEL

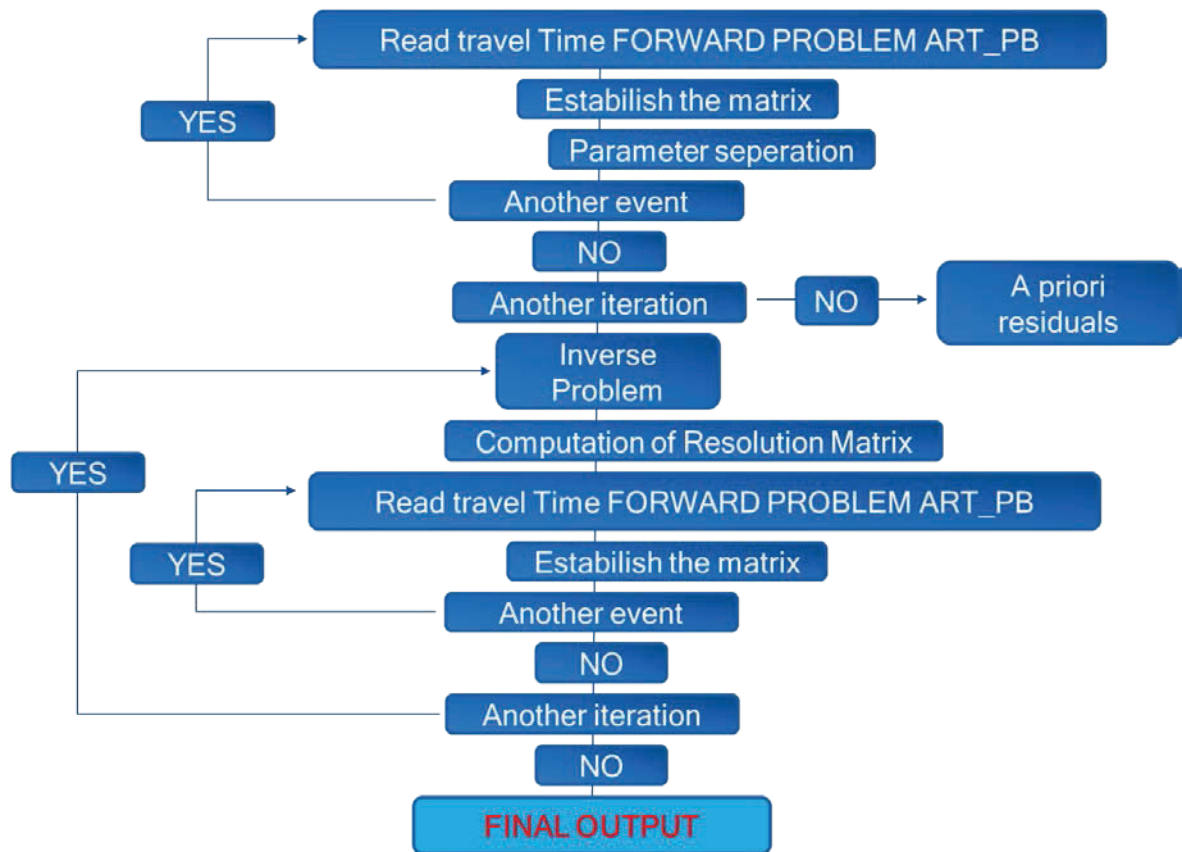| Iteration number	Data Variance (s^2)	% Change Between Iteration Steps	% Change in Total
0	0.7266		
1	0.4019	44.6862	44.6862
2	0.3019	24.8818	58.4493
3	0.2484	17.7211	65.8125
4	0.1976	20.4509	72.8042
5	0.1708	13.5628	76.4927
6	0.1528	10.5386	78.97
7	0.1437	5.9555	80.2225
8	0.1380	3.9666	81.007
9	0.1349	2.24638	81.4336
10	0.1331	1.33432	81.6814
11	0.1326	0.375657	81.7502
12	0.1327	-0.0754148	81.7364
13	0.1334	-0.527506	81.6401
14	0.1329	0.374813	81.7089
15	0.1321	0.601956	81.819
16	0.1309	0.908403	81.9841
17	0.1300	0.687548	82.108
18	0.1292	0.615385	82.2181
19	0.1289	0.232198	82.2594
20	0.1294	-0.387898	82.1906

APPENDIX B. SUPPLEMETARY FIGURES
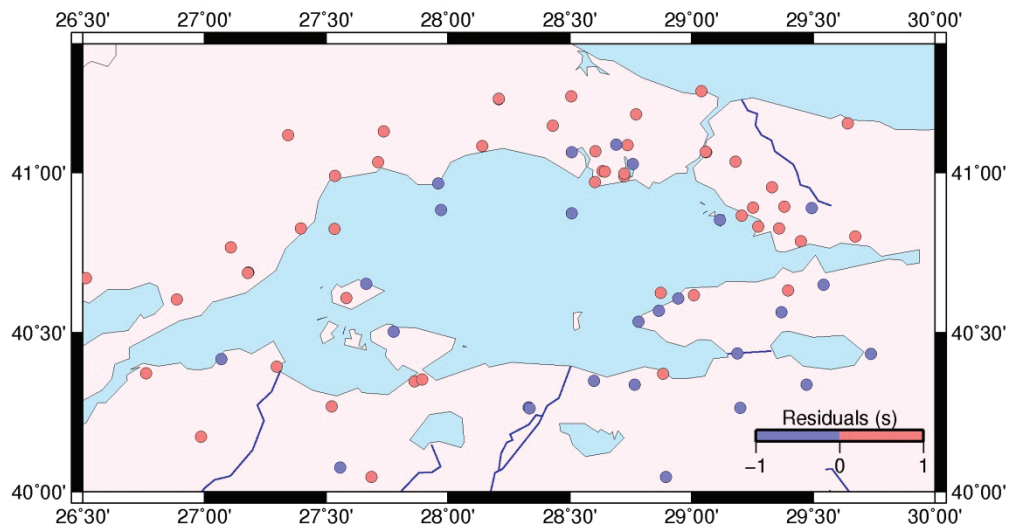
B. 1. Station corrections for resulting 3D model
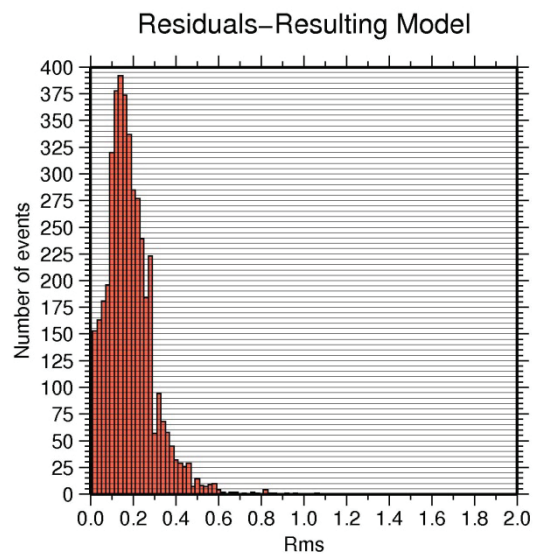
B. 2. A posteriori residuals of all earthquakes

APPENDIX C. FLOW DIAGRAM OF 3D TOMOGRAPHIC INVERSION

C. 1. Flow diagram of 3D tomographic inversion